Cell free protein expression and in depth biophysical analysis of small molecule binding characteristics using SPR and NMR

Dissertation
zur Erlangung des Doktorgrades
der Naturwissenschaften

vorgelegt beim Fachbereich
Biochemie, Chemie und Pharmazie (FB 14)
der Goethe-Universität
in Frankfurt am Main

von
Christopher Erich Hein
aus Werne

Frankfurt am Main 2015
(D 30)

Vom Fachbereich Biochemie, Chemie und Pharmazie (FB 14) der Goethe-Universität als Dissertation angenommen.

Dekan:	Prof. Dr. Michael Karas
Gutachter:	Prof. Dr. Volker Dötsch
	Prof. Dr. Peter Güntert

Datum der Disputation:

„Eritis sicut Deus, scientes bonum et malum."
Johann Wolfgang von Goethe

Eidesstattliche Erklärung

Ich erkläre hiermit an Eides statt, dass ich die vorgelegte Dissertation mit dem Titel „Cell free protein expression and in depth biophysical analysis of small molecule binding characteristics using SPR and NMR“ selbständig angefertigt und mich anderer Hilfsmittel als der in ihr angegebenen nicht bedient habe. Ich erkläre weiterhin, dass Entlehnungen aus Schriften, soweit sie in der Dissertation nicht ausdrücklich als solche bezeichnet sind, nicht stattgefunden haben. Ich habe bisher an keiner anderen Universität ein Gesuch um Zulassung zur Promotion eingereicht oder die vorliegende oder eine andere Arbeit als Dissertation vorgelegt.

Frankfurt am Main, den 24. September 2015

_____

Christopher Erich Hein

Table of contents

List of figures

Summary

Small molecule drug discovery is strongly supported by biophysical data. In the reach of this thesis, cell free protein expression was used to produce human target proteins for ligand binding assays using Surface Plasmon Resonance spectroscopy (SPR). In the second step the binding and interaction characteristics of small molecules and fragments were analyzed using Nuclear Magnetic Resonance spectroscopy (NMR).

The first target protein was the human acid sensing channel 1 (ASIC1a). ASIC1a is a pH dependent cation channel, which is essential for nociception and pain. ASIC1a was expressed in a cell free expression system based on *E.coli* lysate. To optimize the expression, several parameters including fusion tags, ion concentrations and different hydrophobic environments were tested. The expression of the full length protein was achieved using an N-terminal tag as expression enhancer and optimizing the Mg^{2+} concentration during the expression.

The adaption of the folding environment for ASIC1a needed more optimization, because it is a very challenging target to express in an *in vitro* system. ASIC1a is a trimer with a large soluble domain as well as a transmembrane domain. This makes it important to find a hydrophobic environment that supports the folding of both domains. In addition, the protein contains seven disulfide bridges that need to be formed correctly. Three different expression modes were employed to find a suitable folding environment. The expression as precipitate with subsequent solubilization did not yield any folded protein. The direct expression in detergent in the D-CF mode showed some soluble protein using the detergents Digitonin and Brij98. These samples however did not show a homogeneous peak in the size exclusion chromatography. The most promising tool was the use of nanodiscs for protein stabilization, because these particles combine the advantages of a lipid environment with the behavior as soluble particles. This expression yielded some soluble, full length ASIC1a, but the activity of this protein could not be tested due to the lack of a suitable quality assessment.

SPR binding studies with ASIC1a were performed with chicken ASIC1a expressed in insect cells. The immobilization of cASIC1a and the used buffer conditions were tested using Psalmotoxin 1, a naturally occurring peptide venom which binds strong to the trimeric form of ASIC1a. Since the toxin exclusively binds to the trimeric protein, the injection of a concentration series to the protein surface shows that the immobilized protein is probably correctly folded and the immobilization method yields highly active chip surfaces. Compound characterization experiments were performed with a variety of different ligands including amiloride, a general blocker of the whole ENaC protein family. None of the used ligands showed titration curves that would match a simple 1:1 binding model. For the optimization of the experimental conditions, different pH values in the running buffer and different detergent mixtures to stabilize the protein were tested. The pH values were varied to induce different conformations in cASIC1a and the detergent mixtures were varied to probe for unspecific effects between detergent and ligands. The experiments either show no binding signal or signal that could be interpreted as unspecific binding. Even amiloride that should be binding the protein shows no signals that fit a simple binding model.

Another target protein that was investigated, is the soluble prolyl *cis/trans* isomerase Cyclophilin D (or peptidyl prolyl isomerase F – PPIF). This protein is involved in the regulation of the mitochondrial permeability transition pore and therefore a potential drug target to treat neurodegenerative diseases. Small molecule binding was tested with CypD using SPR. For this purpose CypD was expressed in a cell free expression system based on *E.coli* lysate. The construct includ-

ed a C-terminal Avi fusion tag on CypD, which is site specifically biotinylated, when the protein is co-expressed with BirA. The co-translational biotinylation allows the direct immobilization of CypD from the expression mixture without any prior purification. This fast and unproblematic immobilization resulted in highly active and stable chip surfaces, that were used for the binding analysis of a variety of different ligands. Following the kinetic analysis of small molecule ligands, the binding position of different binding fragments was analyzed. These fragments originated from a SPR based fragment screen and gave no co-crystal structures with CypD (data not disclosed, personal communication Daniel Schwarz, Merck Serono). Therefore NMR was used to investigate the binding position of these fragments. CL7 and CL5 were used as control ligands, because co-crystal structures with CypD were available (data not disclosed, personal communication Daniel Schwarz, Merck Serono). An analysis of the chemical shift perturbations upon ligand addition revealed that the NMR analysis was in line with the results gathered by x-ray crystallography. The fragments with unknown binding position however, all bind to a specific patch slightly outside the binding pocket. This patch includes many residues that are reported to be important for the catalytic activity of CypD or close to the substrate binding pocket (Phe60, Ile117, Asp120 and Trp121). It can be speculated, that the examined fragments did not yield co-crystals, because the binding site is involved in crystal contacts in the available CypD crystal structures, which can be disturbed by the ligands.

The ligand CL1 showed a special behavior in the NMR experiments. Upon addition to CypD, it produced large shifts on many signals of the protein, accompanied by a severe line broadening. The shift perturbations were so numerous and large that the spectrum had to be reassigned in complex with the ligand. The line broadening however prevented the use of NH detected 3D experiments for signal assignment. Therefore triple selective labeling was applied to allow a fast and nearly complete signal assignment. The possibility to use highly sophisticated labeling schemes, is one of the advantages of cell free protein expression. The use of specific scrambling inhibitors in combination with the availability of differently labeled amino acids guarantees the specificity of the labeling. After the assignment of the complex spectrum, the chemical shift perturbations were analyzed and quantified. The residues showing the strongest CSPs are also identified in the crystal structure to be involved in the binding of CL1, giving a consistent picture. The numerous and large shift perturbations, produced by CL1 led to the assumption, that the ligand induces a conformational change in CypD, which is not represented in the co-crystal structure. This conformational change was characterized by a NMR based structure determination. CypD apo yielded a defined bundle, whose folded regions overlap well with the corresponding crystal structure. The loop regions in contrast show differences between the x-ray and the NMR structure. This suggests that the loop regions are flexible, which could be needed to accommodate a range of different proteins that are substrates of CypD. In addition the loop flexibility is needed for an induced fit mechanism during substrate binding.

For the calculation of the CypD-CL1 complex structure, the sidechain resonances needed to be assigned. Due to line broadening it was only possible to record a HCCH TOCSY and 3D ^{15}N and ^{13}C NOESY spectra to gain information about the sidechain resonances. The resonances were assigned using an automated assignment approach with the software FLYA. The calculation of the CypD-CL1 complex structure did not result in a defined bundle. While parts of the protein converge in a well folded state, the region around the active site shows no defined folding. Careful analysis of the structure calculation suggests that the problems during structure calculation did not originate from an incorrect resonance assignment, but rather from a lack of NOE crosspeaks. This might be due to a broadening of the corresponding NOE crosspeaks or the coexistence of many different conformations. This leads to the conclusion, that the protein conformation is not defined by the NMR data and could be in a dynamic interchange between multiple structures.

This hypothesis is supported by other observations. The line broadening of the signals in the complex is pronounced in the area around the active site and the substrate binding pocket, hinting

to a connection between catalytic activity and protein dynamics. In addition many NMR signals are sensitive to changes in the measurement field strength and the temperature. A comparison of $^{15}N,^{1}H$ HSQC spectra recorded at 500 MHz and 900 MHz shows that many signals show a splitting at 900 MHz that is not seen at 500 MHz. This field dependent splitting suggest dynamic conformational changes in the protein between at least two different conformations on a millisecond timescale.

The current working model is that CL1 binds to CypD and induces the catalytic cycle and the connected conformational changes in CypD. As a result the proline like moiety in CL1 is constantly switching between the *cis* and the *trans* conformation. Due to the high affinity of CL1, the inhibitor does not leave the binding pocket after successful catalysis, but stays bound in the pocket stimulating further catalytic cycles. The protein motions are hereby happening on the millisecond timescale, which means that the motions are in the intermediate exchange regime under the used NMR conditions. These findings as well as the working model are well in line with data published for Cyclophilin A, another member of the cyclophilin family, thereby supporting the model.

Zusammenfassung

Die Entwicklung und Optimierung von kleinen organischen Molekülen zu medizinischen Wirkstoffen ist ein langer und aufwendiger Prozess. Ist das Zielprotein, dessen Aktivität moduliert werden soll, bekannt, müssen zuerst Startstrukturen gefunden werden, die in folgenden Prozessen optimiert werden. Biophysikalische Daten zu Bindungsort und Bindungskinetik sind eine wichtige Grundlage dieser Optimierung.

Das Ziel dieser Arbeit war die zellfreie Expression medizinisch relevanter Zielproteine sowie die Suche und Analyse potenzieller niedermolekularer Inhibitoren. Hierbei lag ein Augenmerk auf der zellfreien Protein Produktion, da diese einige Vorteile für etwaige spätere Anwendungen bietet. Hierbei wurden das Membranprotein ASIC1 (*acid sensing channel 1*), sowie die Prolyl *cis/trans* isomerase CypD (*Cyclophilin D*) untersucht.

Die zellfreie Expression von ASIC1 wurde in einem System auf Basis eines *E.coli* Zelllysats opimiert. Die ersten Schritten beinhalteten die Optimierung des Expressionskonstrukts, sowie der verwenden Ionenkonzentrationen. Als Basiskonstrukt diente das humane ASIC1a. Mit einer Größe von mehr als 60 kDa pro Monomer ist ASIC1a ein recht großes Zielprotein für die zellfreie Proteinsynthese, da diese eine geringere Prozessivität als das zelluläre System aufweist und deshalb zum vorzeitigen Abbruch der Translation neigt. Dies führt zu C-terminal verkürzten Proteinfragmenten. Aus diesem Grund wurde als erster Optimierungsschritt eine "*tag variation*" durchgeführt. Die Benutzung des AT tags als N-terminales Fusionspeptid erhöhte nicht nur die Gesamtausbeute, sondern führte zusätzlich zu einer Reduktion an Nebenprodukten nach der Translation. Nach einer Optimierung der Ionenkonzentrationen während der Expression wurde die Faltungsumgebung im System optimiert. ASIC1a stellt hierbei große Anforderungen an das System, da es sowohl eine große lösliche Domäne als auch eine Transmembrandomäne enthält, die sehr unterschiedliche Milieus für eine korrekte Faltung benötigen. Transmembrandomänen benötigen zur korrekten Faltung meist eine hydrophobe Umgebung die zB durch Detergenzien bereitgestellt werden kann. Diese Umgebung stabilisiert die hydrophoben Bereiche in Lösung. Bei löslichen Domänen hingegen kann die Verwendung von Detergenzien dazu führen, dass hydrophobe Teile maskiert werden und der hydrophobe Proteinkern nicht korrekt gebildet werden kann. Lipide zeigen diese Problematik weniger, sind aber meist unlöslich, was weitere Schwierigkeiten bei der späteren Verarbeitung der Proben hervorrufen kann. Aus diesem Grund wurden neben Detergenzien auch Nanodiscs in die Optimierung mit eingeschlossen, da diese viele Vorteile von Detergenzien und Lipiden verbinden. Zusätzlich zeigt sich die Schwierigkeit, dass ASIC1 über sieben Disulfid Brücken verfügt, die korrekt gebildet werden müssen, wobei die zellfreie Proteinsynthese klassischerweise unter reduzierenden Bedingungen durchgeführt wird, um eine optimale Funktion zu gewährleisten. Nach der Optimierung kam das Problem auf, dass kein brauchbarer Test vorhanden war um die Qualität der produzierten Proben zu evaluieren. Die Entwicklung eines Verfahrens scheiterte am Fehlen einer Positivkontrolle.

An diesem Punkt des Projekts lieferte die Firma Proteros ASIC1a, das in Insektenzellen produziert und aus diesen gereinigt wurde. Es handelte sich hierbei um eine Isoform aus dem Huhn. Dieses Protein wurde verwendet, um SPR Studien durchzuführen und die Bindung einiger Ligan-

den zu untersuchen. Zuerst wurde die Proteinqualität und die gewählte Immobilisierungsmethode getestet. Hierfür wurde Psalmotoxin1 (PcTx1) benutzt, ein natürlich vorkommendes Peptidtoxin. PcTx1 bindet hochaffin und ausschließlich an die trimere Form von ASIC1a und eignet sich deshalb besonders gut zur Qualitätsprüfung. Da die erhaltenen Ergebnisse im Einklang mit publizierten Daten stehen, wurde die Analyse auf weitere Liganden ausgeweitet. Einige dieser Liganden wurden bereits in zellbasierten Tests, sowie elektrophysiologisch untersucht (Daten nicht freigegeben, persönliche Kommunikation mit Daniel Schwarz, Merck Serono) und zeigten einen inhibitorischen Effekt. Zusätzlich wurde Amilorid als Positivkontrolle verwendet, da dieses ein genereller Inhibitor für die die gesamte ENaC Familie ist. Nachdem erste Tests, unter den gleichen Bedingungen unter denen auch PcTx1 analysiert wurde, keine Bindung zeigten, wurden einige Parameter variiert und optimiert. So wurde unter anderem der pH Wert der verwendeten Puffer verändert. Da ASIC1 durch verschiedene pH Werte gesteuert wird, wurde die pH Änderung benutzt um verschiedene Konformationen zu induzieren oder zumindest stärker zu populieren. Die Experimente wurden einerseits bei pH 7,5 durchgeführt, was den Kanal im geschlossenen Zustand halten sollte, andererseits bei pH 6,3, was den Kanal aktivieren und somit in einem geöffneten Zustand versetzen sollte. Neben dem pH Wert wurde auch die hydrophobe Umgebung des Proteins modifiziert. Es wurden verschiedene Mischungen von Detergenzien verwendet, um deren Einfluss auf die erhaltenen Messdaten zu untersuchen. Hierbei wurde allerdings in allen Proben DDM verwendet, da das Protein in diesem Detergenz gereinigt und gelagert wurde. Bei diesen Messungen fiel auf, dass Proben die kein CHAPS enthielten weitaus größere Messsignale zeigten als Vergleichsproben, diese Signale aber eher auf eine unspezifische Bindung der Liganden deuten, da es bei einer Verdopplung der Ligandenkonzentration auch zu einer Signalverdopplung kam, obwohl die maximale Konzentration mindestens 100 fach über der zu erwartenden aktiven Konzentration lag. Diese Beobachtung lässt den Schluss zu, dass CHAPS unspezifische Bindung des Liganden unterdrückt. Zusammenfassend lässt sich bemerken, dass keiner der Bindungstest Ergebnisse geliefert hat, die auf eine spezifische Protein-Liganden Interaktion schließen lässt, welche einem einfachen 1:1 Bindungsmodell folgt. Die Messkurven enthalten entweder keine Signale, sehr kleine negative Signale oder Signale die auf unspezifische Bindung hinweisen. Auch eine Analyse von Amilorid, welches binden sollte, hat keine brauchbaren Ergebnisse geliefert.

Es gibt verschiedene mögliche Gründe weshalb die SPR Analyse der Liganden keine Bindung zeigt. Zum einen wurden die zellbasierten und elektrophysiologischen Tests mit der humanen Isoform von ASIC1 durchgeführt, während die SPR Versuche mit der Isoform aus dem Huhn durchgeführt wurden. Die Unterschiede zwischen den Isoformen könnten einen Einfluss auf die Bindung haben, sollten aber keinen großen Einfluss auf Amilorid haben, da dieses eine breites inhibitorisches Spektrum hat. Des Weiteren könnten Detergenz Mizellen entweder die Liganden in Lösung abschirmen, was zu einer Reduktion der scheinbaren Ligandenkonzentration führt, oder hydrophobe Bindestellen im Protein maskieren und somit mit den Liganden konkurrieren. Auch wäre es denkbar, dass ASIC1 permanent verschiedene Konformationen durchläuft, von denen nur wenige die Ligandenbindung ermöglichen. Dieses Problem wurde durch die Verwendung verschiedener pH Werte beleuchtet. Trotzdem könnte konformationelle Selektion zu Problemen bei der SPR Analyse führen, die bei anderen Methoden nicht sichtbar sind, da hierbei das Protein für lange Zeit mit dem Liganden inkubiert wird bevor die Aktivitätsmessung erfolgt.

Der zweite Teil der Arbeit hat sich mit der Prolyl *cis/trans* isomerase CypD beschäftigt. CypD ist ein zentraler regulatorischer Faktor der "*mitochondrial permeability transition pore*" und somit ein guter Angriffspunkt für potenzielle Medikamente zur Behandlung neurodegenerativer Erkrankungen.

CypD wurde zellfrei als lösliches Protein exprimiert. Für SPR Bindungsstudien wurde das Expressionskonstrukt mit einem C-terminalen Avi tag versehen, welcher es ermöglicht CypD in einer spezifischen Erkennungssequenz zu biotinilieren. Diese Reaktion wird von der Biotinligase BirA katalysiert, die mit CypD gleichzeitig exprimiert werden kann. Hierfür müssen lediglich beide Plasmide sowie Biotin (1 mM) zur zellfrei Reaktion gegeben werden. Nach Abschluss der Reaktion kann CypD ohne vorhergehende Reinigung direkt aus der Reaktionslösung auf einem Streptavidin Chip immobilisiert werden. Diese Art der Immobilisierung ist sehr hilfreich, da sie viele Probleme die im Zusammenhang mit Aminkopplung auftreten umgeht. So ist unter anderem die Verwendung von Reduktionsmitteln, hohen Salzkonzentrationen und pH Werten oberhalb des Isoelektrischen Punktes des Proteins möglich, was zu Problemen bei Aminkopplung führen würde. Die Immobiliserungsmethode, Proteinqualität und Testbedingungen wurden mit Cyclosporin A, einem natürlich vorkommenden, hochaffinen Inhibitor für CypD, getestet. Die gemessene Bindungskinetik war sehr ähnlich zu den veröffentlichten Werten und bestätigt somit die Validität der verwendeten Bedingungen. Nachdem diese Kontrollmessung erfolgreich war, wurden die Experimente auf verschiedene kleine Moleküle erweitert. Hierbei wurden Liganden mit verschiedenen Bindungskinetiken vermessen und analysiert.

Für die Entwicklung eines potenten Inhibitors ist es notwendig sowohl Informationen über die Bindungskinetik als auch strukturelle Informationen über den Bindungsort zu erhalten. Merck Serono hat eine groß angelegte Analyse einer Fragmentbibliothek durchgeführt. Die Analyse lieferte 58 Fragmente, deren Bindung bestätigt wurde. Von diesen 58 Fragmenten waren jedoch nur 6 in Kristallstrukturen mit CypD sichtbar. Aus diesem Grund wurde NMR verwendet um die Bindung der anderen Fragmente zu bestätigen und den genauen Bindungsort zu ermitteln. Hierfür wurden die Fragmente mit CypD gemischt und die Veränderungen der chemischen Verschiebungen der CypD Signale im ^{15}N,^{1}H HSQC quantifiziert. Diese Analysemethode führt zu einer Bestimmung der Stellen im Protein, deren chemische Umgebung sich aufgrund der Ligandenbindung ändert. Dies bedeutet in den meisten Fällen, dass die Bindungsstelle des Liganden in räumlicher Nähe zu diesen Resten liegt. Die Liganden CL1 und CL7 wurden als Positivkontrollen verwendet, da von diesen Cokristallstrukturen mit CypD vorhanden sind. Die NMR Ergebnisse über die Bindungsstelle von CL7 decken sich gut mit den Beobachtungen aus der Kristallstruktur (Daten nicht freigegeben, persönliche Kommunikation mit Daniel Schwarz, Merck Serono). Der Ligand bindet direkt in die Bindetasche von CypD und okkupiert einen Großteil dieser Tasche. Eine Ausweitung der Analyse auf die Fragmente mit unbekannter Bindestelle zeigt interessanterweise, das die Fragmente alle an einer sehr ähnlichen Position binden. Hierbei handelt es sich um eine Interaktionsfläche, die sich außerhalb der Substratbindetasche, in der Nähe der Prolin Tasche befindet. Die Interaktionsfläche schließt die Reste Phe60, Ile117, Asp120 und Trp121 ein, welche mitunter essentiell für die Proteinaktivität sind. Eine Analyse der vorhanden Kristallstrukturen zeigt, dass diese Fläche an Kristallkontakten zwischen den CypD Molekülen im Kristallgitter beteiligt ist. Es kann spekuliert werden, ob diese Kontakte die Bindung der Fragmente behindert bzw. die Bindung der Fragmente die Ausbildung der Kristallkontakte während der Cokristallisation stört.

Die Untersuchung von CL1 zeigte einige unerwartete Effekte. Die Zugabe von CL1 zu CypD

führt zu starken Verschiebungen an einer Vielzahl der CypD Signale, begleitet von einer starken Signalverbreiterung. Die starken und zahlreichen Verschiebungen machen es notwendig, das gesamte CypD-CL1 Komplexspektrum neu zuzuordnen. Die Signalverbreiterung jedoch sorgt dafür, dass keine 3D Experimente verwendet werden können, die über NH detektiert werden, da in diesen Spektren die Signale großer Bereiche fehlen. Aus diesem Grund wurde selektive Probenmarkierung verwendet, um zumindest die N und H^N Resonanzen zuzuordnen. Die verwendete Methode beruht auf 3 verschiedenen Proben mit je einem anderen Markierungsmuster. Die selektive Markierung wurde zusätzlich mit *time shared* Experimenten kombiniert, um die Messzeit zu verkürzen. Auf diese Weise konnte eine nahezu vollständige Signalzuordnung erstellt werden. Nun konnte eine Auswertung der Signalverschiebungen erfolgen, die zeigte dass die Position von CL1 in der Bindetasche gut zu den Daten aus der Kristallographie passt.

Allerdings legen die Daten die Vermutung nahe, dass das Protein eine Konformationsänderung vollzieht, die durch den Ligand induziert wird. Um diese Konformationsänderung näher zu beleuchten, wurde eine NMR Struktur von CypD gerechnet. Die Struktur von CypD apo konvergiert in ein definiertes Strukturbündel. Die Sekundärstrukturelemente überlagern gut mit der entsprechenden Kristallstruktur. Die Regionen ohne klare Sekundärstruktur jedoch zeigen eine gewisse Flexibilität in der Strukturrechnung. Da CypD verschiedene Proteine als Substrate erkennt, könnte diese Flexibilität wichtig sein, um die verschiedenen Substrate effizient zu binden. Hierbei könnte der flexible Teil in einen *induced fit* Mechanismus eingebunden sein.

Für die Strukturrechnung des CypD-CL1 Komplexes jedoch konnten aufgrund der Signalverbreiterung nur ein HCCH TOCSY sowie ^{15}N NOESY und ^{13}C NOESY Spektren aufgenommen werden, um die Seitenketten Signale zuzuordnen. Aufgrund des großen Signalüberlapps in diesen Spektren wurden die Signale automatisch mit dem Programm FLYA zugeordnet. Hierbei wurden verschiedene Parameter der Zuordnung optimiert. Die Qualität der Zuordnung wurde an der Anzahl der Zuordnungen gemessen, die vom Programm als stark klassifiziert wurden. Durch die selektive Markierung waren viele H und N^H Resonanzen bereits bekannt. Desweiteren wurden einige C^α und C^β Verschiebungen aus einem HNCA, HNCACB und HN(CO)CACB Spektrum gewonnen. Diese Spektren enthielten nur einen Bruchteil der erwarteten Signale und konnten nur verwendet werden, da die N und H^N Resonanzen bereits bekannt waren. Die beste automatische Zuordnung wurde erstellt, indem die manuell zugeordneten Resonanzen als fest gesetzt wurden und die Resonanzen aus CypD apo als Statistik mit einer geringen Standardabweichung von 0,1 für die Zuordnung benutzt wurden. Die angeschlossene Strukturrechnung jedoch konvergierte nicht zu einer definierten Struktur. Während eine Hälfte der Struktur, inklusive vier Stränge des β-Faltblatts, sowie die zwei zentralen α-Helices, eine definierte Faltung zeigen, ist vor allem der Bereich um das aktive Zentrum und die Substrat Bindetasche ungefaltet. Eine Analyse der Strukturrechung lässt darauf schließen, dass dieses Problem wahrscheinlich durch das Fehlen entscheidender NOE Kreuzpeaks verursacht wird und nicht durch eine fehlerhafte Signalzuordnung. Bei einer Konformationsänderung ist zu erwarten, dass das Protein eine definierte Struktur einnimmt. Die Daten weisen jedoch darauf hin, dass das Protein dynamischen Änderungen unterworfen ist, da die Struktur durch die NMR Daten nicht eindeutig bestimmt wird. Diese Annahme wird durch weitere Beobachtungen gestützt. Eine Analyse der Signalintensitäten im CypD-CL1 Komplex zeigt, dass einige Bereiche stark verbreiterte Signal zeigen. Interessanterweise ist die Signalverbeiterung im Bereich um die Substratbindetasche am stärksten ausgeprägt. Dies weist auf eine Dynamik in diesem Bereich hin. Um diese Annahme

zu überprüfen wurden Spektren bei verschiedenen Feldstärken und verschiedenen Temperaturen aufgenommen. Sollte die Signalverbreiterung ein Ergebnis dynamischer Prozesse sein, sollten die Signale sich abhängig von der Feldstärke und der Temperatur verändern. Interessanterweise kommt es bei Messungen bei höherem Feld (900 MHz) zu einer Aufspaltung der CypD Signale. Viele Signale spalten in zwei Signale mit etwa gleicher Intensität, manche jedoch auch in mehr. Zusätzlich zeigt eine NMR Analyse von CL1, dass die Prolin ähnliche Struktur des Liganden in der freien Form in *cis* und in *trans* Konformation vorliegt und die Konformationen sich auch unkatalysiert ineinander umwandeln. Die Beobachtungen führen zu dem finalen Modell, nach welchem CL1 in die Bindetasche von CypD bindet, wobei der Prolin ähnliche Teil im aktiven Zentrum des Proteins bindet. CypD wird durch den Liganden stimuliert und durchläuft den katalytischen Zyklus der *cis*/*trans* Isomerisierung. Im Gegensatz zu Peptidsubstraten verbleibt der hochaffine Ligand jedoch in der Bindetasche, was zu einem konstanten dynamischen Durchlaufen des aktiven Zyklus führt. Diese Proteindynamik wirkt sich auf eine Vielzahl von Resten im Protein aus, was die zahlreichen Signalverschiebungen erklärt. Die dynamische Konforamtionsänderung erklärt ausserdem die Signalverbreiterung in den Spektren und die Probleme bei der Strukturrechnung. Diese Beobachtungen werden von erst kürzlich publizierten Daten über CypA unterstützt (Chi 2015).

Abbreviations

AcP	Acetyl phosphate
APS	Ammonium persulfate
ASIC	Acid sensing ion channel
β-ME	β-mercaptoethanol
BirA	Bifunctional ligase/repressor A
Brij35	Polyoxyethylen (23) laurylether
Brij58	Polyoxyethylen (20) cetylether
Brij98	Polyoxyethylen (20) oleylether
CECF	Continuous-exchange cell-free
CF	Cell-free
CHAPS	3-[(3-cholamidopropyl)dimethyl-ammonio]-1-propansulfonat
CL1-8	Cyclophilin Ligand 1-8
Cmc	Critical micelle concentration
CsA	Cyclsporin A
CSP	chemical shift perturbation
CV	Column volume
CypA	Cyclophilin A
CypD	Cyclophilin D
D-CF	Cell-free protein synthesis in presence of detergents
DDM	n-Dodecyl β-D-Maltopyranoside
DEG	Degenerin sodium channel family
DMPC	1,2-dimyristoyl-sn-glycero-3-phosphocholine
DMPG	1,2-dimyristoyl-sn-glycero-3-phospho-(1'-rac-glycerol)
DMSO	Dimethyl sulfoxide
dNTP	Deoxynucleotide triphosphate
DOPC	1,2-dioleoyl-sn-glycero-3-phosphocholine
DOPG	1,2-dioleoyl-sn-glycero-3-phospho-(1'-rac-glycerol)
DSC	dynamic scanning calorimetry
DTT	Dithiotreitol
ECL	Enhanced chemoluminescence
EDTA	Ethylenediaminetetraacetic acid
EDTA	Ethylene-diamine-tetraacetic acid
ENaC	Epithelial sodium channel family
et al.	and others
EtBr	Ethidium bromide
EtOH	Ethanol
FM	Feeding mixture
FPLC	Fast protein liquid chromatography
HEPES	4-(2-hydroxyethyl)-1-piperazineethanesulfonic acid
HMQC	Heteronuclear multiple-quantum correlation

HRP	Horseradish peroxidase
HSQC	Heteronuclear single quantum coherence
IMAC	Immobilized metal affinity chromatography
IMAC	Immobilized metal ion affinity chromatography
IPTG	Isopropyl β-D-1-thiogalactopyranoside
ITC	Isothermal titration calorimetry
KD	Equilibrium dissociation constant
koff	Dissociation rate constant
kon	Association rate constant
LB	Lysogeny broth
L-CF	Cell-free expression in presence of liposomes
MitTx	The toxin of the Texas coral snake (Micrurus tener tener)
MSP1	Membrane scaffold protein 1
MSP1E3D1	Membrane scaffold protein 1 with three additional helices and a truncation of helix 1
MWCO	Molecular weight cut-off
Ni-IDA	Nickel iminodiacetic acid
Ni-NTA	Nickel-nitrilotriacetic acid
NMR	Nuclear magnetic resonance
NSAID	Non-steroid anti-inflammatory drugs
NTP	Nucleotide triphosphate
OAc	Acetic acid
OD600	Optical density at 600 nm
PAGE	Polyacrylamide gel electrophoresis
P-CF	Precipitate generating cell-free expression mode
PCR	Polymerase chain reaction
PcTx1	Psalmotoxin 1
PDB	Protein data bank
PEG	Polyethylenglycol
PEP	Phosphoenol pyruvate
pH	Potentia hydrogenii
ppm	Parts per million
PVDF	Polyvinylidene difluoride
RM	Reaction mixture
rpm	Revolutions per minute
RT	Room temperature
S30	E. coli extract centrifuged at 30,000xg
SDS PAGE	Sodium dodecyl sulfate polyacrylamide gel electrophoresis
SDS	Sodium dodecylsulfate
SEC	Size exclusion chromatography
SEC	Size exclusion chromatography
SOC	Super optimal broth with catabolite repression
SPR	Surface Plasmon Resonance
SPR	Surface plasmon resonance

TB	Terrific broth
TEMED	N,N,N',N'-tetramethylethylenediamine
TEV	Tobacco etch virus
TMS	Transmembrane segment
Tris	Tris(hydroxymethyl)aminomethane
TritonX-100	Polyethylene-glycol-P-1,1,3,3-tetramethylbutylphenyl-ether
Tween-20	Polyoxyethylene-sorbitan-monolaurate 20
WB	Western blot

Amino acids are abbreviated using the common single letter and three letter code.

1. Introduction

1.1. General introduction

The aim of this thesis was the cell free production of membrane and soluble proteins as targets for the biophysical characterization of small molecule ligands with SPR and NMR.

1.1.1. Cell free protein production

Cell free protein production is becoming more and more popular in the past years as a tool to produce proteins for structural, biophysical and biochemical analysis. The cell free expression system used for the work described in this thesis, is based on earlier published protocols (Schwarz 2007; Schneider 2010; Kai 2015). These publications describe the process of the *E.coli* lysate and T7 RNA polymerase production as well as the technical details of the self-made reaction containers. Besides the *E.coli* based system several other lysate sources are successfully used. The different lysate sources as well as a comparison of the different systems have already been reviewed (Junge 2008; Aceti 2015), including lists of successfully expressed membrane proteins (Proverbio 2014).

Cell free protein expression is a very valuable tool, because its open nature allows a direct manipulation of the transcription and translation machinery. The expression takes place in a chemically defined environment that can be manipulated to a certain extent. The manipulations include treatment of the lysate (Su 2011; Yin 2012), availability of different metabolic pathways (Kim 2006; Kim 2009) and manipulation of the redox potential (Zimmerman 2014; Xu 2015). The cell free expression allows further to add cofactors, chaperones, modifying enzymes, inhibitors and interaction partners directly to the expression, controlling the co-translational and post-translational modification and folding parameters of the expressed protein. Also co-expression of different proteins is possible and easy to achieve. The cell free expression system tolerates the expression of toxic proteins that would be problematic in cell based system, because they are either pro apoptotic (for eukaryotic systems) or interfere with the cell metabolism by destroying membrane gradients for example. This can be the case for different ion channels, transporters or porins. Besides the already mentioned manipulations the hydrophobic environment in the cell free system can be manipulated. This is important for membrane protein expression, which needs a hydrophobic environment to stabilize the newly synthesized membrane protein. The protein can either be expressed without a hydrophobic environment (P-CF mode), directly in detergent micelles (D-CF mode) or in lipids or nanodiscs (L-CF mode). An overview about the modes and the different hydrophobic environments is given in some reviews (Junge 2011; Hein 2014; Proverbio 2014). A general guideline for optimization strategies and general considerations is given by Henrich et al. (Henrich 2015). The large set of possible optimization parameters can efficiently be used, when cell free expression is combined with automatization technology (Aoki 2009; Beebe 2014; Quast 2015).

Cell free expression is very valuable for labeling of proteins with stable isotopes for NMR analysis (Parker 2004; Staunton 2006; Jeremy Craven 2007; Reckel 2008; Abdine 2011; Löhr 2012; Linser 2014; Löhr 2015), because the system allows to control exactly the pool of available amino acids and to inhibit scrambling between the different amino acid types (Su 2011; Yokoyama 2011).

1.2. Acid sensing ion channels (ASIC)

1.2.1. General properties of ASIC channels

ASICs (Acid Sensing Ion Channels) belong to the epithelial sodium channel/degenerin (ENaC/DEG) superfamily of cation channels. ASICs are ligand gated and voltage independent ion channels that are primarily expressed in the peripheral and central nervous system of vertebrates. ASICs are involved in several physiological functions. They are involved in sensory perception like nociception, taste, mechanosensation and pain. In the central nervous system ASICs are found to be involved in synaptic plasticity, learning and memory, and specific behaviour like fear conditioning (Baconguis 2012; Dawson 2012).

The ASIC family comprises four genes leading to six different proteins: ASIC1a, ASIC1b, ASIC2a, ASIC2b, ASIC3 and ASIC4. ASIC1a and ASIC1b as well as ASIC2a and ASIC2b are different splice variants of ASIC1 and ASIC 2 respectively. These proteins assemble into the active trimeric form, whereby they are able to form different heterotrimers. In addition ASIC1a, ASIC1b, ASIC2a and ASIC3 form stable and active homotrimers. The possibility to form homo- and heterotrimers under native conditions, leads to many different complexes with a variety of biophysical properties (Baconguis 2014).

ASIC isoforms are expressed in many tissues, but dominantly present in nervous tissue. Neurons innervating skin, heart, gut and muscle show mainly expression of ASIC2 and ASIC3 (Wemmie 2006). In contrast in the central nervous system ASIC1a, ASIC2a and ASIC2b are predominantly expressed. ASIC1a seems to be enriched in some brain regions including the glomerulus of the olfactory bulb, whisker barrel cortex, cingulate cortex, striatum, nucleus accumbens, amygdala and cerebellar cortex (Wemmie 2003).

1.2.2. Activity of ASIC channels and effect of ligands

ASICs are activated upon exposure to low pH (Krishtal 1980). Acidification of tissue is often triggered by injury conditions like local inflammation, muscle ischemia and stroke (Wemmie 2006). Experiments on cultured neurons showed that a drop below pH 7.2 is enough to activate some ASIC channels, while pH < 6.8 is sufficient for most ASIC channels. The pH dependency is modulated by the oligomer composition and the Ca^{2+} level (Immke 2003). *In vitro*, the activation of ASIC1 is usually triggered by a pH drop from pH 7.5 to pH 4-6 (Krishtal 1980). Upon longer exposure to pH>7.2 ASIC1 changes to a desensitized state and is no longer available for activation by a drop in pH (Dawson 2012).

ASICs are sodium selective ion channels with a preference for Na^+:K^+ ranging from 3:1 to 14:1 depending on the isoform (Kellenberger 2002; Grunder 2015). They exhibit a small conductivity for Ca^{2+}, but are impermeable for larger ions like Rb^+ or Cs^+ (Palmer 1982; Baconguis 2012; Grunder 2015). ASIC1a is selective for Na^+ and Li^+ with a selectivity over K^+ of 4:1. The general biophysical properties as well as gating behavior, electrophysiological properties and ion selectivity are dependent on the composition of the trimer.

ASIC channels are modulated by many endogenous factors including ions (Baron 2001), small molecules (Immke 2001), peptide ligands (Askwith 2000), proteins (Poirot 2004; Gao 2005) and redox reagents (Andrey 2005). It is speculated that these modifiers interact with the big soluble domain of the protein, for it would be surprising if such a big and well structured domain would only sense protons (Wemmie 2006). Besides the endogenous modulators, there are other natural as well as synthetic ligands binding to ASICs and modulating their activity. Amiloride is a general

blocker of the whole ENaC family and therefore also blocking ASIC channels (Ugawa 2002). Other small molecule modulators are non-steroid anti-inflammatory drugs (NSAID) like Ibuprofen and Aspirin, local anesthetics like Lidocaine, the anti malaria drug Chloroquine and other types. Besides these synthetic compounds some natural compounds of vegetal origin showed regulatory effects (Baron 2015).

Peptide toxins from snake, spider and sea anemone (Baron 2015) recently attracted the attention, because they were used in structural studies and are very potent modulators. Members of this family are the toxin MitTx, derived from Texas coral snake (*Micrurus tener tener*) (Bohlen 2011), Mambalgin derived from the Black mamba (*Dendroaspis polylepis polylepis*) (Diochot 2012), Psalmotoxin 1 derived from American tarantula (*Psalmopoeus cambridgei*) (Escoubas 2000) and APETx2 from the sea anemone (*Anthopleura elegantissima*) (Diochot 2004)

1.2.3. General structure of ASIC1a

Chicken ASIC1a has been crystallized by several groups. In all structures a N- and C-terminal truncation was used. The protein was expressed in insect cells and solubilized in DDM. The structure is shown in figure 1 which was asdopted from Jasti et al.

The functional state of ASIC channels in membranes is a trimer. Each monomer comprises two long transmembrane helices and a large, extracellular soluble domain. The extracellular soluble domain is located between the transmembrane helices. The N- and C-terminus have additional small soluble domains located on the cytosolic site (Jasti 2007). ASIC1a forms a chalice like structure with a threefold symmetry axis. This symmetry is not represented in the transmembrane part, where the helices of each monomer adopt a different conformation. In addition the transmembrane helices are longer than usual and lie tilted in the membrane. The helices are strongly coupled to β-strands of the palm domain and some well ordered loops. This connection is thought to play a key role in translating conformational changes in the soluble domain to the transmembrane part. The single subunits have extensive contacts to each other stabilizing the trimeric structure. These interactions are primarily, but not exclusively palm-palm and palm-thumb interactions. The transmembrane domains also have large interaction interfaces contributing to the overall shape and stability of the complex. The extracellular domain is rich in cysteines and contains seven disulphide bonds. The cysteines involved in these covalent bonds are conserved throughout ASIC, ENaC, FaNaCh, and DEG proteins (Jasti 2007). Especially the thumb domain of the soluble part is outstanding, because it

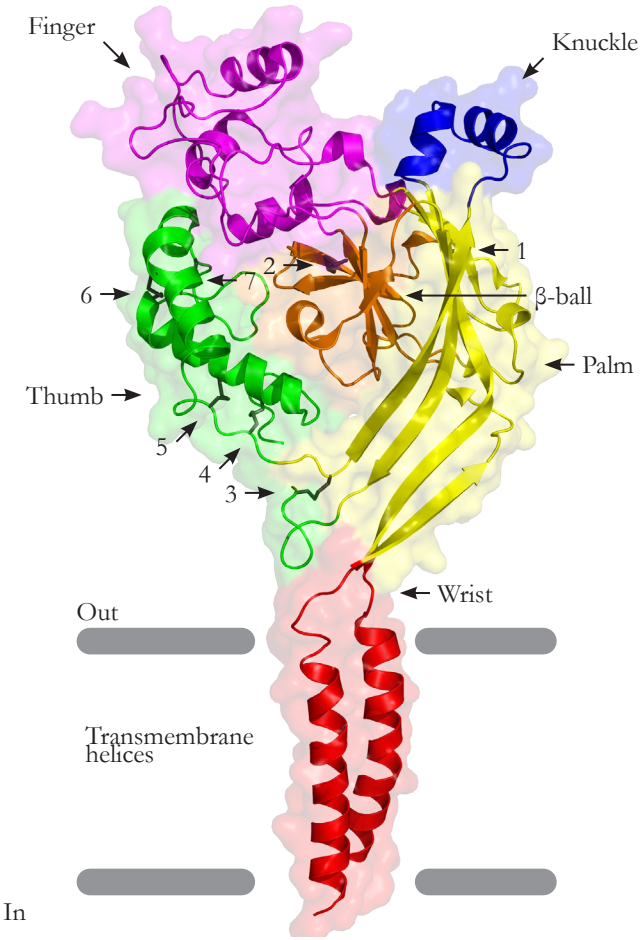

Figure 1: Structure of ASIC1a
Chrystal structure of chicken ASIC1a. Displayed is a monomer from the trimer. The domains are color coded and named according to Jasti 2007 (pdb code: 3S3X) . The seven disulphide bonds are depicted as sticks, colored black and numbered.

contains five disulphide bridges which are linearly oriented (numbers 5-7 in figure 1).

1.2.4. Structures of ASIC1a in complex with peptide toxins

MitTx, the toxin of the Texas coral snake (*Micrurus tener tener*), is a peptide toxin which binds to ASIC1a with a K_D in the nanomolar range. The toxin is a heterodimer of the Tx α subunit with 9.5 kDa and the Tx β subunit with 16.8 kDa. The subunits are stabilized by 10 disulphide bonds, 3 in the Tx α subunit and 7 in the the Tx β subunit. The toxin dimer binds to ASIC1a with a stoichiometry of one toxin dimer per ASIC1a monomer, resulting in a 3:3:3 stoichiometry of Tx α:Tx β:ASIC1a. Each toxin dimer makes contacts to the soluble part of only one ASIC1a monomer resulting in a triskelion like shape, with one toxin molecule reaching out from every ASIC1a monomer. Figure 2 A and C show the side view and the top view respectively.

MitTx induces an open conformation by binding to the wrist, palm and thumb domains suggesting these domains play a major role in gating. The binding of MitTx enlarges the part of the pore that is situated between the transmembrane domains and the wrist domain. This distortion is transferred to the gate part near the GAS motif between the transmembrane domains and opens the gate leading to a channel opening. Importantly the selectivity filter is spatially separated from the gate. While the gate is situated between G436 and G436, the selectivity filter is at the GAS (G443, A444, S445) motif, which is located in the three C-terminal transmembrane helices (Baconguis 2014).

Psalmotoxin 1 (PcTx1) derived from American tarantula (*Psalmopoeus cambridgei*) is a peptide toxin arresting ASIC1a in a closed conformation. PcTx1 only interacts with the homotrimeric form of ASIC1 making it a specific and very potent inhibitor. The binding of PcTx1 depends strongly on a hydrophobic patch as well as a basic cluster on the PcTx1 surface. PcTx1 binds the ASIC1 complex in a 3:3 stoichiometry. The binding site is in the interface between the ASIC1 subunits at the acidic pockets. This location explains how PcTx1 is able to modify the pH dependent gating and why it is specific for ASIC1 homotrimers, for heterotrimers would not display three identical binding sites. While the basic cluster of PcTx1 binds to the acidic pocket on ASIC1, the hydrophobic patch of PcTx1 interacts with helix 5 at the surface of the thumb domain. Binding the thumb and the palm domain, PcTx1 locks the orientation of these two important domains and keeps ASIC1 in a closed desensitized state (Figure 2 B and D).

PcTx1 binding to chicken ASIC1a was analyzed by Dawson et al. who measured a K_D of approximately 2 nM, with slow on and off kinetics (Dawson 2012). In addition to PcTx1, the binding of the small molecule inhibitor A-317567 was tested by SPR. The experiments show that the binding site of the small molecule differs from the binding site of PcTx1, for they can bind at the same time without competing with each other. Although the authors show SPR traces in which they see the binding of the small molecule as well as the PcTx1, they only characterize the binding of PcTx1 in detail. Concerning the small molecule binding the authors only show one trace with an A-317567 concentration of 100 μM. Dubé et al reports IC_{50} values for A-317567 with ASIC1 of 2 μM and for Amiloride with ASIC1 of 30 μM respectively (Dube 2005)

Amiloride, which is a general blocker of ENaCs and ASICs, could be co-crystallized with ASIC1a, shedding light on potential binding sites for small molecules as well as their blocking mechanism. It was found in the co-crystals of ASIC1a and MitTx in the open conformation (Baconguis 2014). The authors assigned some density in the acidic pockets of the extracellular domain to the small molecule, as shown in figure 3 A. The structure reveals two Amiloride molecules binding in the acidic pocket with a head to tail orientation. In addition one molecule per ASIC1a subunit is bound in the transmembrane part making interactions with Asp433 of one subunit and Gln437 of the adjacent subunit. None of these molecules are occluding the pore sug-

gesting that this structure does not reveal the inhibited state. The authors suggest that the Amiloride molecules are binding in the transmembrane part with a subsequent relocation of one molecule at a position where the pore is blocked. They propose that one Amiloride is making contact with its amidino group to the carbonyl of Gly436 which would close the pore. With two Amiloride molecules in the acidic pocket and one molecule in the transmembrane part the complex has a 9:3 stoichiometry.

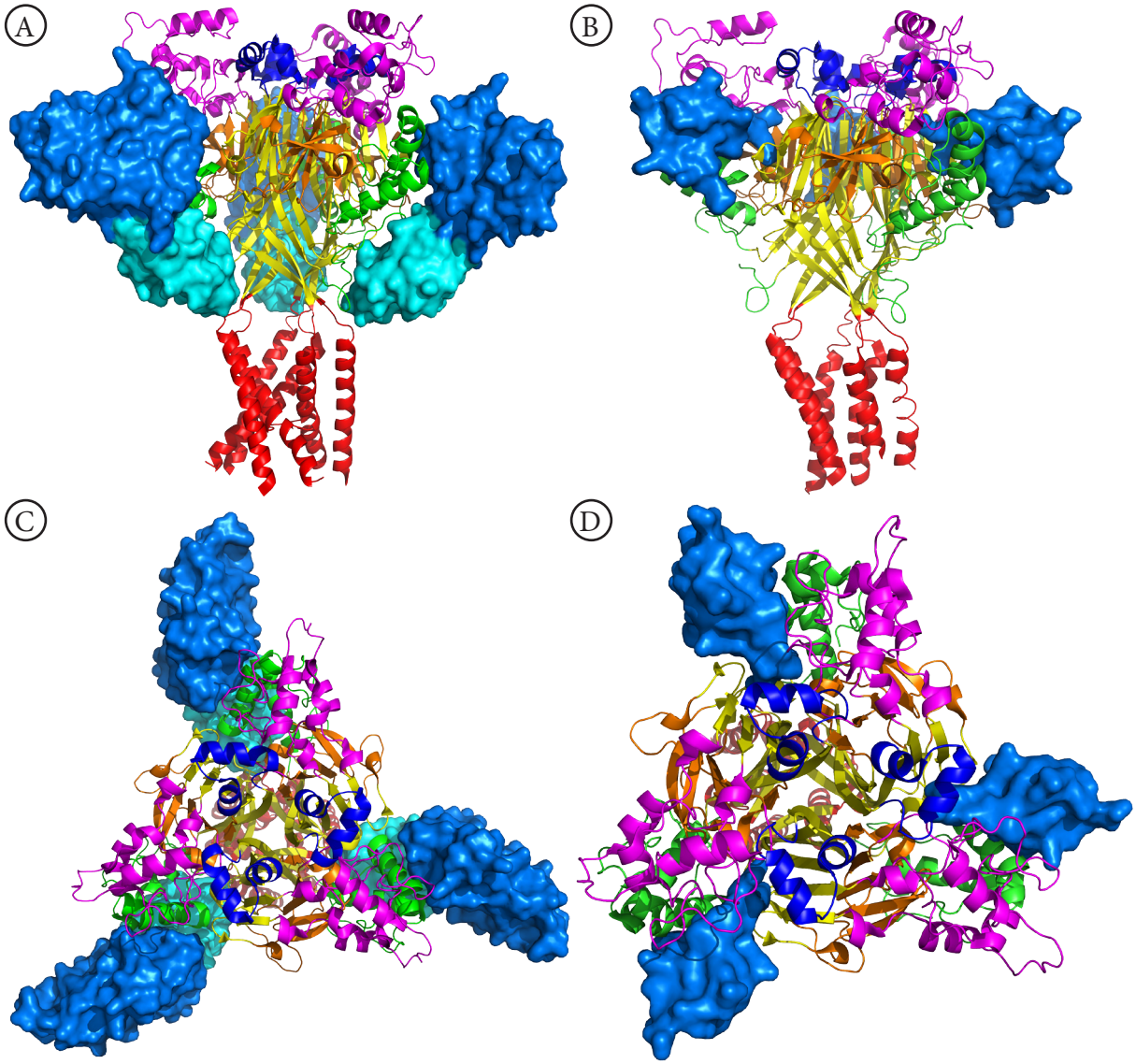

Figure 2: ASIC1a structures with peptide toxins

ASIC1a trimers are depicted as cartoon models and colored according to figure 1. In A and C MitTx is depicted as surface model and colored according to the subunits (pdb code: 3S3X). In B and D PcTx1 is depicted as surface model (pdb code: 4NTX). A and B show the complex in side view, while C and show it from top view. MitTx binds exclusively to the single subunits of ASIC1a, while PcTx1 binds in the interaction interface between the subunits.

1.2.5. Cavities and pores

The proton binding sites are in three acidic pockets on the surface of the soluble domain. Jasti et al propose Asp238-Asp350, Glu239-Asp346, Glu220-Asp408 and Glu80-Glu417 as four pairs of acidic residues that form the proton binding or proton sensing sites (figure 3). These residues are situated on the palm domain as well as between the finger and the thumb domain. This makes sense, for the thumb domain as well as the palm domain are directly linked to the transmembrane part and can transfer conformational changes to this six helix bundle. In addition these sites can easily coordinate Ca^{2+} ions leading to the already described dependency of the activation on the Ca^{2+} concentration (Immke 2003).

The soluble domain of ASIC1a includes a continuous pore throughout the tree fold axis of the protein. The pore has a major constriction in the part enclosed by the transmembrane domains and the wrist domain, while the gate is situated between the transmembrane helices at the GAS motif (Baconguis 2014)

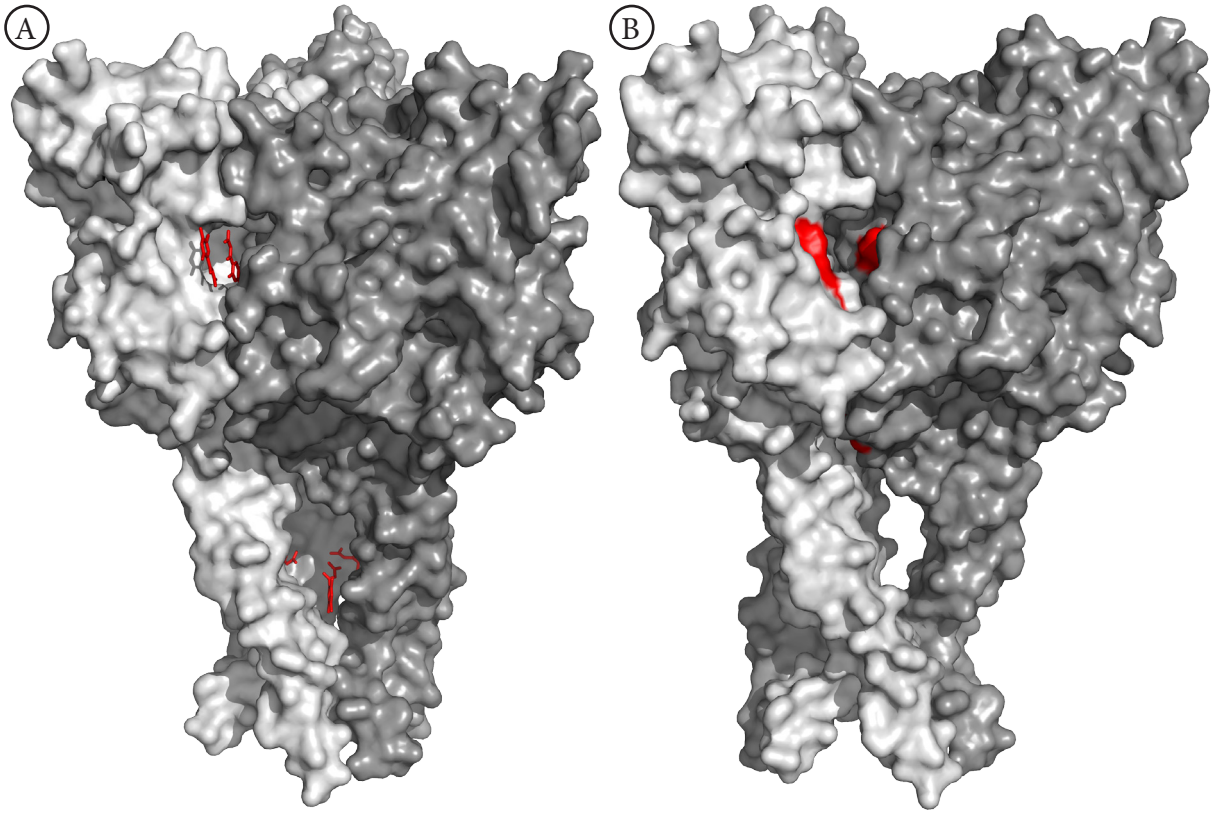

Figure 3: ASIC1a proton sensing site and small molecule binding pockets
Displayed is the trimeric protein complex in surface representation. One subunit is in light grey to highlight the interfaces between the subunits. In A the Amiloride molecules found in the crystal structure are depicted as red stick models. In B the proton sensing site proposed by Jasti et al is colored red. .

1.3. Cyclophilin D as member of the peptidyl-prolyl isomerases

1.3.1. General properties of peptidyl-prolyl isomerases

Peptidyl-prolyl isomerases (PPIases) are a class of enzymes that catalyzes the *cis*/*trans* isomerization of peptidyl-prolyl bonds in proteins and peptides. For a long time their activity was thought to be as chaperone or foldase during co-translational folding (Gething 1992; Galat 1995). It turned out that folding was not the only function of PPIases, as some play a role in virus host interactions (Watashi 2005) and even in signaling processes, as it is the case for Pin1 (Lu 2002) and cyclophilins. Members of the cyclophilin family have been described to be involved in diverse signaling pathways, including mitochondrial apoptosis, RNA splicing and adaptive immunity (Davis 2010).

Cyclophilins are known to bind to the immunosuppressant cyclosporine A (CsA) at nanomolar concentrations, which inhibits their catalytical activity and abolishes target binding (Kallen 1998), with the exception of three family members, which did not show any binding to CsA (Davis 2010). While the human cyclophilin family comprises 17 different isoforms, for most of these isoforms the function and native substrate are unknown (Davis 2010).

1.3.2. The structure of cyclophilin D (CypD)

CypD (also called CypF in mice) belongs to the family of the cyclophilins and is encoded by the *ppif* gene (Wang 2005). It is post translationally imported into mitochondria and therefore possesses a mitochondrial targeting sequence, which is cleaved in the mature protein (Fayaz 2015). The different cyclophilins have a large sequence identity (>50%) between the different isoforms. Given this large degree of identity it is not surprising that they share a very similar fold (Schlatter 2005; Davis 2010). The crystal structure of CypD is shown in figure 4 A. The fold consists of a strongly bended, eight stranded, antiparallel β-sheet and two α-helices that pack against the sheets. In addition, there is a short 3_{10} helix containing the active site residue Trp121 (Kajitani 2008). The active site is a long stretched groove formed by a set of highly structured loops which are well defined in the crystal structure and hold in place by a network of hydrogen bonds. In total the substrate binding groove has a dimension of 10 Å by 15 Å (Davis 2010). It can be subdivided in two individual subpockets. Upon peptide binding, one of these subpockets is occupied by the proline residue, which is isomerized. It will therefore be termed proline pocket and is conserved throughout the cyclophilin family. It contains the catalytic Arg55 and a set of highly conserved residues including Phe60, Met61, Gln63, Ala101, Phe113, Trp121, Leu122, and His126. The other pocket shows some divergence among the family members and is thought to be responsible for substrate specificity (Davis 2010). It will be termed P2 pocket. The P2 pocket is surrounded by a set of gatekeeper residues, modulating the affinity for different peptides, while the pocket itself is quite large and can occupy a large set of different amino acid sidechains. Figure 4 B shows the position of the individual residues on the CypD crystal structure. The active site residues Arg55 and Trp121 are colored in red, the residues forming the proline pocket are highlighted in green and the gatekeeper residues are marked in blue.

Despite the high sequence identity and the common fold, the crystallization properties are quite different. CypD only crystallized after the introduction of the surface mutation K133I, giving crystals with a resolution of 1.6 Å. This mutant was analyzed and behaved basically identical to the wild type form except that the isoelectric point was reduced from 10.2 for the WT to 9.5 for the K144I mutant. The isomerase activity was determined to be around 6 nmol s^{-1}, and the K_D for CsA was around 13 nM (Schlatter 2005). Besides the large active center of the protein, the backside of the cyclophilins is described to be an interaction surface for protein-protein interactions (Davis 2010).

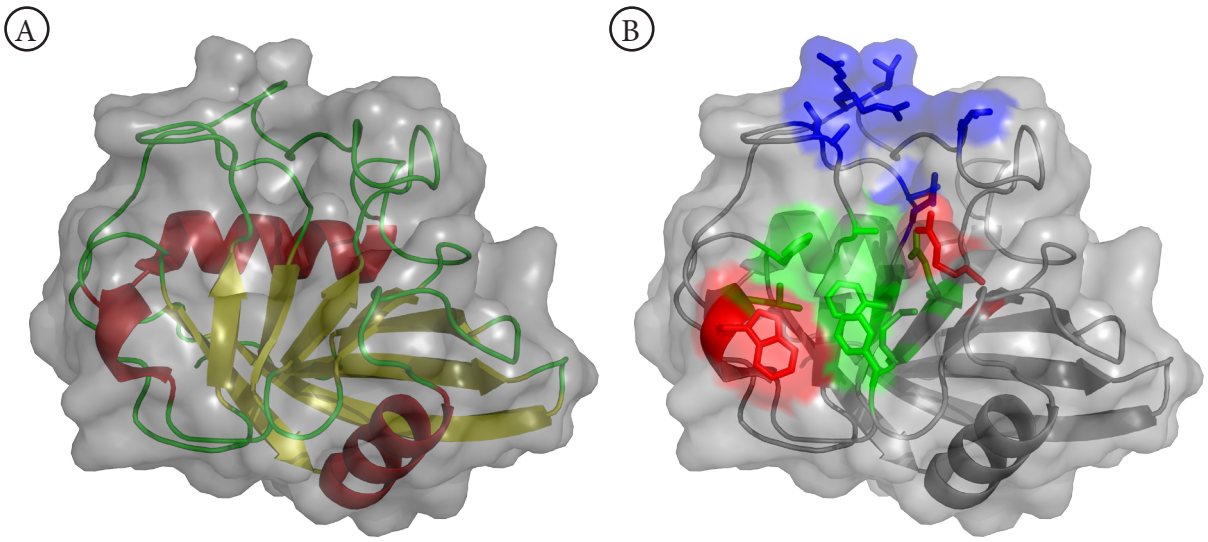

Figure 4: Structure of CypD
(A) Crystal structure of CypD (4J5B). The cartoon representation is colored according to secondary structure elements. α-helices are colored red, β-sheets are colored yellow and loops are colored green. (B) Crystal structure of CypD (4J5B). The active site residues Arg55 and Trp121 are shown in stick representation and colored in red. The residues Phe60, Met61, Gln63, Ala101, Phe113, Leu122, and His126 lining the proline pocket are shown in stick representation and colored in green. The gatekeeper residues Thr73, Ser81, Arg82, Ala103, Thr107, Ser110, and Gln111 lining the P2 pocket are shown in stick representation and colored in blue.

1.3.3. CypD ligands and inhibitors

The most prominent ligand to CypD is cyclosporine A (CsA).It is a tight binding CypD inhibitor and prevents the association of CypD and target proteins by blocking the active site of CypD and thereby inhibiting the opening of the mPTP (Halestrap 1997). CsA is a large cyclic peptide made of 11 amino acids and naturally produced by the fungus *Tolypocladium inflatum* (Svarstad 2000) (Figure 5 A). The Trp121 in the active site is important for CsA binding as only tryptophan or histidine are permissive in this position. The appearance of other residues at this position abolishes CsA binding. Mutation studies demonstrate the crucial role of tryptophan at this position for protein activity (Davis 2010). As shown in figure 6 CsA occupies large parts of the CypD active site making contacts to the proline pocket, Trp121 and the intermediate region between the proline and the P2 pockets. CsA occupies neither the P2 well, nor are there many contacts to the gatekeeper residues. This might explain the unspecific inhibition of the whole cyclophilin family by CsA, since the proline pocket is highly conserved while the P2 pocket may vary between the isoforms. One of the big problems in using CsA as a drug is its ability to inhibit calcineurin and CypA, with the connected immunosuppressive effect as well as its inability to pass the blood-brain barrier. Therefore non immunosuppressive variants like N-Me-Ala-6-cyclosporin A and N-Me-Val-4-cyclosporin were developed, but these still show severe side effects and are still not able to cross the blood-brain barrier (Rao 2014). Clarke et al describe Sanglifehrin A (a macrolide isolated from *Streptomyces sp.*) as an inhibitor for CypD activity while not preventing its binding to target proteins. They concluded, that Sanglifehrin A is not occupying the same site as CsA (Clarke 2002). A co-crystal of cyclophilin A with Sanglifehrin A however showed that it is binding in the active site at the same position as CsA, occupying the proline pocket and reaching out to Trp121 (Kallen 2005). Like CsA, Sanglifehrin A shows immunosuppressive effects and is unable to pass the blood brain barrier. In line with these large inhibitors the decapeptide Amantine from *Amanita phalloides* was found to be a potent inhibitor of CypD and the mPTP (Azzolin 2011). Guo et al screened different quinoxaline derivatives as

potential small molecule inhibitors or as scaffolds for drug development (Guo 2005). These inhibitors showed K_D values in the range of 2 µM – 7 µM and were able to inhibit the catalytic activity of CypD as well as Ca^{2+} dependent swelling of mitochondria.

Apart from the described inhibitors, the protein database contains a lot of co-crystals of CypD with a variety of fragments and small molecules. Among these is the inhibitor CL1, which is published with the structure 4J5B in the protein database and shown in figure 5 B. Important for drug screening experiments is the finding of Schlatter et al. During the crystallization of CypD the DMSO tolerance of the crystal was determined, because co-crystallization with small molecules was planned, which are often dissolved in DMSO. After solving the structure of the soaked crystal to evaluate the damage, Schlatter et al found that the crystal is very tolerant to DMSO, but that at least four DMSO molecules were visible in the structure. Two of these molecules are found to in the active site, making interactions to R55 and N102 (Schlatter 2005). Figure 6 B shows the position of the four DMSO molecules in the structure. It is important to note, that two DMSO molecules directly occupy the active site and one DMSO is making contacts to the P2 pocket.

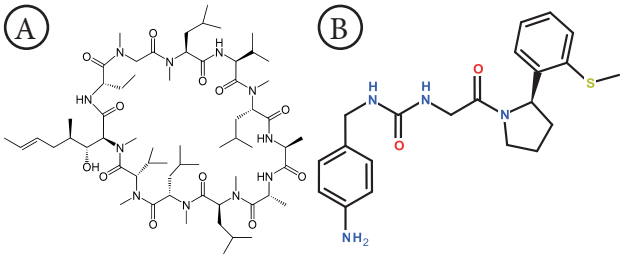

Figure 5: Structure of CsA and CL1
Molecular structures of Cyclosporin A (A) and CL1 (B)

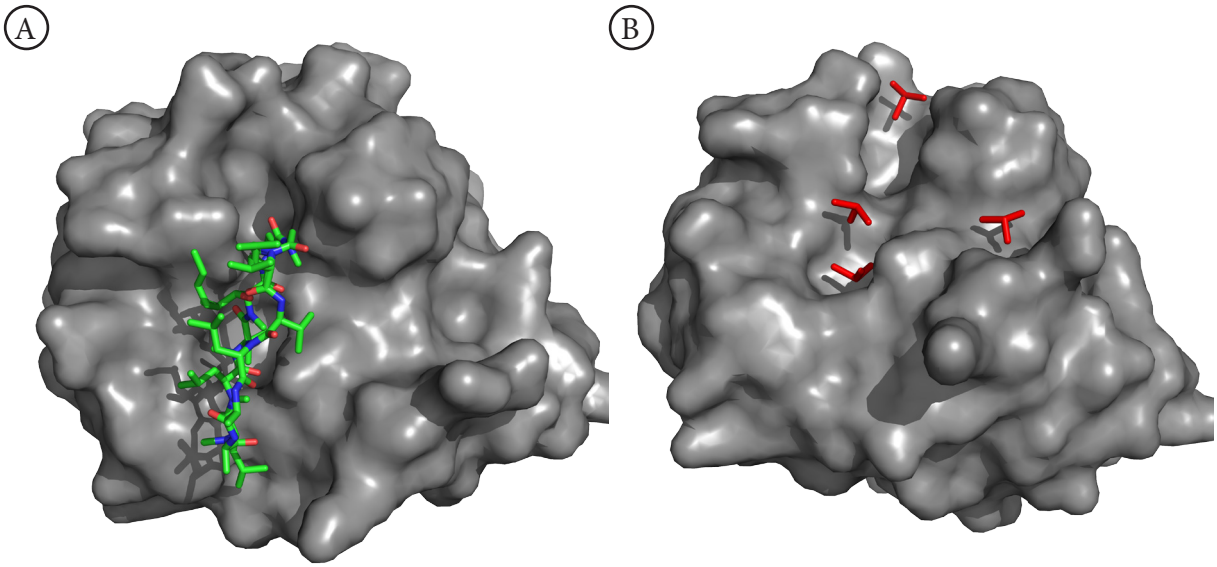

Figure 6: Crystal structures of CypD with cyclosporin A and DMSO
(A) Crystal structure of Cyp in complex with cyclosporin A (2Z6W). CsA occupies the proline pocket and reaches out to Trp121, while the P2 pocket is only poorly occupied and the there are only few contacts to the gatekeeper residues. (B) Crystal structure of Cyp in complex with DMSO (2BIU). Four DMSO molecules are seen in the structure. Two are directly located in the proline pocket and one is situated in the P2 pocket.

1.3.4. The mitochondrial permeability transition pore (mPTP)

The mitochondrial permeability transition (mPT) is defined as a sudden increase in mitochondrial inner membrane permeability for molecules with a mass up to 1.5 kDa (Halestrap 2009). This permeability leads to a loss of membrane potential and massive influx of water, resulting in mitochondrial swelling and subsequent rupture of the organelle. After rupture of the outer mem-

brane, cytochrome C is released followed by induction of apoptosis (Halestrap 2002; Rao 2014). The mPT is enabled by the formation of a pore in the mitochondrial membranes, the so called mitochondrial transition pore (mPTP).

The mPTP is a key component in apoptosis and necrosis. The opening of the mPTP ultimately leads to apoptosis and cell death. The formation of the mPTP is associated with perturbations in the intracellular calcium regulation, phosphate overload, generation of reactive oxygen species (ROS), release of pro apoptotic proteins and deregulation of mitochondrial morphology (Leung 2008; Rao 2014).

1.3.5. Structural components and function of the mPTP

The inner membrane of mitochondria does not contain any porins and the permeability of molecules is only mediated through tightly regulated transporters. The composition of the mPTP is still a controversial issue. Several publications name the voltage-dependent anion channel (VDAC), the adenine nucleotide translocator (ANT), members of the pro and anti-apoptotic Bax-Bcl2 protein family and cyclophilin D (CypD) as key components (Kokoszka 2004; Rao 2014). CypD was identified as a central piece in opening and regulation of the mPTP (Galat 1995). This model proposes that ANT, which is localized in the inner mitochondrial membrane (IMM), forms a tunnel like structure with VDAC in the outer mitochondrial membrane (OMM) upon activation by CypD. This tunnel crosses the IMM and the OMM connecting the mitochondrial matrix with the cytosol (Rao 2014). This tunnel would mediate the permeability of the membranes for small molecules and lead to the already described effects. CypD is usually localized in the mitochondrial matrix and therefore not able to associate with ANT. The association of CypD with ANT is triggered by apoptotic inducers (Du 2008; Rao 2014).

However knockout studies show that none of the named proteins is essential for mPTP formation, although some properties of the pore change dependent on the respective knockout. The adenine nucleotide transporter (ANT) exchanges mitochondrial ATP for cytosolic ADP and is therefore controlling the cell energy level (Kokoszka 2004). With knockout studies Kokoszka et al. showed that cells lacking the major isoforms of ANT can still undergo the mPT, suggesting that the mPTP can be formed without ANT. Nevertheless around threefold more Ca^{2+} than usual is needed to activate the mPTP in absence of ANT and the mPTP is no longer susceptible to ANT ligands like atractyloside or ADP. The authors conclude that ANT is a non-essential component of the mPTP, but does contribute to its regulation (Kokoszka 2004). Interestingly the mPTP without ANT is still sensitive to CsA suggesting that CypD is still involved in mPTP opening. It has to be noted that the experiments were performed with knockout versions of ANT1 and ANT2 but ANT4 was still active and could possibly take the place in the mPTP (Leung 2008).

The voltage dependent channel VDAC was supposed to be part of the complex, because its electrophysiological properties are very similar to those observed during mPT. In addition VDAC is regulated by NADH, Ca^{2+} or glutamate, which are also regulators of the mPTP. To test its role in mPTP assembly and function, Krauskopf et al performed studies with a VDAC1 knockout mice. They found that the basic properties of the mPTP were unaltered. Since mice possess three different isoforms the authors could not rule out that another VDAC isoform is involved in mPTP formation or can take over the position of VDAC1 (Krauskopf 2006).

Leung et al suggest a critical role of the phosphate carrier (PiC) in mPTP formation. They propose that PiC is binding to ANT and CypD in a big complex. This complex would allow for a Ca^{2+} triggered conformational change, which is regulated by CypD and affects ANT and PiC (Leung 2008).

CypD knockout mice do not show a severe phenotype, but they exhibit enhanced anxiety, facil-

itation of avoidance behavior, occurrence of adult-onset obesity (Luvisetto 2008) and a defect in platelet activation and thrombosis (Jobe 2008). Basso et al show that the mPTP can form and can be activated in CypD knockout mice (Basso 2005), but the mPTP opening properties were severely altered. About twice the concentration of Ca^{2+} was needed to activate the mPTP in the absence of CypD. In addition the opening of the pore was no longer influenced by CsA. This suggests that CypD is not essential for the assembly of the mPTP, but it important for the regulation of the Ca^{2+} or oxidative stress dependent opening. (Basso 2005; Basso 2008; Chinopoulos 2012). During mPTP opening CypD was suggested to mask a phosphate binding site (Basso 2008) and to facilitate a Ca^{2+} induced conformational change (Leung 2008).

Besides the already discussed molecular identity of the mPTP, some publications suggest the involvement of the F_1F_O ATP synthase in the mPTP. The data are supported by measurements, showing that the c-subunit can function as a voltage dependent channel (Alavian 2014). They further observed that prolonged exposure to elevated Ca^{2+} levels enlarges the c-ring and unhooks it from the CypD binding site. In addition the properties of the synthase and the c-ring are modulated by phosphate and ADP, fitting the observations made for the mPTP (Alavian 2014). CypD regulates the activity of the F_1F_O ATP synthase by binding to the lateral stalk (Chinopoulos 2012). The association of CypD to the lateral stalk is modulated by phosphate. (Giorgio 2009)

1.3.6. CypD as drug target

Alzheimer's disease (AD), Parkinson's disease (PD), amyotrophic lateral sclerosis (ALS), and Huntington's disease (HD) are the most common human adult-onset neurodegenerative diseases (Rao 2014). The toxic effects of these diseases to the cells are often related to increased mPTP opening and the associated cell death. CypD directly interacts with mitochondrial amyloid-β protein(Aβ) (Rao 2014), which is directly related to Alzheimer's disease (Du 2008). Aβ protein was found to be involved in plaque formation in the late stage of the disease, but also shows cytotoxic effects in the early stages by disrupting mitochondrial functions and thereby enhancing oxidative stress. Inhibition or genetic deletion of CypD significantly reduces the effects of Aβ in mouse models for AD, as these mice show less mitochondrial and neuronal perturbations than wildtype mice (Du 2008). These findings propose CypD inhibition as a valuable target to treat neurodegenerative diseases (Fayaz 2015). Apart from neurodegenerative diseases, CypD dependent mPTP opening is crucial for the cell death connected with ischemia/reperfusion injury affecting the heart (Baines 2005) and brain (Schinzel 2005). CypD knockout or inhibition showed cytoprotective effects in mice models for many organs (Nguyen 2011). CypD inhibition or knockout showed a decreased muscle apoptosis in mice with collagen VI myopathy which was confirmed in human patients using CsA (Merlini 2008). Knockout mice also showed a weaker phenotype in models for muscular dystrophy (Millay 2008) and acute tissue damage (Baines 2005; Basso 2005). Besides these apoptosis related phenomena CypD is involved in the regulation of 362 genes as shown by gene analysis (Elrod 2010).

To target the individual cyclophilin isoforms, the P2 pocket seems to be an attractive drug target, for it might give enough specificity, while the proline pocket is very conserved, making it hard to find a selective binder in respect to all cyclophilin isoforms (Davis 2010).

1.3.7. Selective labeling of proteins to support drug screening with NMR

Structural information of target proteins is crucial for the development of high affinity, low molecular weight ligands. Especially fragment based approaches require the exact binding position of the fragment as well as detection of interactions between the small molecule and the protein of interest. This information is routinely gathered by x-ray crystallography. However in some cases

the desired co-crystals do not grow or diffract poorly. This can be due to conformational changes upon ligand binding or if the binding site is not accessible in the crystal lattice. In these cases NMR is a valuable technique to confirm the binding of potential hits and gives information about the binding location, for the measurement is in solution and allows for conformational changes (Shuker 1996). One drawback of NMR techniques is the requirement for a peak assignment to extract the information about the binding position of the ligand. Peak assignment can be quite time consuming and tedious, especially with increasing protein size or when membrane proteins are used (Weigelt 2002). To achieve a fast backbone assignment, which is necessary for the data analysis, selective labeling schemes have been developed and used (Weigelt 2002; Parker 2004; Wu 2006; Gossert 2011). These labeling schemes have the advantage to reduce signal overlap and in some cases allow the direct unambiguous assignment of several signals. The different labeling schemes include single amino acid type labeling (Dötsch 1996), transmembrane segment enhanced labeling (Reckel 2008), triple selective labeling (Löhr 2012), stereoselective labeling (Kainosho 2006) and the use of fluorinated amino acids as probes (Gee 2015). Different labeling schemes have been used to screen protein interaction interfaces (Reese 2003), enable backbone assignment (Vajpai 2008b) or facilitate NMR structure determination (Reckel 2011). Of special interest for this thesis are the studies that used NMR to identify and characterize protein-ligand interactions (Vajpai 2008a; Jahnke 2010; Gee 2015). In this thesis a combination of triple selective labeling (Löhr 2015) and time shared experiments (Löhr 2014) was used to achieve a fast and complete backbone assignment of CypD in complex with an inhibitor. Besides the use of selective labeling for drug screening, it can assist in making membrane proteins accessible for NMR by simplifying the spectra and decreasing signal overlap (Abdine 2011; Löhr 2012).

Combinatorial labeling relies on the fact, that only certain amino acids are labeled in specific positions. Amino acid scrambling, which occurs in cells for many amino acid types, is therefore a big problem as it exchanges isotopically labeled groups between different amino acid types. Cell free expression systems enable numerous sophisticated tools to label any amino acid type or individual residues. The elimination of amino acid degradation or scrambling enzymes such as transaminases by addition of specific inhibitors (Yokoyama 2011) or by chemical modifications (Su 2011) could furthermore significantly improve the subsequent characterization of CF expressed proteins by nuclear magnetic resonance (NMR) spectroscopy. Reduction of the lysate with $NaBH_4$ inactivates all pyridoxal-phosphate dependent enzymes, which are crucial for the non-desired amino acid metabolisms (Su 2011). Labeled and even perdeuterated proteins can be synthesized with nearly no reduction in expression yields. A valuable advantage upon perdeuteration in CF systems is furthermore that the protein amide positions remain protonated resulting in almost ideal samples for many NMR experiments. Such labeling schemes are often hard to achieve by conventional expression in *E. coli* cells due to reduced growth and expression efficiencies in deuterated media. Moreover, proton exchange of protein amide positions is often incomplete and requires partial denaturation in order to make them solvent accessible (Su 2011). Chemical pre-treatments of lysates as well as the use of specific inhibitors furthermore prevents the scrambling of labeled amino groups and stabilizes carbon alpha positions of amino acids in order to prevent back-protonation and to preserve the desired high degree of protein deuteration (Su 2011; Yokoyama 2011). Deuterated or otherwise labeled detergents or lipids can be implemented for the solubilization of CF synthesized membrane proteins without risking contaminations of endogenous lipids (Hein 2014). Labeling approaches are more economical due to the low CF reaction volumes and even highly sophisticated stereo-array isotope labelling schemes are thus feasible as exemplified with proteorhodopsin (Kainosho 2006).

2. Material

2.1. Equipment

Cell-free extract and T7-RNA polymerase preparation	
Cell disruptor	Constant Systems IUL Instruments (Koenigswinter, Germany)
Fermenter, 10 Liter	B. Braun Biotech (Germany)
French pressure cell disruptor	SLM Aminco Instruments (USA)

DNA template preparation and analysis	
Agarose gel electrophoresis system	Peqlab (Erlangen, Germany)
QIAquick gel extraction kit	Qiagen (Hilden, Germany)
Midi/Maxi DNA preparation kit	Macherey-Nagel (Dueren, Germany)
QIAGEN Plasmid Maxi Kit	Qiagen (Hilden, Germany)
QIAquick PCR purification kit	Qiagen (Hilden, Germany)
Thermocycler	Biometra (Goettingen, Germany), Eppendorf (Hamburg, Germany), Roche (Penzberg, Germany)

General equipment	
Autoclave	Integra (Gießen, Deutschland), Gettinge (Rastatt, Germany)
Centrifuge Sorvall Evolution RC	Thermo Scientific (Langenselbold, Germany)
Centrifuge Sorvall RC 5B, C	Thermo Scientific (Langenselbold, Germany)
Cooled table top centrifuge Micro 22R	Hettich (Tuttlingen, Germany)
Incubating shakers	Infors (Bottmingen, Switzerland), Eppendorf (Hamburg, Germany)
MS2 Minishaker	IKA (Staufen, Germany)
NanoDrop 1000	Peqlab (Erlangen, Germany)

Protein expression and analysis	
Dialysis tubes type 27/30, 12 - 14 kDa MWCO	Spectrum Laboratories (Rancho Dominguez, USA)
Immobilon-P PVDF membrane	Millipore (Merck, Darmstadt, Germany)
Lumi Imager F1	Roche (Penzberg, Germany)
Mini-Protein electrophoresis system	Bio-Rad (Muenchen, Germany)
Slide-A-lyzer dialysis cassette, 10 kDa MWCO	Thermo Scientific (Langenselbold, Germany)

Protein expression and analysis	
Waterbath shaker	Eppendorf (Hamburg, Germany)

Protein processing, quality control and functional analysis	
Äkta prime FPLC system	GE Healthcare (Muenchen, Germany)
Äkta purifier FPLC system	GE Healthcare (Muenchen, Germany)
Amicon (10 kDa MWCO)	Millipore (Merck, Darmstadt, Germany)
Bandelin Sonorex Super RK 510	SCHALLTEC (Moerfelden-Walldorf, Germany)
Biacore 3000	GE Healthcare (Muenchen, Germany)
Bio-Beads SM-2	Bio-Rad (Muenchen, Germany)
Centriprep (10 kDa MWCO)	Millipore (Merck, Darmstadt, Germany)
Cobra II Auto gamma	
Columns (Superdex 200 3.2/30, Superdex 200 10/300, Superdex 75 10/300, Q-sepharose)	PerkinElmer (Rodgau, Germany)
GE Healthcare (Muenchen, Germany)	
GeniosPro microplate spectrophotometer	Tecan (Crailsheim, Germany)
Mini-Extruder	Avanti Polar Lipids (Alabaster, USA)
MultiScreen HTS GF/B filter	Millipore (Merck, Darmstadt, Germany)
MultiScreen HTS vacuum filtration	Millipore (Merck, Darmstadt, Germany)
Ni-NTA resin	Qiagen (Hilden, Germany)
PIERCE Monomeric Avidin Agarose	Thermo Scientific (Langenselbold, Germany)
Sepharose 6 FF resin	GE Healthcare (Muenchen, Germany)
Sonifier Labsonic U	B. Braun Biotech (Germany)
Spectrofluorometer, FP-6500	Jasco Labortechnik (Groß-Umstadt, Germany)
Spectrofluorometer, J-180	Jasco Labortechnik (Groß-Umstadt, Germany)
StrepII-Tactin resin	IBA (Goettingen, Germany)
Ultracentrifuges (L-70, Optima TLX, Optima LE-80K)	Beckmann Coulter (Krefeld, Germany)
Ultra-Clear centrifuge tubes	Beckmann Coulter (Krefeld, Germany)

2.2. Reagents and chemicals

General reagents and chemicals	
1,4-Dithiotreitol (DTT)	Carl Roth (Karlsruhe, Germany)
2-Mercaptoethanol/β-Mercaptoethanol	Carl Roth (Karlsruhe, Germany)
Acetyl phosphate lithium potassium salt (ACP)	Sigma-Aldrich (Taufkirchen, Germany)
Adenosine 5'-triphosphate (ATP)	Roche (Penzberg, Germany)
Amino acids for CF expression	Sigma-Aldrich (Taufkirchen, Germany)
Antifoam Y-30 emulsion	Sigma-Aldrich (Taufkirchen, Germany)
Bactotryptone	Carl Roth (Karlsruhe, Germany)
Bovine serum albumin Fraction V	Sigma-Aldrich (Taufkirchen, Germany)
Complete protease inhibitor cocktail	Roche (Penzberg, Germany)

General reagents and chemicals

Cytidine 5'-triphosphate di-sodium salt (CTP)	Sigma-Aldrich (Taufkirchen, Germany)
Desthiobiotin	IBA (Goettingen, Germany)
Dimethylsulfoxide (DMSO)	Carl Roth (Karlsruhe, Germany)
Dipotassium hydrogenphosphate (K2HPO4)	Carl Roth (Karlsruhe, Germany)
Ethidiumbromide (EtBr)	Carl Roth (Karlsruhe, Germany)
Ethylenediaminetetraacetic acid (EDTA)	Carl Roth (Karlsruhe, Germany)
Folinic acid calcium salt	Sigma-Aldrich (Taufkirchen, Germany)
Gene ruler 100bp, 1kb DNA ladder	Fermentas (Thermo Scientific, Langenselbold, Germany)
Glucose monohydrate	Carl Roth (Karlsruhe, Germany)
Glycerol	Carl Roth (Karlsruhe, Germany)
Guanosine 5'-triphosphate di-sodium salt (GTP)	Sigma-Aldrich (Taufkirchen, Germany)
HEPES	Carl Roth (Karlsruhe, Germany)
Imidazole	Carl Roth (Karlsruhe, Germany)
Isopropyl-β-D-thiogalactopyranosid (IPTG)	Carl Roth (Karlsruhe, Germany)
Lactate dehydrogenase	Roche (Penzberg, Germany)
Lithiumchloride (LiCl2)	Carl Roth (Karlsruhe, Germany)
Magnesium acetate tetrahydrate (Mg(oAc)2)	Sigma-Aldrich (Taufkirchen, Germany)
Magnesium chloride hexahydrate (MgCl2)	Sigma-Aldrich (Taufkirchen, Germany)
Natriumazid (NaN3)	Sigma-Aldrich (Taufkirchen, Germany)
Nicotinamide adenine dinucleotide (NAD+)	Roche (Penzberg, Germany)
PEG 35,000/8,000/6,000/1,000	Sigma-Aldrich (Taufkirchen, Germany)
Peptone, tryptic digest	Carl Roth (Karlsruhe, Germany)
Phenylmethylsufonyl fluoride (PMSF)	Sigma-Aldrich (Taufkirchen, Germany)
Phosphoenol pyruvic acid monopotassium salt (PEP)	Sigma-Aldrich (Taufkirchen, Germany)
PIPES	Carl Roth (Karlsruhe, Germany)
Potassium chloride (KCl)	Carl Roth (Karlsruhe, Germany)
Potassium acetate (KoAc)	Sigma-Aldrich (Taufkirchen, Germany)
Potassium dihydrogenphosphate (KH2PO4)	Carl Roth (Karlsruhe, Germany)
Pyruvate kinase (PK)	Roche (Penzberg, Germany)
Restriction enzymes	NEB (Frankfurt, Germany)
RiboLock RNase inhibitor	Fermentas (Thermo Scientific, Langenselbold,
Sodium chloride (NaCl)	Carl Roth (Karlsruhe, Germany)
T4 DNA-ligase	NEB (Frankfurt, Germany)
TCEP	Thermo Scientific (Langenselbold, Germany)
tRNA E.coli MRE 600	Roche (Penzberg, Germany)
Turbo-Pfu DNA polymerase	Stratagene (Waldbronn, Germany)
Uridine 5'-triphosphate tri-sodium salt (UTP)	Sigma-Aldrich (Taufkirchen, Germany)
VentDNA polymerase	NEB (Frankfurt, Germany)
Yeast extract	Carl Roth (Karlsruhe, Germany)

Antibodies

Anti-biotin goat pAb peroxidase conjugate	Calbiochem (Merck, Darmstadt, Germany)
Anti-mouse IgG HRP conjugate from goat	Sigma-Aldrich (Taufkirchen, Germany)
Anti-penta His IgG from mouse	Qiagen (Hilden, Germany)
T7-tag antibody HRP conjugate	Novagen (Merck, Darmstadt, Germany)
Anti-StrepII-tag IgG from mouse	Qiagen (Hilden, Germany)

Detergents

Brij-35, polyoxyethylene-(23)-lauryl-ether	Sigma-Aldrich (Taufkirchen, Germany)
Brij-58, polyoxyethylene-(20)-cetyl-ether	Sigma-Aldrich (Taufkirchen, Germany)
Brij-78, polyoxyethylene-(20)-stearyl-ether	Sigma-Aldrich (Taufkirchen, Germany)
Brij-98, polyoxyethylene-(20)-oleyl-ether	Sigma-Aldrich (Taufkirchen, Germany)
TritonX-100, polyethylene-glycol-P-1,1,3,3-tetramethylbutylphenyl-ether	Sigma-Aldrich (Taufkirchen, Germany)
Cholic acid	Sigma-Aldrich (Taufkirchen, Germany)
Digitonin	Sigma-Aldrich (Taufkirchen, Germany)
CHAPS, 3-[(3-Cholamidopropyl)-dimethylammonio]-1-propansulfonat	Carl Roth (Karlsruhe, Germany)
SDS, sodium-dodecyl-sulfate	Carl Roth (Karlsruhe, Germany)
Sodium cholate	Carl Roth (Karlsruhe, Germany)
Tween-20, polyoxy-ethylene-sorbitan-monolaurate 20	Carl Roth (Karlsruhe, Germany)
DDM, n-dodecyl-β-D-maltoside	Anatrace (Affymetrix, USA)
DM, n-decyl-β-D-maltoside	Anatrace (Affymetrix, USA)
DPC, Fos-12, n-dodecylphosphocholine	Anatrace (Affymetrix, USA)
LMPC, 1-myristoyl-2-hydroxy-sn-glycero-3-[phospho-rac(1-choline)]	Anatrace (Affymetrix, USA)
LMPG, 1-myristoyl-2-hydroxy-sn-glycero-3-[phospho-rac-(1-glycerol)]	Anatrace (Affymetrix, USA)
LPPG, 1-palmitoyl-2-hydroxy-sn-glycero-3-[phospho-rac-(1-glycerol)]	Anatrace (Affymetrix, USA)
DHPC, 1,2-diheptanoyl-sn-glycero-3-phosphocholine	Avanti Polar Lipids (Alabaster, USA)

Lipids

DMPC, 1,2-dimyristoyl-sn-glycero-3-phosphocholine	Avanti Polar Lipids (Alabaster, USA)
DMPG, 1,2-dimyristoyl-sn-glycero-3-phospho-(1'-rac-glycerol)	Avanti Polar Lipids (Alabaster, USA)
DMPS, 1,2-dimyristoyl-sn-glycero-3-phospho-L-serine	Avanti Polar Lipids (Alabaster, USA)
DOPC, 1,2-dioleoyl-sn-glycero-3-phosphocholine	Avanti Polar Lipids (Alabaster, USA)

Lipids	
DOPE, 1,2-dioleoyl-sn-glycero-3-phosphoethanolamine	Avanti Polar Lipids (Alabaster, USA)
DOPG, 1,2-dioleoyl-sn-glycero-3-phospho-(1'-rac-glycerol)	Avanti Polar Lipids (Alabaster, USA)
DOPS, 1,2-dioleoyl-sn-glycero-3-phospho-L-serine	Avanti Polar Lipids (Alabaster, USA)
DPPC, 1,2-dipalmitoyl-sn-glycero-3-phosphocholine	Avanti Polar Lipids (Alabaster, USA)
POPC, 1-palmitoyl-2-oleoyl-sn-glycero-3-phosphocholine	Avanti Polar Lipids (Alabaster, USA)
POPS, 1-palmitoyl-2-oleoyl-sn-glycero-3-phospho-L-serine	Avanti Polar Lipids (Alabaster, USA)
Cholesterol	Sigma-Aldrich (Taufkirchen, Germany)
Asolectin, L-α-phosphatidylcholine from soybean	Sigma-Aldrich (Taufkirchen, Germany)

Proteins and peptides	
Psalmotxin 1 (PcTx1)	Peptanova (Sandhausen, Germany)
chicken ASIC1a 26-463	Proteros (Müchen, Germany)

2.3. Working solutions and media

2.3.1. Media and expression solutions

LB Medium	
Yeast extract	5 gL^{-1}
Peptone	10 gL^{-1}
NaCl	10 gL^{-1}

LB Agar plates	
Yeast extract	5 gL^{-1}
Peptone	10 gL^{-1}
NaCl	10 gL^{-1}
Agar Agar	15gL^{-1}

TB Medium	
Yeast extract	24 gL^{-1}
Peptone	12 gL^{-1}
Glycerol	4 gL^{-1}

SOC Medium	
Yeast extract	5 gL^{-1}
Peptone	20 gL^{-1}
NaCl	0,5 gL^{-1}
KCl	1 M

2xYTPG Medium	
Yeast extract	10 gL^{-1}
Peptone	16 gL^{-1}

2xYTPG Medium	
NaCl	5 gL^{-1}
Glucose	19.8 gL^{-1}
KH2PO4	3gL^{-1}
K2HPO4	6.9gL^{-1}

TFBI buffer	
KCl	100 mM
$MnCl_2$	100 mM
KOAc	30 mM
$CaCl_2$	10 mM
pH 5.8	

TFBI buffer	
MOPS HCl, pH 7	10 mM
KCl	10 mM
$CaCl_2$	75 mM
Glycerol	15% (v/v)

Component	Concentration
Kanamycin 1000x	25 $mgml^{-1}$ kanamycin sulfate in 50% glycerol
Ampicillin 1000x	100 $mgml^{-1}$ sodium ampicillin in 50% ethanol
IPTG 1000x	1 M

2.3.2. Buffers for SDS PAGE

5x SDS sample buffer	
Tris HCl, pH 7	150 mM
SDS	12% (w/v)
Glycerol	30% (v/v)
β-Mercaptoethanol	6 % (v/v)
Coomassie G250	0.05% (w/v)

4x SDS sample buffer with Urea	
Tris HCl, pH 6.8	100 mM
Urea	8 M
SDS	20% (w/v)
Glycerol	15% (v/v)
β-Mercaptoethanol	6 % (v/v)
Bromphenoleblue	0.12% (w/v)

Anode buffer	
Tris HCl, pH 8.9	1 M

Cathode Buffer	
Tris HCl, pH 8.25	1 M
Tricine	1 M
SDS	0.1% (w/v)

APS	
APS	10% (w/v)

Tricine gel buffer (3x)	
Tricine, pH 8.45	3 M
SDS	0.3% (w/v)

2.3.3. Buffers for Western Blot analysis and Comassie staining

Transfer buffer	
Tris	25 mM
Glycine	192 mM
Methanol	15% (v/v)
ph self-adjusts to 8.36	

TBS-T	
Tris HCl, pH 7.5	25 mM
NaCl	150 mM
Tween-20	0.05% (v/v)

ECL 1	
Tris HCl, pH 7.5	100 mM
Luminol	2.9 mM
p-cumaric acid	0.4% (w/v)

ECL 2	
Tris HCl, pH 7.5	100 mM
H_2O_2	0.06% (v/v)

Fixing solution	
Ethanol	50% (v/v)
Acetic acid	10% (v/v)

Colloidal staining soliution	
Aluminium sulfate hydrate	5% (w/v)
Comassie G250	0.02% (w/v)
Ethanol	10% (v/v)
o-phosphoric acid	2% (v/v)

2.3.4. Stock solutions for cell-free expression

Component	**Comments**
Acetyl phosphate (AcP)	1 M, pH 7.0, adjusted with KOH
Amino acid stock	25 mM of each amino acid
RCWMDE mix	16.67 mM Arg, Cys, Trp, Met, Asp, Glu
Complete protease inhibitor (50x)	1 tablet in 1 ml ddH_2O results in 50x stock
Dithiothreitol (DTT)	500 mM
Folinic acid	10 $mgml^{-1}$
HEPES/EDTA buffer (24x)	2.4 M HEPES, 20 mM EDTA adjust to pH 8 with KOH
$Mg(OAc)_2$	1 M
NTP mix (75x)	90 mM ATP, 60 mM GTP, CTP and UTP, adjusted to pH 7 with KOH
Phosphoenolpyruvic acid (PEP)	1.5 M, adjusted to pH 7.0 with KOH
PEG 8000	40% (w/v)
KOAc	4 M
Pyruvate kinase (PK)	10 $mgml^{-1}$
RiboLock RNase inhibitor	40 $U\mu l^{-1}$
NaN_3	10% (w/v)
E.coli tRNA	40 $mgml^{-1}$

S30 buffer A	
Tris Acetate, pH 8.2	10 mM
$Mg(OAc)_2$	14 mM
KCl	60 mM
β-Mercaptoethanol	6 mM

S30 buffer B	
Tris Acetate, pH 8.2	10 mM
$Mg(OAc)_2$	14 mM
KCl	60 mM
Dithiotreit (DTT)	1 mM
PMSF	1 mM

S30 buffer C	
Tris Acetate, pH 8.2	10 mM
$Mg(OAc)_2$	14 mM
KOAC	60 mM
Dithiotreit (DTT)	0.5 mM

2.3.5. Protein purification buffer

IMAC Buffer A	
HEPES, pH 8	50 mM
NaCl	300 mM
β-Mercaptoethanol	20 mM

IMAC Buffer B	
HEPES, pH 8	50 mM
NaCl	100 mM
β-Mercaptoethanol	20 mM
Imidazole	25 mM

IMAC Buffer C	
HEPES, pH 8	50 mM
NaCl	100 mM
β-Mercaptoethanol	20 mM
Imidazole	300 mM

Stripping Buffer	
Tris HCl, pH 8	20 mM
NaCl	500 mM
EDTA	100 mM

Ni-solution	
$NiSO_4$	100 mM

Q sepharose buffer A	
Tris HCl, pH 8	30 mM
NaCl	50 mM
EDTA	1 mM
β-Mercaptoethanol	10 mM
Glycerol	5% (v/v)

Q sepharose buffer B	
Tris HCl, pH 8	30 mM
NaCl	1 M
EDTA	1 mM
β-Mercaptoethanol	10 mM
Glycerol	5% (v/v)

T7 RNAP resuspension buffer	
Tris HCl, pH 8	30 mM
NaCl	1 M
EDTA	10 mM
β-Mercaptoethanol	10 mM
Glycerol	5% (v/v)

Q sepharose buffer B	

T7 RNAP resuspension buffer	
Complete Protease inhibitor	1x

MSP buffer 1	
Tris HCl, pH 8	40 mM
NaCl	300 mM
Triton X-100	1% (v/v)

MSP buffer 2	
Tris HCl, pH 8	40 mM
NaCl	300 mM
Cholic acid	50 mM

MSP buffer 3.1	
Tris HCl, pH 8.9	40 mM
NaCl	300 mM

MSP buffer 3.2	
Tris HCl, pH 8	40 mM
NaCl	300 mM

MSP buffer 4	
Tris HCl, pH 8	40 mM
NaCl	300 mM
Imidazole	50 mM

MSP buffer 5	
Tris HCl, pH 8	40 mM
NaCl	300 mM
Imidazole	300 mM

MSP buffer 6	
Tris HCl, pH 8	40 mM
NaCl	300 mM
Glycerol	10% (v/v)

HBS-N	
HEPES, pH 7.4	10 mM
NaCl	150 mM

2.3.6. SPR buffer

HBS-N	
HEPES, pH 7.4	10 mM
NaCl	150 mM

HBS-EDT	
HEPES, pH 7.4	20 mM
NaCl	150 mM
EDTA	0.1 mM
DTT	1 mM
Tween20	0.05%
(DMSO)	2%

ASIC buffer 1	
Sodium citrate, pH 6.3	20 mM
NaCl	300 mM
(DDM)	0.05%
(CHAPS)	0.05%
(CHS)	0.01%
(DMSO)	2%

ASIC buffer 2	
HEPES, pH 7.5	20 mM
NaCl	300 mM
(DDM)	0.05%
(CHAPS)	0.05%
(CHS)	0.01%
(DMSO)	2%

NMR buffer	
Sodium Phosphate, pH 7	50 mM
DTT	1 mM

3. Methods

3.1. Molecular biological methods

3.1.1. Preparation of chemically competent *E.coli* cells

For preparation of chemically competent *E.coli* cells, the cells of a defined strain were incubated in 3 mL LB medium overnight. The next morning the OD_{600} was determined and fresh LB medium (100 mL) was inoculated with a defined volume of overnight culture to give a final OD_{600} = 0.03. Growth at 37°C was followed to a final OD_{600} of 0.4 – 0.5 before cells were harvested (2,200xg, 10 min, 4° C). Cells were carefully resuspended in 15 mL ice-cold TFBI-buffer (100mM KCl, 100 mM $MnCl_2$, 30 mM KOAc, 10 mM $CaCl_2$, 15% (v/v) glycerol, pH 5.8) and incubated for 1 h on ice. After pelleting the cells again (2,200xg, 10 min, 4° C) the cells were carefully resuspended in 4 ml ice-cold TFBII-buffer (10 mM MOPS HCl, 10 mM KCl, 75 mM $CaCl_2$, 15% (v/v) glycerol, pH 7.0). Aliquots of 50 µL were prepared, flash frozen in liquid nitrogen and stored at -80° C. To determine the transformation competence, the user's manual was used (e.g. OneShot Top 10 competent cells, Life Technologies, Darmstadt, Germany).

3.1.2. Transformation of *E.coli* cells

E. coli strains for protein expression or DNA production are transformed by mixing 50 µl of chemically competent cells with 40 ng - 80 ng of the corresponding plasmid. After a ligation or a quick change 10 µl of the sample are used. The sample is incubated on ice for 5 minutes. Followed by a heat shock at 42°C for 1 minute. The cells are cooled on ice for 5 min and resuspended in 400 µl SOC medium. Afterwards the cells are incubated for 60 minutes at 37°C to develop the corresponding antibiotic resistance. The transformed cells are pelleted by centrifugation at 3000 rpm for 1 minute, resuspended in 100 µl SOC-medium and spread on LB agar with the appropriate antibiotic. The plates are incubated at 37°C overnight. NEB DH-5-alpha competent *E. coli* High Efficiency cells are used for DNA-preparation and molecular cloning, while T7 Express Competent *E. coli* High Efficency (NEB T7) are chosen for protein expression.

3.1.3. Plasmid-DNA preparation

Plasmid DNA extraction was performed according to the manufacturer's protocol using Nucleo Spin® Plasmid Kit (Macherey-Nagel GmbH & Co. KG, Düren) or Plasmid Plus Kits (Qiagen, Hilden). For sequencing and further cloning procedures, DNA is purified from 5 ml *E.coli* cultures. For cell-free expression DNA was isolated from 200 ml cultures using a midi-preparation. NEB DH 5-alpha Competent *E.coli* High Efficiency cells are transformed with the desired plasmid. A single colony is subsequently used to inoculate the appropriate volume of LB medium supplemented with a suitable antibiotic. The *E.coli* culture is incubated overnight at 37°C with constant shaking at 180 rpm.

3.1.4. Polymerase-chain reactions for cloning and tag-variation

Polymerase-chain reaction is a tool for the amplification of double stranded DNA. This in vitro technique is applied in all cloning strategies to generate new DNA-fragments and modified plasmids. PfuUltra HF DNA Polymerase (Stratagene, Agilent Technologies Sales & Services GmbH & Co. KG) is used for the amplification of single genes and for the amplification of whole plasmids, for example during site directed mutagenesis. Table 1 shows the composition of a PCR-reaction. Reactions can be optimized by the addition of 5% DMSO or 50 µM $MgCl_2$.

Table 1: Preparation and procedure of a PCR reaction.
The left side of the table shows the composition of a PCR sample. The right side of the table shows the protocol used to amplify the DNA samples.

Component	Amount
DNA template	40 ng - 80 ng
Primer forward	0.5 µM
Primer reverse	0.5 µM
dNTPs	20 µM
Reaction buffer (10x)	5 µl
Polymerase	1 µl
ddH2O	add to 50 µl

Step	Temp [°C]	duration [s]
1) Denaturation	98	45
2) Denaturation	98	30
3) Annealing	T_m-3	60
4) Elongation	68	120/kb
5) Elongation	68	600
Steps 2) - 4) are repeated for 25 cycles		

3.1.5. Cloning of DNA inserts

Cloning with restriction enzymes was performed as recommended by the manufacturer (NEB, Frankfurt, Germany). 2 µg - 7 µg of template DNA (PCR product or plasmid) were incubated with 10 - 20 U restriction enzyme (each for double digest) in the appropriate 1x NEB-buffer at +37° C for 3 - 5 hrs. 1 µL of restriction sample was analyzed on a 1% (w/v) agarose gel in 1x TAE-buffer (40 mM Tris-Acetate, 1mM EDTA, pH 8.0). The remaining vector was gel purified with QIAquick gel extraction Kit (Qiagen, Hilden). For dephosphorylation of the restricted and purified vector 1 µg - 3 µg of vector was incubated in 20 µL with 1x reaction-buffer and 5 U Antarctic phosphatase (NEB, Frankfurt, Germany) for 30 min at +37° C. Heat inactivation was completed by incubation at 60° C for 20 min followed by centrifugation to remove the denaturized enzyme (16,000xg, 10 min, 4° C). Ligation was achieved by combining 50 ng – 100 ng of vector with the insert in a molar ratio of 1:2 within 20 µL with 10 U T4 DNA-ligase (NEB, Frankfurt, Germany) in 1x ligation-buffer for 1 h at room temperature. Following ligation 10 µL of sample was used to transform chemically competent DH5α cells as described in section 3.1.1.

3.1.6. Insertion and excision of DNA seqences from plasmids

For the insertion of DNA sequences at the C-terminus or the N-terminus of proteins the corresponding sequence is synthesized on a primer annealing to the protein. A second primer is created that anneals on the backbone, right after the position where the sequence should be inserted. In addition both primer contain an idntical restriction site, in most cases for BamHI. In a first PCR step the primers are used to amplify the whole plasmid. THe PCR results in a linear DNA sequence, that contains the gene of interest containing the new DNA sequence as well as the restriction site. This DNA template is digested with the respective restriction enzyme (in most cases BamHI) and DpnI. DpnI digests methylated DNA and therefore removes all template DNA originated from an *E.coli* isolated plasmid. The resulting linear plasmid is religated using T4 DNA-ligase as described in 3.1.5. This method is also suited to remove specific part of the sequence to create truncated genes.

3.1.7. Two-step overlap PCR for tag-variation

The procedure is performed as described by Haberstock et al (Haberstock 2012). Four different primer were needed for the PCR reaction in order to generate a library of tag fragments and a target fragment. Primer 1 (P1): A universal forward primer annealing upstream of the T7 promoter. Primer 2 (P2): Reverse tag-specific primer, for each tag a specific P2 primer is needed. P2 anneals at the ribosome binding site and contains a 5' linker with a specific tag sequence. For the PCR overlap region, protease cleavage sites e.g. for TEV or PreScission protease could be used, allowing the removal of the expression leader after protein expression. Primer 3 (P3): This primer is target gene specific, annealing at the start of the coding sequence and carrying a 5' linker with the PCR overlap region. Primer 4 (P4): A universal reverse primer annealing downstream of the T7 terminator.

First a tag fragment library was produced by PCR using a vector containing the T7 promoter as template (e.g. pET21a(+) Merck, Darmstadt, Germany) and the primer P1 and P2. Second a linear target fragment was produced by PCR with the primer P3 and P4 and with a vector carrying the coding sequence of the target protein under T7 control. All synthesized PCR fragments were purified using either standard PCR purification kits or agarose gel extraction kits (e.g. QIAquick, Qiagen, Hilden, Germany or Jet Sorb, Genomed, Loehne, Germany). Both PCRs were performed in large scale (200 µL) as the products were required for further optimization steps. Annealing temperature for both reactions were optimized in most cases to 50°C - 54°C with the standard PCR program. DNA concentrations were determined using the NanoDrop (Peqlab, Erlangen, Germany) and samples were stored at -20° C before further use.

In the overlap PCR step, linear target fragments were mixed with individual fragments from the tag library in equal molar ratios using 50 ng of gene fragment and corresponding amounts of tag fragments. The overlap PCR was performed with the primer P1 and P4. Annealing temperature was optimized to 52°C with the standard PCR program. The resulting PCR fragments were purified by PCR purification kits (QIAquick, Qiagen, Hilden, Germany) and analyzed for purity on a 1% (w/v) agarose gel. DNA concentrations were determined using the NanoDrop (Peqlab, Erlangen, Germany) and samples were store at -20°C before further use. The purified PCR fragments could be directly added into the CF reaction as templates.

3.1.8. Template design for cell-free expression

High level protein production in the *E.coli* based cell-free expression system is usually directed by standard T7 regulatory sequences. T7 promoter as well as T7 terminator must be present in the DNA template. Suitable vectors containing the T7 promoter sequence include the pET (Merck, Darmstadt, Germany) and pIVEX (Roche, Penzberg, Germany) series. In addition, few further parameters regarding template design should be considered. (I) Purification tags. The presence of small tags at the C-terminal of the target protein is a valuable tool for the detection of expression and for full-length protein purification. Poly(His)6/10-tags or StrepII-tags may be used for protein detection by immune-blotting or for efficient membrane protein purification. (II) Expression monitoring. Fusions with reporter proteins such as sGFP allows the fast monitoring of expression and may accelerate the optimization of the reaction conditions for improved protein target production. (III) Codon usage. In rare cases, cluster of non-frequent codons or the formation of unfavorable secondary structures within the coding sequence may cause amino acid mis-incorporation or premature terminations of the protein product. Such problems should be addressed by expression of synthetic genes. (IV) Expression tags. In most cases, inefficient initiation of translation is the reason for low expression efficiency. This problem is addressed by the tag-variation screen by fusing small tags to the N-terminus of the target protein (Haberstock 2012).

3.1.9. Agarose Gel Electrophoresis

Digested DNA-fragments or PCR-products are separated according to their size on 0.8 % agarose gels. Therefore, 3 g of agarose are dissolved in 375 ml of boiling TAE-buffer. 40 ml of the solution are cooled to 60°C before ethidium bromide is added to a final concentration of 1 $\mu g ml^{-1}$. The gel is inserted into the running chamber (Peqlab Biotechnologie GmbH, Erlangen),which is filled with TAE-buffer. Samples are mixed with loading buffer (Thermo Scientific, Darmstadt) and loaded in the gel. Gel Electrophoresis is performed by applying a constant voltage of 120 V for 30 min to 40 min. DNA in the gel is visualized by UV-light. Bands can be extracted from the gel by purification according to QIAquick® Gel Extraction Kit (Qiagen GmbH, Hilden).

3.1.10. DNA Sequencing

After every cloning procedure, DNA sequences are validated. Therefore, plasmids are prepared according to section 3.1.3. The constructs are sequenced by Seqlab –Sequence Laboratories Göttingen GmbH. Sample and primer concentrations are used as specified by Seqlab.

3.1.11. Photometric determination of DNA-concentrations and purity

DNA concentrations are measured by UV/Vis spectroscopy using a NanoDrop™ 1000 spectrophotometer (Peqlab Biotechnologie GmbH, Erlangen). Therefore, the absorbance of the sample at 260 nm is detected. The concentration is calculated using the extinction coefficient of double stranded DNA at this wavelength, which is 0.020 $\mu g ml^{-1} cm^{-1}$. The absorbance of water or DNA elution buffer at 260 nm is used as a reference value in the measurement. The purity of DNA is estimated by the ratio of absorbances in the UV spectrum. The quotient of the absorbances at 260 nm and 280 nm should be $\geq$ 1,85.

3.1.12. Expression of the membrane scaffold proteins MSP1 and MSP1E3D1

MSP1 and MSP1E3D1 were expressed with an N-terminal 6xHis-tag followed by the TEV cleavage site without any linker regions (MGSSHHHHHHENLYFQG) (Denisov 2004). The MSP1 construct contains the full-length first helix of the membrane scaffold protein, whereas the first helix is truncated (Δ1 - 11, indicated by D1) in the elongated construct (MSP1E3D1). The following basic expression protocol was applied for MSP1 as well as for MSP1E3D1 production.

For expression the MSP expression plasmid was freshly transformed into BL21 Star (DE3) (Invitrogen, Life Technologies, Darmstadt, Germany) and used to inoculate a 150 ml LB overnight culture with kanamycin. The following day, 600 ml sterile TB medium with kanamycin in a 2 L culture flask were inoculated with 50 ml of fresh LB overnight cultures. Cell growth was performed at 37° C, expression was induced with 1 mM IPTG at OD_{600} = 1. Following induction, cells were incubated for 3 h at 37° C. Harvesting was done by centrifugation (6,000xg, 10 min, 4° C). Cell pellets were stored at -20° C until further processing.

3.2. Proteinbiochemistry methods

3.2.1. Photometric determination of Protein-concentrations

Protein concentrations are measured by UV/Vis spectroscopy using a NanoDrop™ 1000 spectrophotometer (Peqlab Biotechnologie GmbH, Erlangen). The UV-light absorbance of the solu-

tion at 280 nm is determined with the spectrometer and used to calculate the protein concentration. The absorbance of the respective buffer at 280 nm is used as a blank value, which is subtracted in the measurement. Protein concentrations are calculated from the absorbance using the law of Lambert-Beer (Swinehart 1962). The protein concentration is obtained through the division of the measured extinction by the pathlength of the light multiplied with the molar extinction coefficient at 280 nm ε_{280}. The value of ε_{280} is calculated by the ProtParam tool on the ExPASy Proteomics Server for each protein (Wilkins 1999).

3.2.2. Tricine SDS-Polyacrylamide gel electrophoresis (SDS-PAGE)

Expressed proteins are separated by their size using denaturating discontinuous SDS polyacrylamide gel electrophoresis (SDS-PAGE) according to Schägger et al. (Schagger 1987; Schagger 2006). This technique enables an adequate resolution especially for smaller proteins. In this method samples are mixed with SDS sample buffer and incubated at RT for 10 minutes. The discontinuous Tricine gel consists of a resolving gel containing 11% polyacrylamide and a stacking gel with only 4% polyacrylamide. The gels are prepared and used in combination with the miniProtean III system (Bio-Rad, Muenchen, Germany). The gel mixtures are prepared and poured between two glass plates provided in the gel system (Table 2). At first, the resolving gel is casted and overlaid with water to generate an even edge. After the gel is completely polymerized, the water is removed and the stacking gel is poured on top of the resolving gel. Finally a comb is placed in the gel chamber, so that samples can be injected. The gels are placed into a running chamber, which is filled with anode buffer. Cathode buffer is poured between two fixed gels, before protein samples in a volume of 5 µl to 15 µl are loaded. To estimate the molecular weight of a protein, 10 µl of a size marker are also injected. The resulting gels are either stained with coomassie or analyzed by Western Blot

Table 2: Preparation and procedure of a SDS PAGE.
The left side of the table shows the composition of a SDS gel. The right side of the table shows the protocol used to separate the samples.

Component	4% stacking gel	11% separation gel	Voltage	Time
30 % (w/v) Polyacrylamid (37,5:1)	0.825 ml	4.4 ml	80 V	20 min
Gelbuffer (3x)	2 ml	4 ml	130 V	55 min
Glycerol 50 % (v/v)	-	1 ml		
ddH2O	3.175 ml	2.6 ml		
APS 10 % (w/v)	50 µl	100 µl		
TEMED	10 µl	10 µl		

3.2.3. T7-RNA polymerase for cell-free expression

The T7-RNA polymerase (T7-RNAP) is one of the most essential and most expensive compounds for the cell-free synthesis of proteins. Although the polymerase is commercial available (Roche, Penzberg, Germany), efficient expression protocols have been established in the past (Schwarz 2007) resulting in high amounts of active T7-RNAP. The T7-RNAP is characterized by a molecular mass of 98 kDa, a pI of 6.77 and is highly dependent on Mg^{2+}-ions as co-factors.

Overexpression of the T7-RNAP in BL21 Star (DE3) (Invitrogen, Life Technologies, Darmstadt, Germany) was achieved from the plasmid pAR1219 carrying ampicillin resistance. An overnight culture was prepared in LB medium completed with ampicillin at 37°C. The following day, 1 L of

TB medium containing ampicillin was inoculated 1:100 (v/v) in a 2 L culture flask with the freshly prepared overnight culture and incubated at 37°C with vigorous shaking to reach an OD_{600} of 0.6 - 0.8. Expression of the T7-RNAP was induced by addition of 1 mM IPTG. After induction cells were further grown for additional 5 hrs at 37°C and finally harvested by centrifugation (4,500xg, 15 min, 4° C). Cell pellets were stored at -80° C before further processing.

The pellet was resuspended in 30 mL T7-RNAP resuspension-buffer per litre expression culture. Cells were disrupted by ultrasonification cycles (3x 60 sec and 3x 45 sec) with equal cooling times in between each run. The cell debris were removed by centrifugation (20,000xg, 30 min, 4°C). The supernatant was subsequently kept on ice and adjusted drop-wise to a final concentration of 2% (w/v) streptomycin sulfate to precipitate DNA. In order to gently mix after each addition of streptomycin sulfate, the mixture was inverted six to eight times. DNA precipitate was removed from the turbid supernatant by a second centrifugation step (20,000xg, 30 min, 4°C). The DNA-free supernatant was subjected to purification by anion exchange chromatography.

The purification of the T7-RNAP was performed at 16°C with an Äkta purifier system (GE Healthcare, Muenchen, Germany). A self-packed fast flow Q-sepharose column with an approximate volume of 75 mL and a pressure limit set to 0.3 MPa was used. Flow rates were set to 2 ml - 4 ml/min. The column was washed and pre-equilibrated with 2 CV H_2O followed by 2 CV of Q sepharose-buffer A. Subsequently, half of the lysate obtained from 1 L expression was loaded onto the column at a flow rate of 2 ml/min by an external pump. The column was washed with Q sepharose-buffer A until a stable baseline was reached. Since the T7-RNAP eluted at very low salt concentrations, the continuous gradient was set to moderate steepness from 50 mM - 500 mM NaCl in 90 min at a flow rate of 4 ml/min using Q-sepharose-buffers A and B. The purification was followed by measurements of the absorbance at 280 nm. The elution fractions were analyzed using SDS-PAGE prior to dialysis and concentration. It is necessary to note that the T7-RNAP did elute widely spread without being highly pure. Best fractions were pooled and dialyzed at 4° C overnight against dialysis-buffer for T7-RNAP (10 mM K_2HPO_4, 10 mM NaCl, 0.5 mM EDTA, 1 mM DTT, pH 8.0). A final concentration of 10% (v/v) glycerol was added to the dialyzed protein solution before concentrating the protein to approximately 1 mg/ml - 4 mg/ml using Amicon filter devices (10 kDa MWCO; Millipore, Merck, Darmstadt, Germany). The T7-RNAP preparation was finally adjusted to 50% (v/v) glycerol and stored at -80°C or at -20°C if in use.

3.2.4. *In vitro* expression of membrane proteins using *E. coli* S30 extracts

Cell-free expression is an established but still developing technique to express membrane proteins outside of living cells and based on cell extract containing most essential compounds for *in vitro* protein production. The expression system used in this work is based on crude extracts from *E.coli*. In this thesis only the continuous-exchange cell-free setup (CECF) was used, the batch setup for high-throughput screening was not applied. CECF expression in the P-CF, D-CF and L-CF mode were performed as previously described (Schwarz 2007; Schneider 2010).

3.2.5. Extract preparation

The extract preparation protocol is similar to published protocols (Zubay 1973), but contains an additional run-off step to reduce the intrinsic mRNA level. As in principle many different *E.coli* cell-lines demonstrated to bear the potential for *in vitro* protein production, only some of them are frequently used. In this work the RNase deficient *E.coli* strain A19 was used as this led to high yield expression. For cell cultivation a 10 L fermenter was used (B. Braun Biotech, Germany), which allows aeration and optimal cell growth to high optical densities. The extract production procedure takes an overall time of approximately 3 days and results in 50 ml - 80 ml crude extract, sufficient

for the expression of up to 300 mg of membrane protein. Thus 100 mL of LB medium were prepared and sterilized by autoclaving. The medium was carefully inoculated with *E.coli* cells of strain A19 from a fresh LB agar plate without antibiotics, as no expression plasmid was introduced into the bacterial cell. The pre-culture was incubated overnight at 37° C with vigorous shaking.

Cell growth for extract preparation is done in 10 L 2xYTPG medium. Thus the medium was prepared without glucose and phosphate buffer and autoclaved in the fermenter. The medium was supplemented with sterile filtrated 10x glucose stock, to give a final concentration of 100 mM, with autoclaved 10x phosphate-buffer and filled up to 10 L with autoclaved MilliQ water. During extract preparation Antifoam Y-30 emulsion (Sigma-Aldrich, Taufkirchen, Germany) was added to reduce foam production. A19 pre-culture was used to inoculate pre-warmed extract medium (37° C, 500 rpm), growth was followed by measuring OD_{600}. When mid-log phase was reached (OD_{600} ~ 4) the bacteria suspension was rapidly cooled within the fermenter by applying an external cooling source. Cooling should not exceed 45 min to avoid extensive cell-division. *E.coli* cells were harvested when reaching 20°C by centrifugation (8,000xg, 20 min, 4° C).

The cell pellet was carefully resuspended in pre-chilled S30-buffer A (300 ml, 4°C) with a glass pistil and centrifuged afterwards (8,000xg, 10 min, 4° C). The washing step was repeated twice. The resulting cell pellet was resuspended in 110% (v/w) of pre-cooled S30-buffer B for cell lysis.

Cells were mechanically lysed using a French press cell disruptor (SLM Aminco Instruments Inc., USA) with a constant pressure of 20,000 psi. The disrupted cells were centrifuged (30,000xg, 30 min, 4° C) to pellet the cell debris. The non-turbid supernatant (ca. 66% - 75% of the supernatant) was collected and subjected to a second centrifugation step as previously described. Only non-turbid extract was kept for following steps. Subsequently, the modified run-off step was performed to remove endogenous mRNA. Therefore, the supernatant was adjusted step by step to a final concentration of 400 mM NaCl and the extract was incubated in a water bath at 42° C for 45 min. This treatment causes some proteins in the extract to precipitate. The cloudy extract was transferred to dialysis tubes (12 - 14 kDa MWCO) and dialyzed against 5 L of pre-cooled S30-buffer C for at least 2 h at 4° C. The buffer was refreshed and dialysis was carried out overnight (> 12 hrs). Following dialysis, the extract was centrifuged again (30,000xg, 30 min, 4° C). The supernatant was immediately aliquoted to appropriate volumes and shock-frozen in liquid nitrogen. The frozen extract was stored at -80° C for several months. Total protein content in the extract was analyzed by the Bradford assay and was found to be 20 mg/ml - 40 mg/ml.

3.2.6. Basic protocol for the continuous-exchange cell-free setup

Analytical scale continuous-exchange cell-free (CECF) reactions are suitable for any kind of screens such as Mg^{2+}-optimization screens, tag-variation screens or ND lipid screens and can be performed in Mini-CECF reactors (Schneider 2010) or in suitable D-Tube dialyzers (Merck, Darmstadt, Germany) with RM volumes of 50 µl - 100 µL. Here the FM is applied to 24-well microplates (Greiner bio-one, Frickenhausen, Germany). If Mini-CECF reactors were used, appropriate dialysis membranes with MWCO 12 - 14 kDa (Roth, Karlsruhe, Germany) were applied to separate RM from FM. In general the RM volume was set to 50 µL with a RM to FM ratio of 1:17 (v/v). The identified optimal reaction parameters could then be scaled up in a 1:1 ratio into preparative scale CECF reactions with RM volumes of several ml by using Maxi-CECF reactors (Schneider 2010). Here a RM to FM ratio of 1:16 (v/v) was applied to the CF expression experiment. CF reactions were incubated for 16 h - 20 h with gentle shaking at 30° C. Analytical scale expressions were always prepared in dublicates to average the results, although variations between the reactions minimized as good as possible.

Optimal concentrations of Mg^{2+}- and K^{+}-ions have to be determined for every S30 extract

batch and for every target construct. For soluble expression in D-CF mode the detergents were solubilized in distilled water (1 - 10% w/v) and stored at -20° C. The detergents were applied in the RM as well as in the FM in concentrations as indicated and replaced a defined volume of water in the pipetting scheme. For further additives (e.g. liposomes, Nanodiscs) the volume of water was reduced in the RM and/or/not in the FM. Table 3 shows a general scheme for a cell free reaction. The according stock solutions are presented in section 2.3.4

Table 3: Composition of a continuous exchange cell free expression.
Concentrations of stock solutions are shown in section 2.3.4

Feeding mix		Reaction mix	
Component	**Final concentration**	**Component**	**Final concentration**
NaN_3	0.05%	NaN_3	0.05%
PEG8000	2%	PEG8000	2%
KOAc	ca 290 mM	KOAc	ca 290 mM
$Mg(OAc)_2$	ca 16 - 24 mM	$Mg(OAc)_2$	ca 16 - 24 mM
HEPES/EDTA	1x	HEPES/EDTA	1x
Complete	1x	Complete	1x
Folinic acid	0.1 mg/ml	Folinic acid	0.1 mg/ml
DTT	2 mM	DTT	2 mM
NTP mix	1x	NTP mix	1x
PEP	30 mM	PEP	30 mM
AcP	20 mM	AcP	20 mM
Amino acids	0.5 mM	Amino acids	0.5 mM
RCWMDE	1 mM	RCWMDE	1 mM
		Pyruvate Kinase	40 µg/ml
		E.coli tRNA	0.5 mg/ml
		T7 RNAP	ca 60 µg/ml
		Ribolock	0.3 U/µl
		Plasmid template	15 µg/ml
S30 buffer C	30% - 40%	S30 extract	30% - 40%

3.2.7. Co-translational biotinylation of CypD

CypD was cloned with a C-terminal Avi tag (GLNDIFEAQKIEWHE) in a pIVEX vector as described in section 3.1.8. The expression was performed using the standard expression protocol except the addition of the plasmid containing BirA and biotin. BirA was cloned in a pet21 vector with a C-terminal His tag (Plasmid #20857 at Addgene). In addition 1mM biotin was added to the feeding and the reaction mix. BirA can also be expressed in E.coli and added as purified protein, but the co expression was used for the SPR experiments. Prior to the protein immobilization on the SA chip, the reaction mix was dialysed in HBS-N with 1 mM DTT to remove the free biotin, which would otherwise saturate the SA chip surface. Alternatively the biotin removal can be done using a desalting column.

3.2.8. Purification of the membrane scaffold proteins MSP1 and MSP1E3D1

Bacterial pellets of 2 L expression were resuspended in 50 ml MSP buffer 1 supplemented with 1 tablet Complete protease inhibitor cocktail (Roche, Penzberg, Germany). Cells were disrupted by ultrasonification (3x 60 sec and 3x 45 sec) with equal cooling times in between each cycle. Centrifugation was performed (30,000xg, 20 min, 4° C) to clarify the lysate. The supernatant was filtered (0.45 µm pore size) prior to further purification steps.

IMAC column (20 ml bed volume, Sepharose 6 FF, GE Healthcare, Muenchen, Germany) was loaded with Ni^{2+}-ions and equilibrated with 5 CV MSP-buffer 1. The filtered supernatant of cell disruption was then loaded onto the column using a peristaltic pump. The column was washed with 5 CV MSP buffer 1, 1 CV MSP buffer 3.1, 5 CV MSP buffer 2, 1 CV MSP buffer 3.1, 5 CV MSP buffer 3 and 5 CV MSP buffer 4. Elution was achieved with MSP buffer 5 in 2 ml fractions. MSP containing fractions, were pooled and immediately set to 10% (v/v) glycerol to prevent precipitation. MSP stocks were dialyzed overnight at 4° C against 5 L of MSP buffer 6 with one buffer exchange after 2 h. MSP concentration was determined by A_{280} using the NanoDrop (Peqlab, Erlangen, Germany) with the molar extinction coefficient A_{280} ε = 26930 $M^{-1}cm^{-1}$ (MSP1) or A_{280} ε = 28420 $M^{-1}cm^{-1}$ (MSP1E3D1) and the molecular weight of M_W = 26.3 kDa (MSP1) or M_W = 31.96 kDa (MSP1E3D1). Stocks of purified MSPs were stored at -80° C and thawed on ice before usage.

3.2.9. TEV cleavage of proteins

The tobacco etch virus (TEV) protease specifically hydrolyzes peptide bonds in a defined position within the protease recognition site (ENLYFQG). The TEV protease was prepared as common stocks from members of the group of Prof. Doetsch (University Frankfurt, Germany). The TEV cleavage of MSP was performed in MSP buffer 6 supplemented with 20 mM β-mercaptoethanol overnight at 4°C with a MSP:TEV molar ratio of 50:1. The cleavage of cell free expressed CypD was performed in HBS-N supplemented with 20 mM β-mercaptoethanol overnight at 4°C with a CypD:TEV molar ratio of 20:1. Following the cleavage IMAC purification was performed to separate the His-tagged TEV and the unprocessed protein molecules from the truncated versions.

3.2.10. Assembly of empty nanodiscs

For the assembly of homogeneous nanodiscs with a defined size, the MSP to lipid ratio needs to be optimized. The ratio depends on the used MSP version and on the used lipid. The experiments were performed with the optimized ratios determined by Roos et al (Roos 2012). Lipid powders were resuspended in water at a final concentrations of 50 mM and solubilized with sodium cholate supported by vortexing or incubating at 37° C in an ultrasonic water bath. The solubilization was completed when the suspension turned clear. Required sodium cholate concentrations for complete solubility were: DMPC – 100 mM; DOPG- 200 mM; DOPC, DMPG, DOPE – 300 mM. Lipids were filtered (pore size 0.45 µm), stocks were stored at -20° C and thawed on ice before usage. The MSP, the lipids and additional sodium cholate are mixed and afterwards the detergent is removed. ND assembly was induced by dialysis (10 kDa MWCO) against a large volume (e.g. 5 liters for a sample to buffer ratio (v/v) of at least 1:1000) of a detergent free buffer for 72 hrs at 4° C. The buffer was exchanged every 24 h to guarantee an efficient detergent removal. The assembly mixture was centrifuged (16,000xg, 20 min, 4° C) and the supernatant was stored on ice until further analysis.

3.2.11. Concentration and storage of empty nanodiscs

For ND concentration Centriprep (Millipore, Merck, Darmstadt, Germany) and Amicon (Millipore, Merck, Darmstadt, Germany) filter devices (10 kDa MWCO) were equilibrated with dialysis buffer. Centripreps and Amicons were operated at 4° C as described in the user's manual. Samples were suspended after each 30 min to reduce the risk of precipitation. At described time points the remaining volume was determined and concentration of MSP1 was determined

Large amounts of ND for cell-free expression experiments were concentrated by the Centriprep method. Following concentration, ND stocks were centrifuged (16,000xg, 10 min, 4° C), the final protein concentration was determined by Uv absorbance. For short time storage (<12 hrs) the ND stocks were incubated on ice. Long time storage (up to month) was achieved by flash freezing in liquid nitrogen and storage at -80°C. Extensive numbers of freeze-thaw cycles were avoided as this would probably destroy the NDs. Thus larger amounts of NDs were aliquoted before freezing in liquid nitrogen. ND stock solutions were thawed on ice before usage.

3.2.12. Post-translational MP/ND complex formation

The post-translational incorporation of MPs into nanodiscs requires extensive optimization if homogeneous samples are required. As the MSP associates with a fixed number of lipids, the MSP to lipid to target protein ratio needs to be properly adjusted for each MSP/lipid/target combination. For post-translational incorporation of MPs into nanodiscs the detergent purified protein was mixed with soluble MSP1 (or MSP1E3D1) and lipids under a defined ratio of MP to MSP to lipid (mol:mol:mol). Lipids were solubilized in sodium cholate and mixed with the detergent solubilized MP and MSP. The concentration of the detergent stabilizing the MP was kept at 2x CMC to avoid MP precipitation . The mixture was incubated for 1 h at 4°C. Detergent was dialyzed out for three days at 4°C against HBS-N buffer with a buffer excess of at least 1:1000 (v/v). Buffer was exchanged two times during dialysis over 72 hrs. After dialysis the samples were centrifuged (16,000xg, 20 min, 4° C) to remove possible aggregates.

For ASIC1 reconstitution the protein was cotranslationally solubilized in Digitoinin. The purified protein was mixed with the lipid and the according MSP. Digitonin solubilized protein was used for this experiment because Digitonin can be removed via dialysis (CMC=0.09%).

3.2.13. Immobilized metal affinity chromatography (IMAC) with Ni^{2+} ions

Immobilized metal affinity chromatography (IMAC) was performed to purify poly His-tagged proteins from CF reactions or from cell lysates. Plasmide templates were designed including His-tags at in general the C-terminus of the polypeptide chain. Hexa-histidine repeats were used for soluble proteins, while deca-histidine repeats were used for MP purification. The purification process bases on the reversible interaction between consecutive histidine side chains and immobilized metal ions (Porath 1988). For the purification of recombinant proteins either Ni-NTA (Qiagen, Hilden, Germany) or self-loaded Sepharose 6 FF (GE Healthcare, Muenchen, Germany) were used. Ion-loading was achieved by washing the resin with at least 10 column volumes (CV) of MilliQ water to remove the storage ethanol, followed by washing with 10 CV of 100 mM $NiSO_4$. Unbound ions were washed out with MilliQ water and IMAC buffer C.

For purification a defined volume of Ni-NTA resin (e.g. 100 µL resin for each 250 µL of RM) was equilibrated with 5 CV IMAC buffer A either containing detergent at detergent-working concentration (when working with detergent solubilized MPs after solubilization of P-CF pellets or after D-CF expression) or without detergents (when working with soluble or ND solubilized MP). Cell free reaction mixtures were diluted 1:10 (v/v) in IMAC buffer A and applied to the resin. Af-

ter binding to the matrix, the resin was washed with 5 CV IMAC buffer A and 5 CV IMAC buffer B. The samples were eluted with 5 CV IMAC buffer C which were collected as fractions of 1 CV each. During the purification of MP stabilized by detergent, the appropriate detergent was added to every buffer. Flow through of binding and washing as well as the elution fractions were usually analyzed on SDS-PAGE, by size exclusion chromatography or by NMR.

3.2.14. Purification of CypD 43-207 for NMR

CypD was purified using IMAC purification. After the purification the protein was digested using TEV protease to remove the N-terminal 6xHis tag. The cleavage was performed over night at 4°C in HBS-N buffer supplemented with 20 mM β-mercaptoethanol in a Slide-A-Lyzer dialysis cassette (10 kDa MWCO, Thermo Scientific). After TEV treatment the protein was applied again to the IMAC purification to remove the TEV protease and the uncleaved CypD. After the second IMAC purification the Flow through and the wash fractions were pooled and dialysed against the NMR buffer usign a dialysis bag (Spectra Por 6-8 kDa MWCO). This dialysis was performed overnight at 4°C with one buffer exchange to remove residual salts from the IMAC. The final protein sample was concentrated using Amicon (Millipore, Merck, Darmstadt, Germany) filter devices (10 kDa MWCO). The filter device was equilibrated with NMR buffer and operated at 4°C according to the user's manual. Samples were mixed after each 10 min to reduce the risk of protein precipitation. The final concentration was determined using the absorbance at 280 nm.

3.2.15. Size exclusion chromatography

Size exclusion chromatography (SEC) analysis of all samples was performed using an Äkta purifier HPLC system (GE Healthcare, Muenchen, Germany). Samples were centrifuged (16,000xg, 10 min, 4° C) to remove aggregates before loading on a column. In most cases a Superdex 200 3.2/30 was used. The Superdex 200 3.2/30 column (GE Healthcare, Muenchen, Germany) was operated with a flow rate of 50 µl/min. Fractions were collected in 100 µl volumes if indicated. Elution was monitored at 280 nm and 260 nm simultaneously. Columns were equilibrated and chromatographic runs were performed with HBS-N buffer which was supplemented with detergent if needed.

3.2.16. SPR experiments

Ligand binding experiments to CypD surfaces

The ligand binding experiments with CypD were performed on a S51 Biacore instrument (GE Healthcare). CypD was expressed in the cell free system using a construct with a C-terminal Avi tag. The biotin ligase BirA was co-expressed with CypD using the basic cell free expression protocol supplemented with 1 mM biotin. After expression the cell free reaction mixture was dialyzed over night in HBS-N buffer with 1 mM DTT in order to remove free biotin from the solution. For immobilization the dialyzed reaction mixture was diluted 200 times with HBS-EDT and injected on a SA chip (flow: 10 µl/min, time: 6 min). The titration was performed using HBS-EDT with 2% DMSO as running buffer and a flow of 30 µl/min. The ligand samples were injected for 150 s with a dissociation time of 300 s. Running buffer was injected as regeneration step. Solvent correction cycles were performed after every ligand titration series. Ligands were injected in a 1:2 dilution series with 10 different ligand concentration and 2 blank injections. The maximum used ligand concentrations are indicated in the corresponding figure captions.

All SPR experiments are double referenced, which means that the signal was referenced with a blank channel and the blank injections were subtracted.

Ligand binding experiments to ASIC1 surfaces

For ligand binding experiments with chicken ASIC1 the immobilization was performed using a NTA chip. The NTA chip was prepared prior to immobilization by injecting 100 mM EDTA (10 µl/min, 3min) followed by 50 µM NiCl2 (10 µl/min, 3min). Afterwards the chip surface was treated with EDC and NHS to prepare the amine coupling procedure. This chip preparation allows to attach the protein to the chip surface using the His tag of the protein and facilitate the covalent coupling. ASIC 1 was diluted in ASIC buffer 1 to a final concentration of 10 µg/ml and injected with a flow of 10 µl/min for 7 or 15 min. This results in high immobilization levels of around 10000 RU. The immobilization procedure can also be performed in ASIC buffer 2, although this results in much lower final surface densities of ca 2500 RU.

The injection series of Psalmotoxin1 was performed on a Biacore 3000 instrument. PcTx1 was titrated in ASIC buffer 1 with or without 2% DMSO as running buffer and a flow of 30 µl/min. The ligand sample was injected for 300 s with a dissociation time of 600 s. Solvent correction cycles were performed after the ligand titration series. PcTx1 was injected in a 1:2 dilution series with 10 different ligand concentration and 1 blank injection. The maximum used ligand concentration was 100 nM.

The concentration series of the small molecule ligands were performed on a Biacore S51 instrument. The according running buffer is indicated in the figure captions. All small molecules were titrated with 2% DMSO added to the running buffer and a flow rate of 30 µl/min. The ligand samples were injected for 300 s with a dissociation time of 300 s. Running buffer was injected as regeneration step. Solvent correction cycles were performed after every ligand titration series. Ligands were injected in a 1:2 dilution series with 10 different ligand concentration and 2 blank injections. The maximum used ligand concentrations are indicated in the corresponding figure captions. The expected answer for a 300 Da compound is approximately 1,25 RU per 1000 RU of immobilized cASIC1a and per binding position of the ligand. The binding of 3 ligands per trimer and a surface desnsity of 5000 RU would therefore result in an expected answer of 19 RU.

All SPR experiments are double referenced, which means that the signal was referenced with a blank channel and the blank injections were subtracted.

Compound characterization was done using a simple 1:1 binding model with a global R_{max} and a constant bulk RI effect if not statet differently. If the binding kinetics could not be resolved by SPR, a steady state analysis was performed. In this case only a K_D value is given and no k_{on} and k_{off} rate constants. All SPR experiments were performed at 25°C.

3.2.17. NMR experiments

All NMR experiments were recorded by Dr. Frank Löhr (Institute for biophysical Chemistry, Frankfurt). Therefore the technical details are only briefly summarized. For NMR measurements CypD was expressed using the cell free system and purified as described in section 3.2.14. For triple selective labeling the according amino acids were used at a final concentration of 0.5 mM. The isotope scrambling was inhibited using O-Carbox-ymethylhydroxylamine hemihydrochloride (AOA) (20 mM final concentration), D-Malic Acid (2.7 mM final concentration) and D-Cycloserine(10 mM final concentration). The final labeled samples were dialyzed in NMR buffer using a dialysis membrane with a MWCO of 10 kDa. Samples were measured in 5 mm sample tubes or 5 mm Shigimi tubes. The used protein concentrations in the experiments ranged from ca 200 µM to ca. 500 µM.

For samples containing CypD and a ligand, the ligands were dissolved in DMSO at a concentration of 100 mM. The amount needed for a final ligand concentration of approximately 700 µM in

the NMR sample was put in a freeze drying machine to remove the DMSO. The resulting powder was directly dissolved in the NMR sample to reach maximum ligand concentration in the sample.

All experiments concerning the determination of the ligand binding positions were recorded on a Bruker Avance 500 MHz spectrometer without a cryo probe at 293 K. All experiments concerning the triple selective labeling are performed on a Bruker Avance 500 MHz spectrometer without a cryo probe at 303 K. This spectrometer was also used for the HNCA, HNCACB and HNCO type experiments. These experiments were performed at 293 K and 303 K. All TOCSY type experiments were recorded on a Bruker Avance 600 MHz spectrometer at 293 K. The HCCH TOCSY was in addition measured at 303 K. NOESY type experiments and HSQC experiments to analyze the field dependent signal splitting were recorded on a Bruker Avance 900 MHz and 950 MHz spectrometer at 293 K. and 303 K, except for the 3D ^{13}C NOESY spectra. The samples of the CypD-CL1 complex were measured using non uniform sampling to reduce the measurement time.

The experiments were recorded with the standard pulse sequences or the published sequences in the case of the time shared experiments. Topspin (Bruker, Karlsruhe, Germany) was used for data acquisition and processing. SPARKY (Goddard and Kneller, SPARKY 3) was used for spectra analysis.

4. Results

4.1. Nanodisc formation

MSP was purified as described in the methods section. The purification procedure includes 4 different washing steps. First of all it is important to use the dertgent Triton X-100 during cell lysis, because MSP associates with membranes and would be removed with the residual membrane fragments and cell debris during the centrifugation step. Triton X-100 weakens this interaction and even dissolves most of the lipids leading to soluble MSP in the supernatant. After binding to the Ni matrix, the MSP is first washed with a high salt buffer containing Triton X-100. During this step the detergent and the high salt are used for washing to reduce the amount of unspecific bound protein, DNA, RNA and lipids that are still attached to the MSP. The second washing buffer contains cholate as detergent to remove as many E.coli lipids as possible. This step is needed to reduce lipid contaminations during the nanodisc assembly. Before the use of MSP buffer 2, buffer 3 is used to adjust the pH value, because cholate is only soluble at pH 8.9. After the detergents a washing step containing 50 mM imidazole is used to further reduce the amount of unspecific bound protein. Figure 7 A shows a SDS PAGE analysis of purified MSP1. The major band at around 25 kDa is the MSP1. There are a few impurities, mainly a band at 14 kDa. The identity of this contamination was not further investigated. If needed the N-terminal His tag of MSP can be removed by

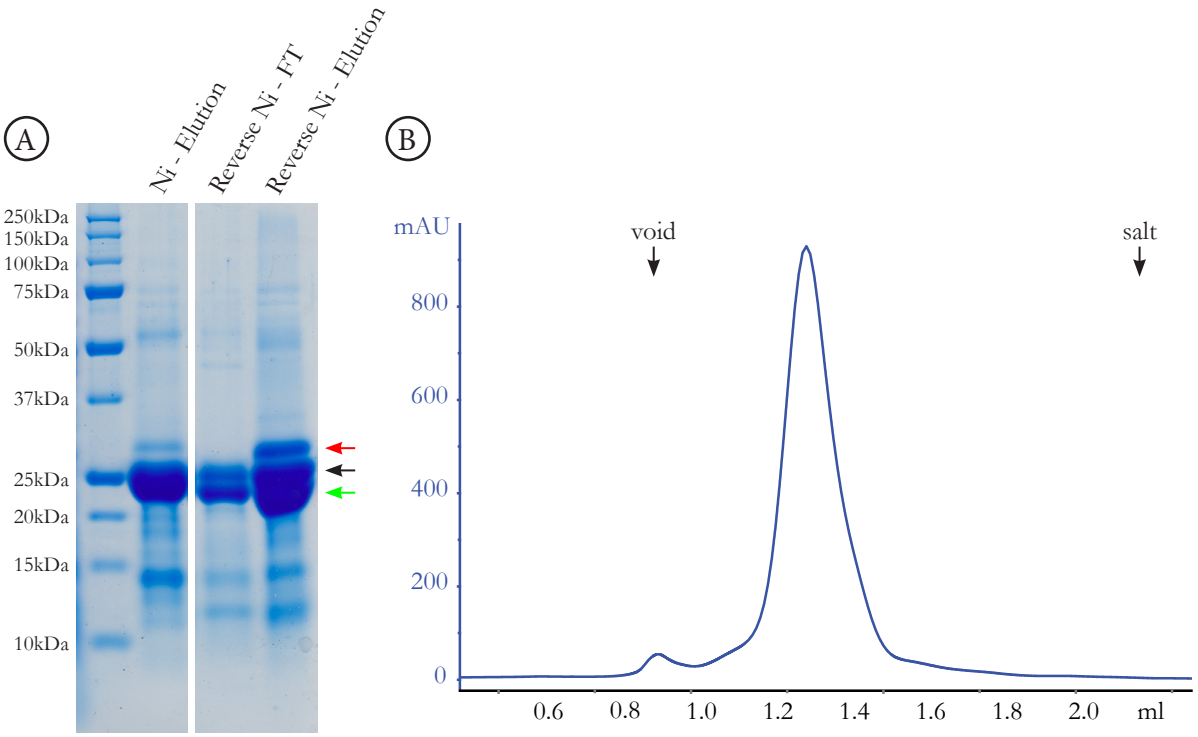

Figure 7: Purification of MSP1 and SEC analysis of empty nanodiscs

(A) MSP1 is first purified by Ni-purification, followed by cleavage of the N-terminal His tag using TEV protease and a final reverse Ni-purification to remove the TEV protease and further impurities. The samples were separated on a 11% Tricine gel. The black arrow indicates the uncleaved MSP1, the green arrow the cleaved MSP1 and the red arrow the TEV protease. (B) The assembled MSP1 DMPG nanodiscs were then analyzed using SEC. Shown is the absorbance at 280 nm. The SEC was performed on a Superdex 200 3.2/30 column. The void volume of the column as well as the salt exchange are labeled accordingly.

TEV digestion. As shown in figure 7 A the cleavage efficiency is poor. Only around 50% of the MSP are cleaved. In addition, the cleaved MSP1 cannot completely be separated from the uncleaved MSP1 using reverse IMAC. Therefore the MSP1 and MSP1E3D1 are mostly used with the His tag to avoid the losses during cleavage. The pure MSP is then mixed with the lipid and detergent to induce nanodisc formation. The optimized MSP:lipid ratios were taken from (Roos 2012). Figure 7 B shows a SEC analysis of the assembled empty nanodiscs. The chromatogram shows a single symmetric elution peak at an elution volume of 1.3 ml. Only a very small shoulder in the void volume is visible. This suggest a homogenous nanodisc population.

4.2. Acid sensing channels (ASIC)

4.2.1. Optimization of ASIC1a cell free expression

The aim of the project was to express human ASIC1a in a cell free expression system to perform binding tests with small molecules to find modulators of the protein function. The human ASIC1a gene was codon optimized for *E.coli* and synthesized by Geneart. The gene was cloned in the pIVEX and pET21 vector with a C-terminal 10x His tag. The expression was best in the pET21 vector system, although the expression level did not yet reach the desired level (<200 µg/ml). Further optimization of the expression yield was reached using tag variation as described by Haberstock et al. (Haberstock 2012). The screen included the AT tag, GFP tag, sHis tag and HA tag. These tags add an AT rich regions at the 5' end of the gene mRNA leading to increased expression levels, probably due to higher initiation rates. The screen was performed in P-CF mode and the resulting protein pellet was analyzed by SDS-PAGE as well as anti-His Western Blot. The P-CF mode is well suited for the optimization of expression yield, because the expressed membrane protein precipitates completely in the absence of a hydrophobic environment. Figure 8 shows the SDS PAGE of the corresponding pellets. AT, GFP and sHis tag show high ASIC1a expression, while the HA tag is less effective. Expression without any N-terminal tag leads to expression yields lower than for the HA tag. Therefore the construct bearing the AT tag was used for further experiments. The resulting construct bears the full length human ASIC1a with a N-terminal AT tag and a C-terminal 10x His tag and will be termed only ASIC1a throughout the text. A quantification of the expression yield is difficult at this stage, for this would require either purification of the protein or specific labeling e.g. incorporation of radioactive amino acids.

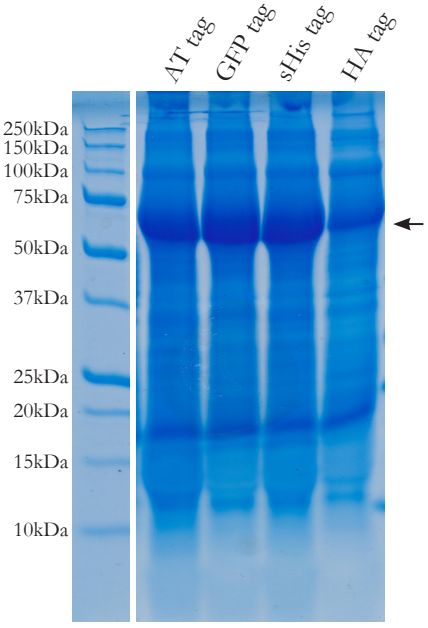

Figure 8: Tagvariation
SDS-PAGE of ASIC1a pellets with different N-terminal tags. The different constructs were expressed in analytical scale and treated equally. The samples were separated on a 11% Tricine gel and stained with coomassie. The black arrow indicates the ASIC1a band. The identity of the band was confirmed by immunoblotting against the C-terminal His tag.

4.2.2. Usage of different detergent environments to support protein folding

After optimization of the expression yield, the protein needs to be expressed in a functional form. Therefore different hydrophobic environments are available, that solubilize the protein and stabilize it in solution. Cell free expression

offers the possibility to solubilize the protein either cotranslational or posttranslational in a suitable hydrophobic environment. The different hydrophobic environments are reviewed by Hein et al. (Hein 2014). The D-CF mode allows for co-translational solubilization in a variety of different detergents and detergent mixtures. Figure 9 shows a detergent screen for ASIC1a including the detergents Brij35, Brij58, Brij98, DDM, and Digitonin. The Brij class of detergents showed a good compatibility with the cell-free expression system and proved successful for a variety of target proteins (Hein 2014). Brij detergents in general have a low CMC and a poor binding to biobeads, which makes it hard to exchange them to another hydrophobic environment. DDM is one of the most used detergents in structure biology and was successful in many crystallization and functional studies. Digitonin is a very mild detergent that is extracted from a natural source making it more

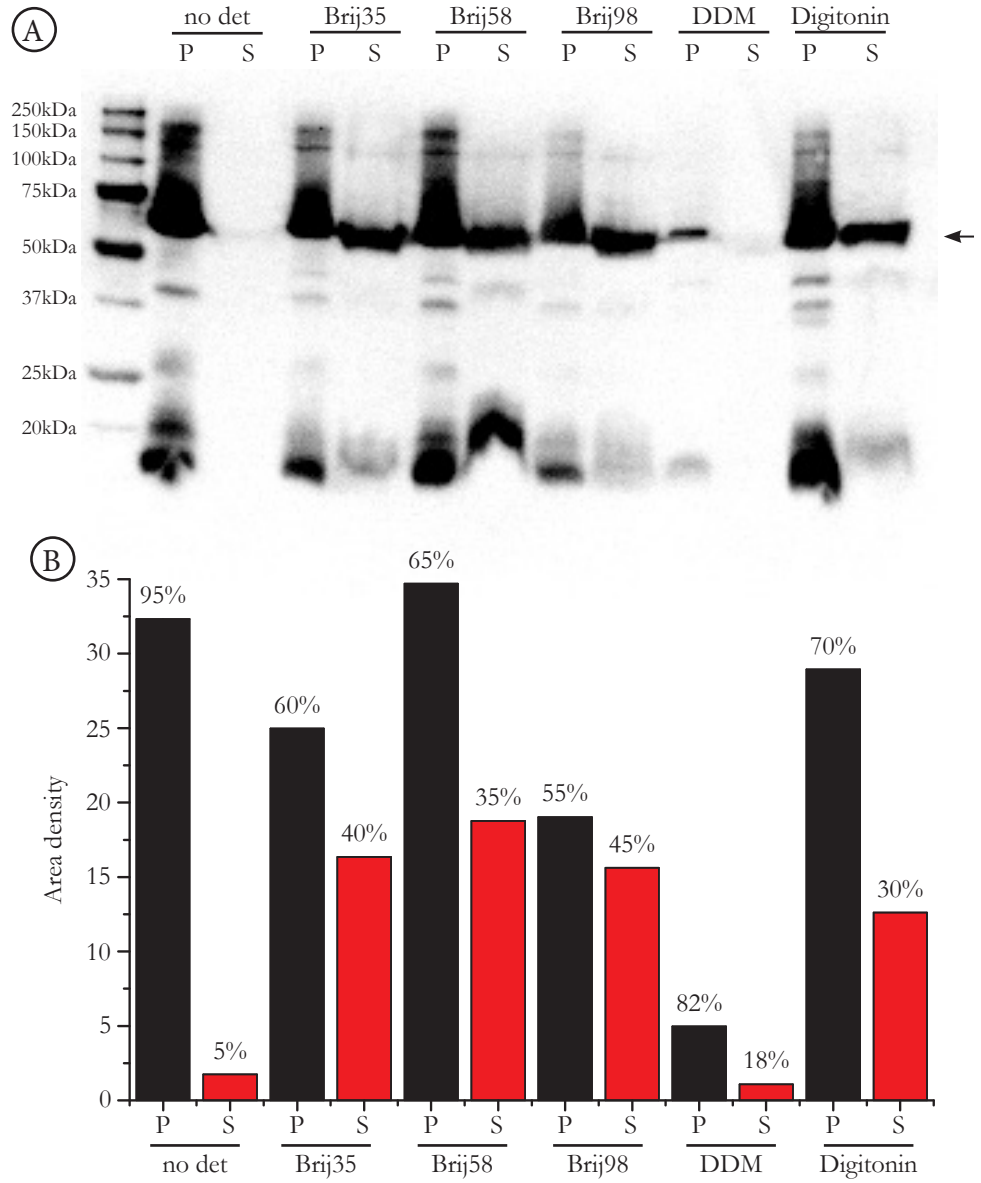

Figure 9: ASIC1a D-CF detergent screen

ASIC1a was expressed in D-CF mode supplemented with different mild detergents. The expressions were done in analytical scale and pellet (P) and supernatant (S) were separated by centrifugation. **A** The samples were analyzed by Western Blot using an antibody directed against the C-terminal His Tag. The black arrow marks the full length ASIC1a band. The ASIC band was quantified in every lane and the resulting area density is displayed in **B**. The quantification can be used to compare the total amounts of soluble full length product. The numbers above the columns indicate the percentage of soluble/ insoluble protein normalized to the total expression.

heterogeneous as the other tested detergents. Digitonin displays in addition a high batch to batch variation and starts precipitating after longer storage. Nevertheless Digitonin shows good compatibility with the cell-free expression system and was successfully used by Reckel et al. (Reckel 2011) in combination with D-CF expression. ASIC1a showed some solubility in the Brij detergents and in Digitonin. Concerning the Brij class of detergents all tested members showed comparable total amounts of soluble ASIC1a. In Brij98 the highest percentage of soluble protein was reached with around 45% of total expressed protein being in the supernatant. However, in DDM only about 18% of the expressed protein was soluble and the total expression yield dropped dramatically. Digitonin was able to solubilize about 30% of the expressed ASIC1a, but the total amount of soluble protein was less than for the Brij detergents. Digitonin and Brij98 were chosen for further analysis, for Brij98 solubilized the highest percentage of ASIC1a, and Digitonin is easier to remove for reconstitution experiments, because its CMC is approximately 10 times higher than the CMC of the Brij detergents.

Following the detergent screen, ASIC1a was expressed in Brij98, purified by IMAC and analyzed by SEC. Figure 10 shows the SEC profile. The profile shows four dominant peaks. A Western Blot analysis of the fractions was performed to test which of the populations contains ASIC1a, for the protein was not completely separated from contaminants. The analysis showed, that the major part of ASIC1a was in the void fraction and therefore seemed to form soluble aggregates. Some ASIC1a could be detected in fractions 5 and 6, belonging to the second peak, but the signal intensity of the band was much weaker than in fraction 1 and could originate from the tailing of the void peak. It seems that although Brij98 kept ASIC1a in solution, the protein did not adopt a correct fold, for it formed soluble aggregates.

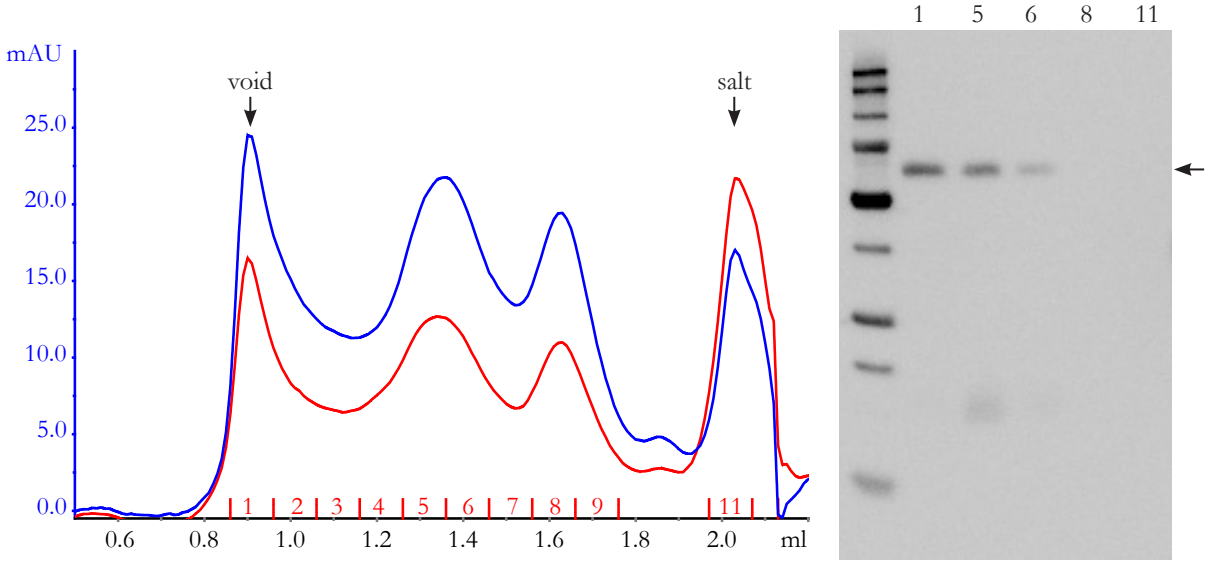

Figure 10: SEC analysis of ASIC1a expressed in Brij98

ASIC1a was expressed in D-CF mode supplemented with Brij98. The sample was purified using IMAC. The quality of the purified sample was assessed using SEC. The left figure shows the SEC run and the right figure shows a Western Blot analysis of the indicated fractions to determine which peak corresponds to ASIC1a. The blue line shows the UV absorbance at 280 nm, the red line the absorbance at 260 nm. The black arrow on the right indicates the ASIC1a full length band. The SEC was performed on a Superdex 200 3.2/30 column. The void volume of the column as well as the salt exchange are labeled accordingly.

To test another class of detergents ASIC1a was expressed in the D-CF mode using Digitonin. The protein was purified by IMAC and analyzed by SDS PAGE as shown in figure 11. The gel shows that the elution sample still contains major impurities, but a strong ASIC1a band is visible. A SEC analysis did not work with this sample, for the used Digitonin was very prone to precipitation and clogged the FPLC system. The good result after purification suggests that Digitonin could

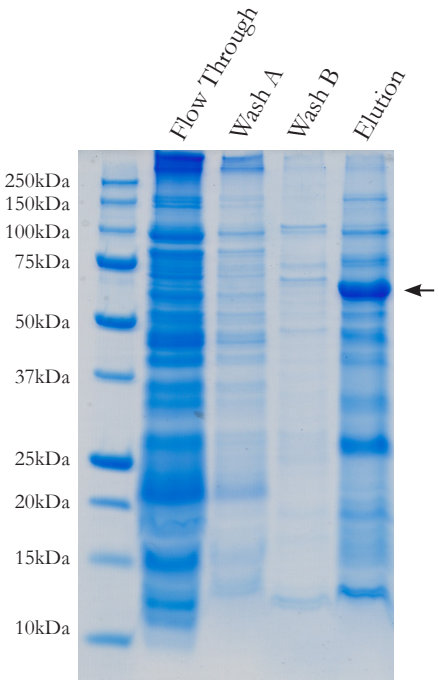

Figure 11: Purification of ASIC1a
SDS-PAGE of ASIC1a IMAC purification. ASIC1a was expressed in D-CF mode supplemented with Digitonin. The supernatant was purified on a Ni-NTA column. The different fractions were analyzed by SDS PAGE. The black arrow indicates the ASIC1a band.

stabilize ASIC1a in a soluble form, but due to the analysis issues using Digitonin, it is not the hydrophobic environment of choice for further experiments. Therefore the hydrophobic environment was changed and ASIC1a was reconstituted into MSP1 DMPG nanodiscs. Three different MSP to lipid ratios were used to get homogeneous samples. The detergent was removed via extensive dialysis. The resulting samples were analyzed by SEC and SDS PAGE. Figure 12 shows an overlay of the different SEC chromatograms on the left side as well as a SDS PAGE of the indicated fractions on the right side. The chromatogram reveals a large void peak and a broad double peak with maxima around 1.3 ml and 1.5 ml. Empty nanodiscs are expected to give a peak around 1.3 ml. The SDS PAGE revealed that nearly all ASIC1a was in the void peak and did not co elute with the MSP, while the MSP eluted in the broad central peak suggesting inhomogeneous, empty nanodiscs. This result shows that ASIC1a was probably already unfolded before the reconstitution or did not survive the long reconstitution time. Extensive dialysis to remove the detergent during reconstitution takes around 3 days time, stressing the protein stability and possibly leading to the formation of soluble aggregates. It is also possible that Digitonin kept the aggregates in solution during

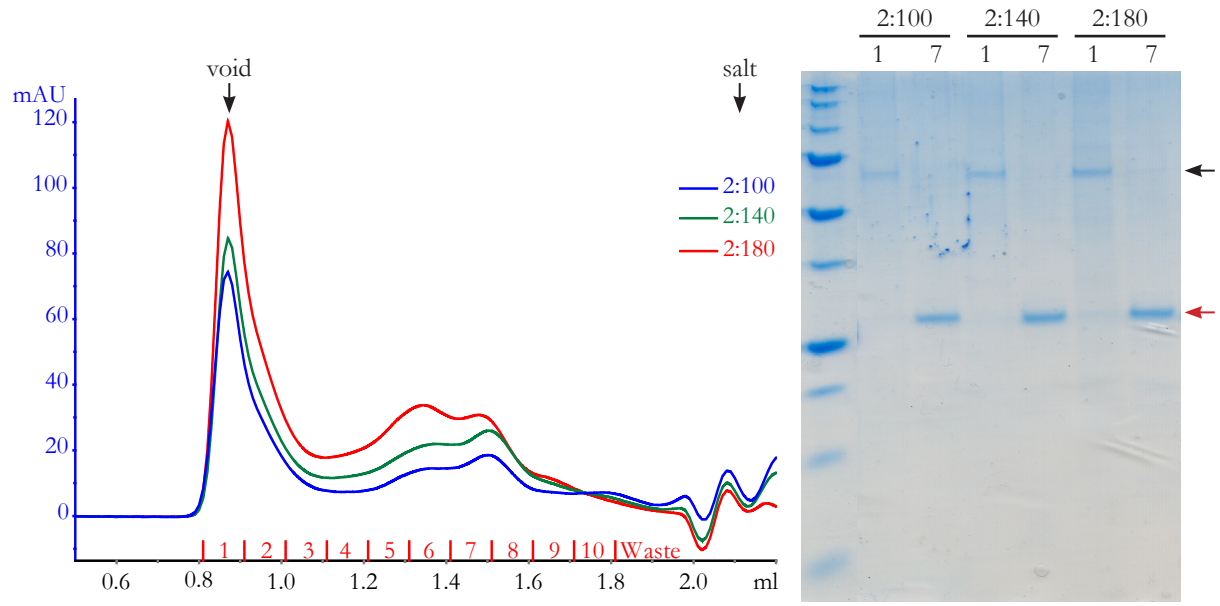

Figure 12: SEC analysis of ASIC1a reconstitution into nanodiscs from a detergent solubilized state
ASIC1a was expressed in D-CF mode supplemented with Digitonin. The sample was purified using IMAC (Figure 11). The detergent solubilized protein was reconstituted into MSP1 DMPG nanodiscs using three different MSP:lipid ratios. The assembled nanodiscs were then analyzed using SEC. The left figure shows the SEC run and the right figure shows a SDS-PAGE of the indicated fractions. The lines in the left figure show the absorbance at 280 nm. The blue line shows sample with a MSP:lipid ratio of 2:100, the green line of 2:140 and the red line of 2:180. The black arrow on the right indicates the ASIC1a full length band, while the red arrow indicated the MSP1 band. The SEC was performed on a Superdex 200 3.2/30 column. The void volume of the column as well as the salt exchange are labeled accordingly.

expression and purification, as it was the case for Brij98.

Since the P-CF and the D-CF mode did not yield well folded ASIC1a, the L-CF mode was used to screen different nanodiscs for co translational insertion. For the screen, two different nanodisc sizes as well as different lipids were used. The screen was analyzed with Western Blot to determine the amount of ASIC1a that resides in the supernatant. The blot is shown in figure 13 and reveals that all used species were able to stabilize ASIC1a in solution. Unfortunately the major amount of ASIC1a is still in the pellet fraction, leaving the impression that the used nanodiscs are not able to stabilize the protein sufficiently.

The presented SEC data shows, that ASIC1a is able to form soluble aggregates under different conditions. This fact makes it necessary to perform a SEC analysis of every sample to check for aggregate formation. SEC analysis is time consuming and not suited to screen a wide range of expression and purification conditions. Therefore a fast screening method is needed to assess the folding of ASIC1a for many conditions. The problem with the setup of such a method is the lack of a positive control. We could not get well folded ASIC1a so far, making it nearly impossible to develop an activity assay for it is always unclear, if the test conditions are wrong or if the used protein is just not active.

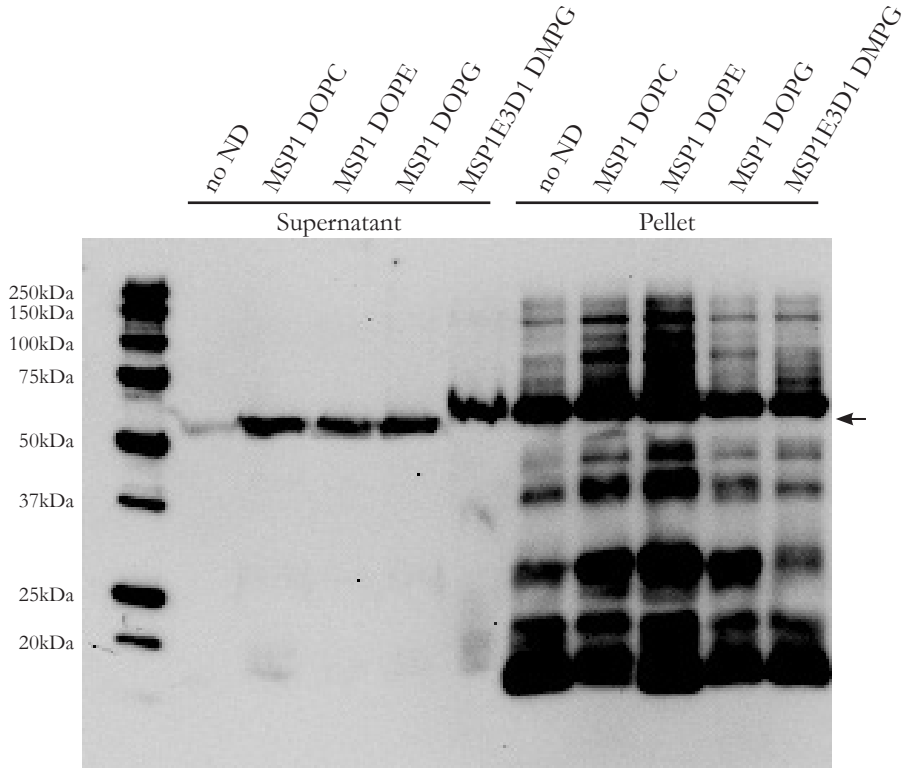

Figure 13: ASIC1a L-CF Nanodisc screen

ASIC1a was expressed in L-CF mode supplemented with different Nanodiscs. The synthetic lipids DOPG, DOPE and DMPG were used for disc assembly. In addition, the two different scaffold proteins MSP1 and MSP1E3D1 were used to sample different disc sizes. The expressions were done in analytical scale and pellet and supernatant were separated by centrifugation. The samples were analyzed by Western Blot using an antibody directed against the C-terminal His Tag. The black arrow marks the full length ASIC1a band. MSP1 and MSP1E3 do not give a signal in the Western Blot although they bear a His tag. For nanodiscs behave like soluble particles inserted or attached ASIC1a is expected to be in the supernatant.

At this point of the project Proteros (München, Germany) provided chicken ASIC1a 26-463 with N-terminal His tag, expressed in insect cells and purified in DDM. This protein was used to

study the binding of PcTx1 and various small molecules by SPR to assess the binding behavior of these ligands and a potential use as activity test.

4.2.3. SPR binding studies with chicken ASIC1a 26-463

The binding studies were performed using cASIC1a provided by Proteros. Dawson et al. analyzed the binding of PcTx1 to cASIC1a by SPR before. Therefore the experiment was repeated to test the integrity of the provided protein as well as the influence of DMSO on the binding, because small molecules usually require the use of 2% DMSO in the running buffer to stay solubilized. cASIC1a was coupled to the chip surface and different concentrations of PcTx1 were injected to the protein surface. The toxin binds strong to cASIC1a with a k_{off} rate that is too slow to reach baseline level after injection in a reasonable amount of time. Therefore regeneration conditions would be useful for multi cycle injections. Dawson et al. circumvented the problem by using single cycle kinetics. Single cycle kinetics suffer from the fact, that most of the k_{off} rate information is gathered during the last dissociation period, making it more error-prone. Every error in the k_{off} rate will affect the K_D determination and the k_{on} rate determination. We decided to use multi cycle kinetics without a regeneration step, because this setup allows for a more accurate fit of the k_{off} and k_{on} rate. To correct for the increasing surface density after every injection the used fit model allowed for a local R_{max}. In addition, a drifting baseline model was used to correct for the dissociation of the complex between the injections. The fitted data are shown in figure 14 A. The fit matches the data very well and yields a k_{on} of $4.25 \cdot 10^6\ M^{-1}s^{-1}$; a k_{off} of $4.31 \cdot 10^{-3}\ s^{-1}$ and a K_D of 1 nM for the sample without DMSO and a k_{on} of $4.1 \cdot 10^6\ M^{-1}s^{-1}$; a k_{off} of $1.31 \cdot 10^{-3}\ s^{-1}$ and a K_D of 0.3 nM for the sample with DMSO. In addition, the cumulated R_{max} matches the estimated value for a 3:3 complex, proving a high rate of binding active cASIC1a on the surface. The addition of DMSO to the running buffer does not abolish the binding of PcTx1 to cASIC1a as shown in figure 14 B. The fitted kinetic parameters are similar and in line with the published data (Dawson 2012).

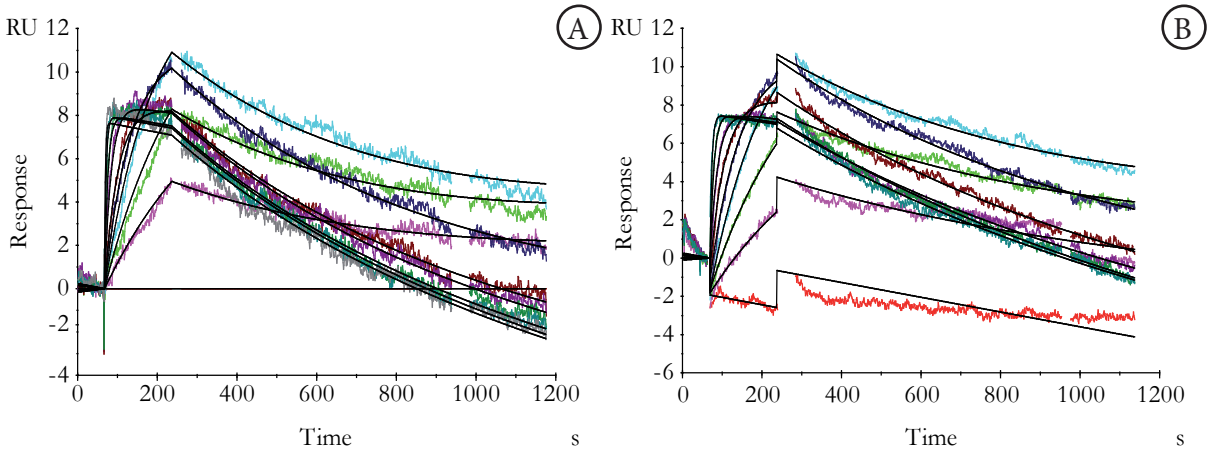

Figure 14: cASIC1a SPR titrations PcTx1

The panels show the SPR traces of titrations with PcTx1. In all experiments chicken ASIC1a in DDM was coupled to a CM5 chip via amine coupling. The experiments were performed on a Biacore 3000 instrument. The compound was injected in a 1:2 dilution series with 10 concentrations and 1 blank injection. In panel A the running buffer contained 20 mM sodium citrate, pH 6.3, 300 mM NaCl, 0.05% DDM, 0.05% CHAPS, 0.01% CHS and in panel B the same with 2% DMSO added. The immobilization level was 642 RU in A and 664 RU in B. The maximal used compound concentration was 100 nM. The shown traces are double referenced, which means that the signal was referenced with a blank channel and the blank injection was subtracted. In addition, artefacts due to buffer mismatch at the beginning and the end of the injection were removed. No regeneration was performed after each injection. The black lines represent a global fit of the data with drifting baseline, local R_{max} and a constant bulk contribution for panel B. The fitted data are k_{on}: $4.25 \cdot 10^6\ M^{-1}s^{-1}$; k_{off}: $4.31 \cdot 10^{-3}\ s^{-1}$; K_D: 1 nM for A; k_{on}: $4.1 \cdot 10^6\ M^{-1}s^{-1}$; k_{off}: $1.31 \cdot 10^{-3}\ s^{-1}$; K_D 0.3 nM for B

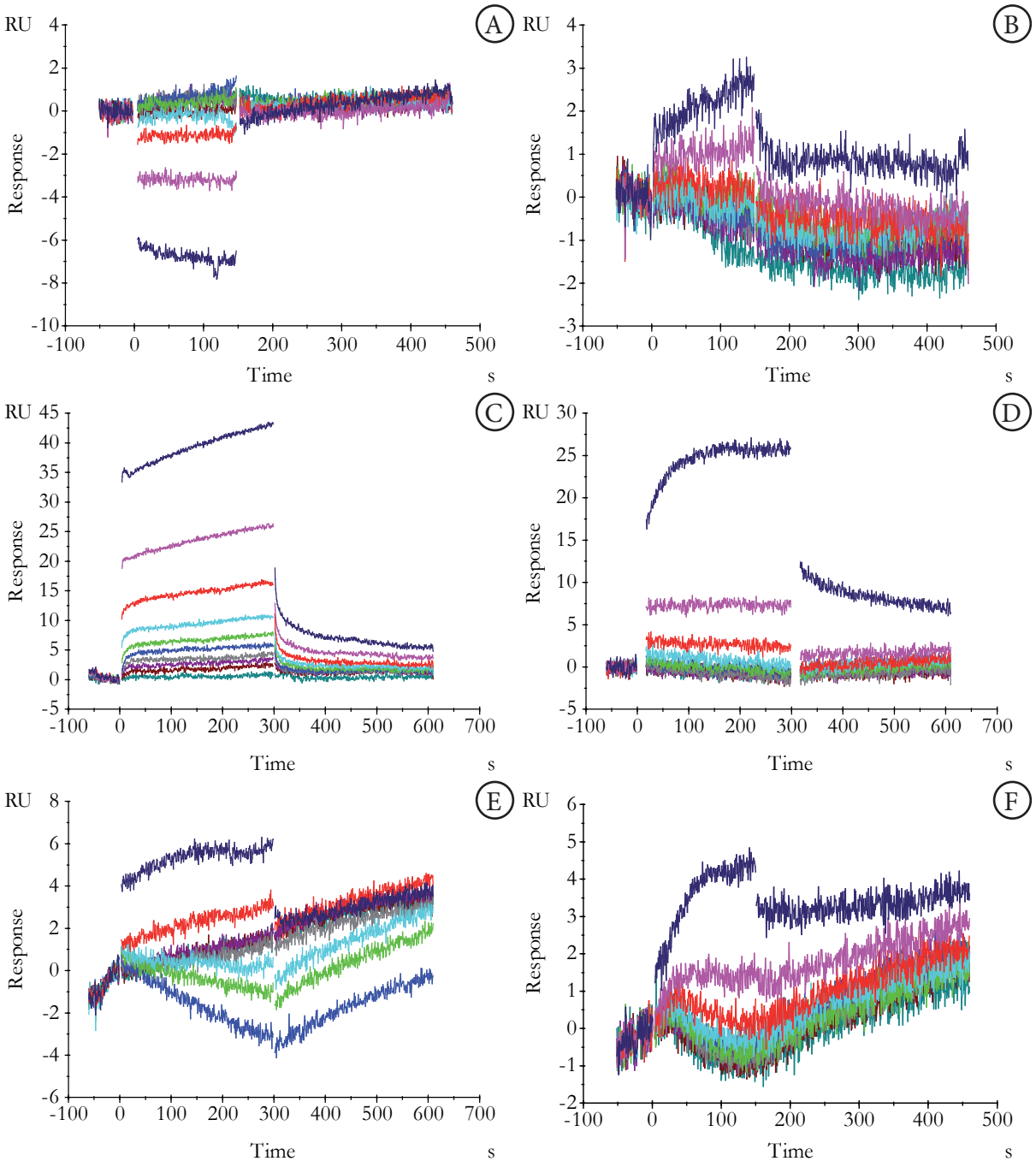

Figure 15: cASIC1a SPR titrations with reference compound 1

The panels show the SPR traces of titrations with reference compound 1. In all experiments chicken ASIC1a in DDM was coupled to a CM5 chip via amine coupling. The experiments were performed on a Biacore S51 instrument. The compound was injected in a 1:2 dilution series with 10 concentrations and 2 blank injections. In panels A, C, E the running buffer contained 20mM sodium citrate, pH6.3, 300 mM NaCl, 2% DMSO as well as 0.05% DDM, 0.05% CHAPS, 0.01% CHS in A; 0.05% DDM in C; 0.05% DDM, 0.05% CHAPS in E. In panels B, D, F the running buffer contained 20mM Hepes, pH7.5, 300 mM NaCl, 2% DMSO as well as 0.05% DDM, 0.05% CHAPS, 0.01% CHS in B; 0.05% DDM in D; 0.05% DDM, 0.05% CHAPS, 10 nM PcTx1 in F. The immobilization levels were 5406 RU for A, 2240 RU for B, 9418 RU for C, 8519 RU for D, 7544 RU for E and 3831 RU for F. The maximal used compound concentration was 10 µM for A,B and D; 100 µM for C; 20 µM for E and F. The shown traces are double referenced, which means that the signal was referenced with a blank channel and the blank injections were subtracted. In addition, artefacts due to buffer mismatch at the beginning and the end of the injection were removed.

Having established immobilization conditions for cASIC1a to the sensor chip surface and shown its binding activity, the binding of small molecules was tested. The titrations were done at two different pH values to force cASIC1a either to the open (pH 6.3) or the closed (pH 7.5) conformation. The titration at different pH values was done to assess if the two states display different binding pockets and if the molecules can force the protein to a certain state or just stabilize one distinct state. Figure 15 shows a compilation of the traces with reference compound 1. The IC_{50} of this compound was determined to be 60 nM - 120 nM in cell based and electrophysiology experiments with human ASIC1a (data not disclosed; personal communication Daniel Schwarz Merck Serono). The traces in figure 15 A, C and E are all done at the same pH with different hydrophobic environments in the running buffer. These traces show fast k_{on} and k_{off} rates that could not be resolved, which is not unusual for small molecules. Although all traces are done with high immobilization levels and compound concentrations at least 100 times above the IC_{50} value, the responses to the injections are very low, except for C. A shows negative signals, which was unexpected and the signal intensity doubles with rising compound concentration. This is a sign for unspecific binding of the compound or a complex binding mode which does not fit a simple 1:1 model. In contrast the signals in C show a positive response, which still doubles with rising compound concentration. E shows binding signals which appear randomly distributed and very small. Therefore they likely are just background signals. As a general trend it seems as if CHAPS suppresses unspecific binding of the compound, because A and E show very low signals while DDM alone (C) seems to display a high unspecific signal. A similar behavior is seen for the samples at pH 7.5, displayed in figure 15 B,D and F. Again the sample without CHAPS shows high responses which look like unspecific binding, while traces B and F show only very low responses. The addition of PcTx1 to the running buffer, to lock the protein in a defined state seems not to promote the binding of reference compound 1 (Figure 15 F). In summary the results do not match a simple 1:1 binding model and have signs of unspecific or no binding of the compound to the protein.

Amiloride is a general blocker of ASICs and other ion channel family members and was therefore chosen as second reference. Amiloride was co crystallized with chicken ASIC1a (Dawson 2012) and should therefore bind the used protein. The results are presented in figure 16. The results are similar to those of reference compund 1, presented in figure 15. The traces in figure 16 A,B and D show only minor signals, and C shows traces that give negative signals with an unusual shape, leading to the conclusion that no compound binding is observed. A broad variety of other small molecules was screened (data not shown), but all of them gave traces similar to those presented in figure 15. Possible reasons for these results and potential solutions are discussed in chapter 5.

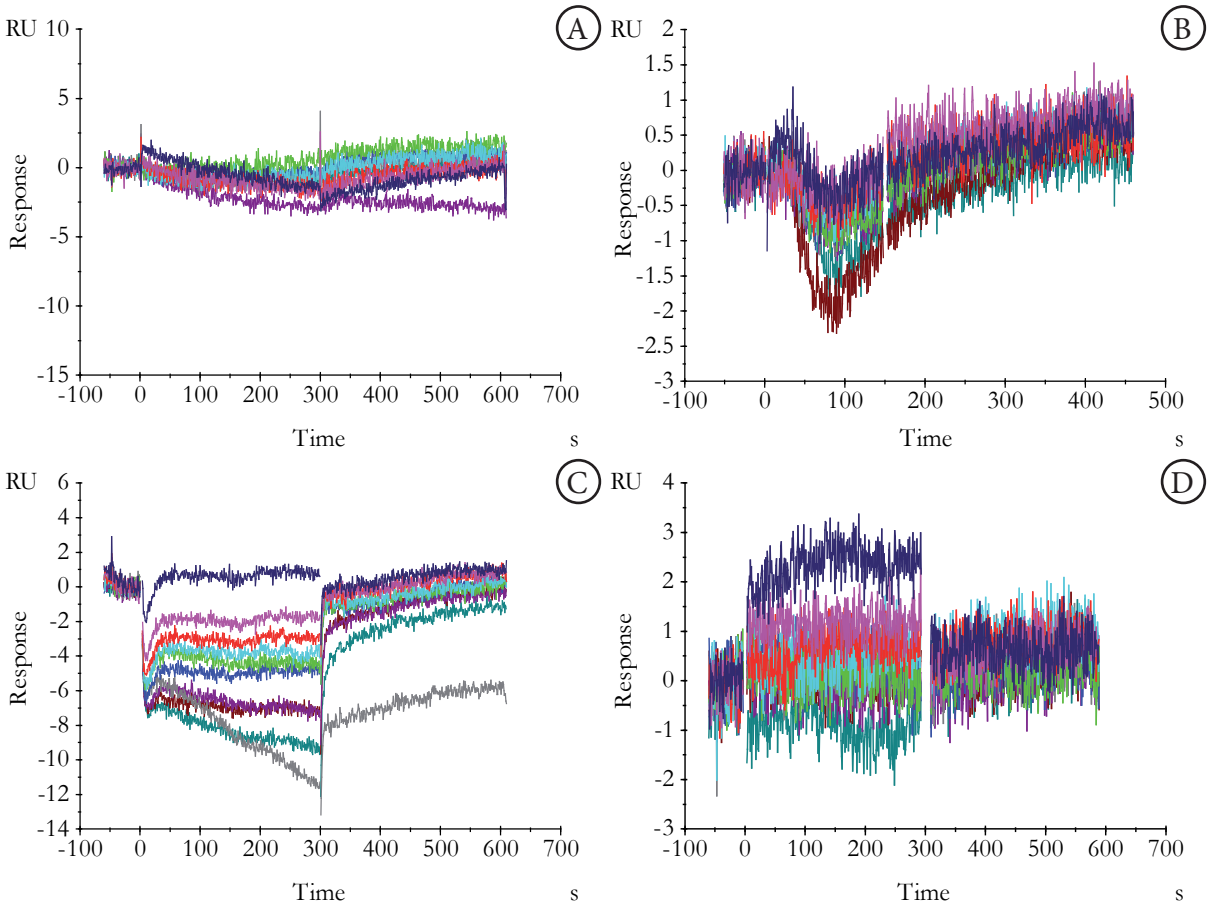

Figure 16: cASIC1a SPR titrations with amiloride

The panels show the SPR traces of titrations with amiloride. In all experiments chicken ASIC1a in DDM was coupled to a CM5 chip via amine coupling. The experiments were performed on a Biacore S51 instrument. The compound was injected in a 1:2 dilution series with 10 concentrations and 2 blank injections. In panels A and C the running buffer contained 20mM sodium citrate, pH6.3, 300 mM NaCl, 2% DMSO as well as 0.05% DDM and 0.05% CHAPS in A; 0.05% DDM in C. In panels B and D the running buffer contained 20mM Hepes, pH7.5, 300 mM NaCl, 2% DMSO as well as 0.05% DDM, 0.05% CHAPS, 10 nM PcTx1 in B; 0.05% DDM in D. The immobilization levels were 7544 RU for A, 3831 RU for B, 9418 RU for C and 8519 RU for D. The maximal used compound concentration was 20 µM for A and B; 100 µM for C; 10 µM for D. The shown traces are double referenced, which means that the signal was referenced with a blank channel and the blank injections were subtracted. In addition, artefacts due to buffer mismatch at the beginning and the end of the injection were removed.

4.3. Cyclophilin D (CypD)

4.3.1. Expression and purification

The aim of this project was the chracterization of small molecule to cyclophilin D (CypD) interaction by various biophysical techniques. All experiments in this section were done with human CypD which will be only named CypD in this thesis. The binding kinetics were assessed with SPR and the binding position was determined using NMR. CypD is described as a drug target (section 1.3.6) for the treatment of a variety of diseases. It would therefore be of great interest, to find a small molecule inhibitor that is selective for CypD over other PPIases and could cross the blood brain barrier to be available for the treatment of neurodegenerative diseases. The expression was performed using a cell free expression system, because it enables a fast and easy expression and bears the potential for specific NMR labeling schemes as described in section 1.3.7 .

The used expression construct did not contain the N-terminal mitochondrial targeting sequence of CypD (amino acid 1-42). CypD 43-207 was cloned in a pIVEX vector with a N-terminal 6x-His tag and a TEV cleavage site. In this thesis the amino acids of CypD are counted as in the crystal structure of Schlatter et al. (2BIU) starting with G2 and ending with S165. The protein was expressed in the cell free reaction system as soluble protein, although approximately 50% of the expressed CypD was insoluble and precipitated. The soluble fraction was purified using IMAC purification. To optimize the washing steps, several different imidazole concentrations were tested. A SDS PAGE analysis in combination with a western blot is shown in figure 17 A. The gel shows that the protein binds well to the resin, since no CypD stays in the flow through. As soon as imidazole was added to the washing buffer, CypD slowly starts to elute from the column. Even 25 mM of imidazole leads to an elution of the protein. Because the protein could only be washed with 25 mM imidazole, the elution still contained many impurities. To remove the residual impurities, CypD was digested with TEV protease and again applied to the Ni-resin. The cleaved CypD is now found in the flow through and the impurities stay bound to the resin. The final sample is properly purified and suitable for further biophysical analysis (figure 17 B). The final yield of CypD after purification is around 1 mg per ml of reaction mix, which is enough to support NMR experiments.

SEC analysis of the final sample shows a single elution peak with a slight tailing to smaller protein sizes (figure 18). This shows the homogeneity of the sample and the absence of soluble aggregates. The peak tailing might be due to the used buffer, which contains only low salt concentrations and might lead to unspecific interactions of CypD with the gel filtration resin.

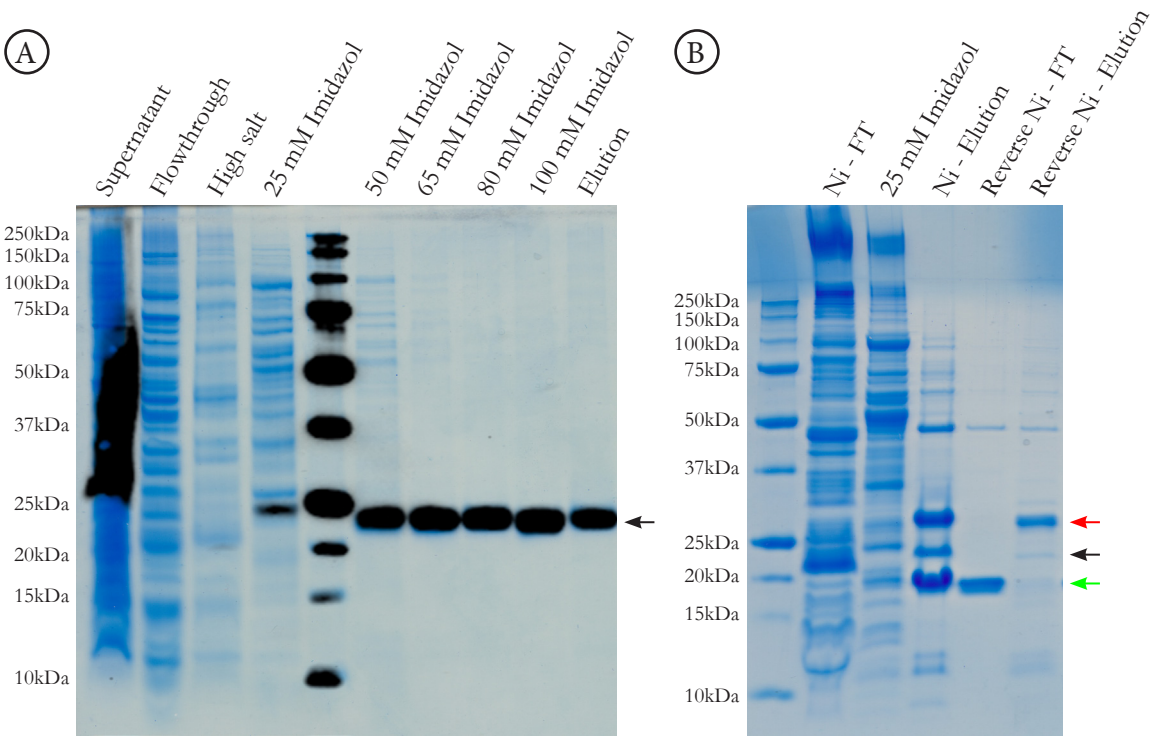

Figure 17: Optimization of CypD purification

(A) Test of different imidazol concentrations in the wash buffer. Shown is an overlay of the coomassie stained gel and a western blot against the N-terminal His tag. B: Analysis of the different steps in the optimized purification scheme. The protein is first purified by Ni-purification, followed by cleavage of the N-terminal His tag using TEV protease and a final reverse Ni-purification to remove the TEV protease and further impurities. The samples were separated on a 11% Tricine gel. The black arrow indicates the uncleaved CypD, the green arrow the cleaved CypD and the red arrow the TEV protease.

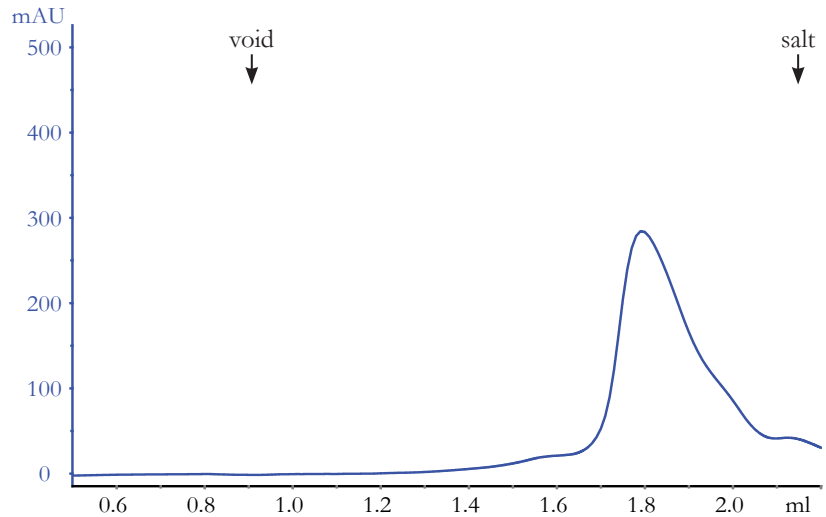

Figure 18: SEC analysis of CypD

CypD was expressed using cell-free expression. The sample was purified as described in the methods section. The quality of the purified sample in the NMR buffer (50 mM NaPi, 1 mM DTT, pH 7) was assessed using SEC. The blue line shows the UV absorbance at 280 nm. The SEC was performed on a Superdex 200 3.2/30 column. The void volume of the column as well as the salt exchange are labeled accordingly.

4.3.2. SPR binding analysis of small molecules

SPR was used to probe the binding of several ligands to CypD. Protein immobilization on the chip surface is one of the key steps when using SPR. A common method is the immobilization by amine coupling. The covalent coupling produces very stable surfaces that show a minimum signal drift and can be used for long periods, if the protein stability is accordingly. In addition, covalent coupling allows to produce dense surfaces, which is needed when the ligand, that is titrated is very small compared to the immobilized protein. Amine coupling however is problematic in many cases, because the coupling of the protein and the activated carboxy groups to be in close proximity. Therefore the protein is enriched on the surface using electrostatic attraction between the protein and unmodified carboxy groups. To enable the electrostatic attraction, the protein of interest needs to be immobilized at a pH that is below the isoelectric point of the protein. Additionally the immobilization buffer should not contain buffer substances that bear amine groups and should contain low salt concentrations, because the protein needs to attach to carboxyl groups on the chip surface. This treatment is not tolerated by many proteins, which unfold and aggregate or are inactive after immobilization. In addition the coupling is unspecific bearing the possibility that catalytically active residues, which often show increased reactivity, are modified covalently. An alternative immobilization method is the indirect immobilization using an antibody coated surface. The used antibody can be directed against the protein directly or against an attached fusion peptide. This method allows to immobilize a variety of different proteins and can usually be regenerated by a pH jump. However the binding kinetics of the antibody can differ substantially between the used antibodys and shows a drift of the signal over time. This drift can be disturbing in some cases.

To circumvent these problems CypD was immobilized using a biotinylated CypD and a streptavidin coated chip (SA chip). For this purpose CypD was cloned with a C-terminal Avi tag. The Avi tag was site specifically biotinylated during expression by the use of BirA biotin ligase. BirA recognizes the 15 amino acid long avi tag and biotinylates a lysine residue in this tag. BirA can directly be co-expressed in the system by only adding the plasmid to the expression, saving time and resources. The site specific biotinylation leaves all important residues of the protein untouched and has only minor effects on the protein. The biotin streptavidin interaction is very strong leading to surfaces with a stability comparable to covalent coupling.

After cell free expression, the biotinylated protein can be directly immobilized from the reaction mixture without prior purification using a SA chip. Only free biotin needs to be removed before the immobilization.. The immobilization is insensitive to DTT, redox systems, high salt, cofactors and pH. This allows to keep the protein in optimal buffer conditions, which is not possible using covalent coupling. Especially reducing agents are very difficult to use in combination with amine coupling or antibodys. Besides this, the immobilization method is very fast and can be used for fast screening of different constructs or mutants, because the immobilization doesn't need any protein purification or cell disruption.

Figure 19 shows the SPR binding curves of four different ligands that were titrated to CypD. The natural product CsA was used to test and validate the CypD quality and the immobilization method, because it is a well-established positive control and gave a k_{on} of $1.39 \cdot 10^5$ $M^{-1}s^{-1}$, a k_{off} of $5.41 \cdot 10^{-3}$ s^{-1} and a K_D of 39 nM. This is very similar to the kinetics published for CypA (Huber 2004). As second control the ligand CL1, which was published in the protein database (4J5B) by Colliandre et al., was used (figure 19). The results from these control experiments are basically identical to the results obtained with *E.coli* expressed protein (data not disclosed; personal communication Daniel Schwarz Merck Serono). In addition, other ligands were tested to probe small molecules with a variety of different affinities and binding kinetics. The results of two of these ligands are shown in figure 19 C and D. The used ligands covered a range of affinities from 39 nM to 20 μM. In addition, binding kinetics ranging from slow k_{on} and k_{off} rates as it is the case for CsA,

to fast k_{on} and k_{off} rates as it is the case for CL4 are observed. This leads to the conclusion that the used construct and immobilization method are well suited for the ligand tests. The next step would be a larger high throughput ligand screen, to identify suitable inhibitors or molecular scaffolds that could be used as starting points for an inhibitor development. For this purpose Merck Serono (Darmstadt) performed a large fragment screen on CypD. The fragment screen has the advantage, that fragments binding to different subpockets can be distinguished and fragments binding outside of the active site can be considered to gain binding selectivity over other family members. After the initial fragment screen the different hits were validated and the binding position of the fragments was analyzed by x-ray crystallography (data not disclosed; personal communication Daniel Schwarz Merck Serono). The screen yielded 58 confirmed fragment hits, however only 6 fragment-protein crystal structures could be obtained (data not disclosed; personal communication Daniel Schwarz Merck Serono). For the other fragments the binding position stayed unclear. At this point NMR was used to identify the binding position of the fragments.

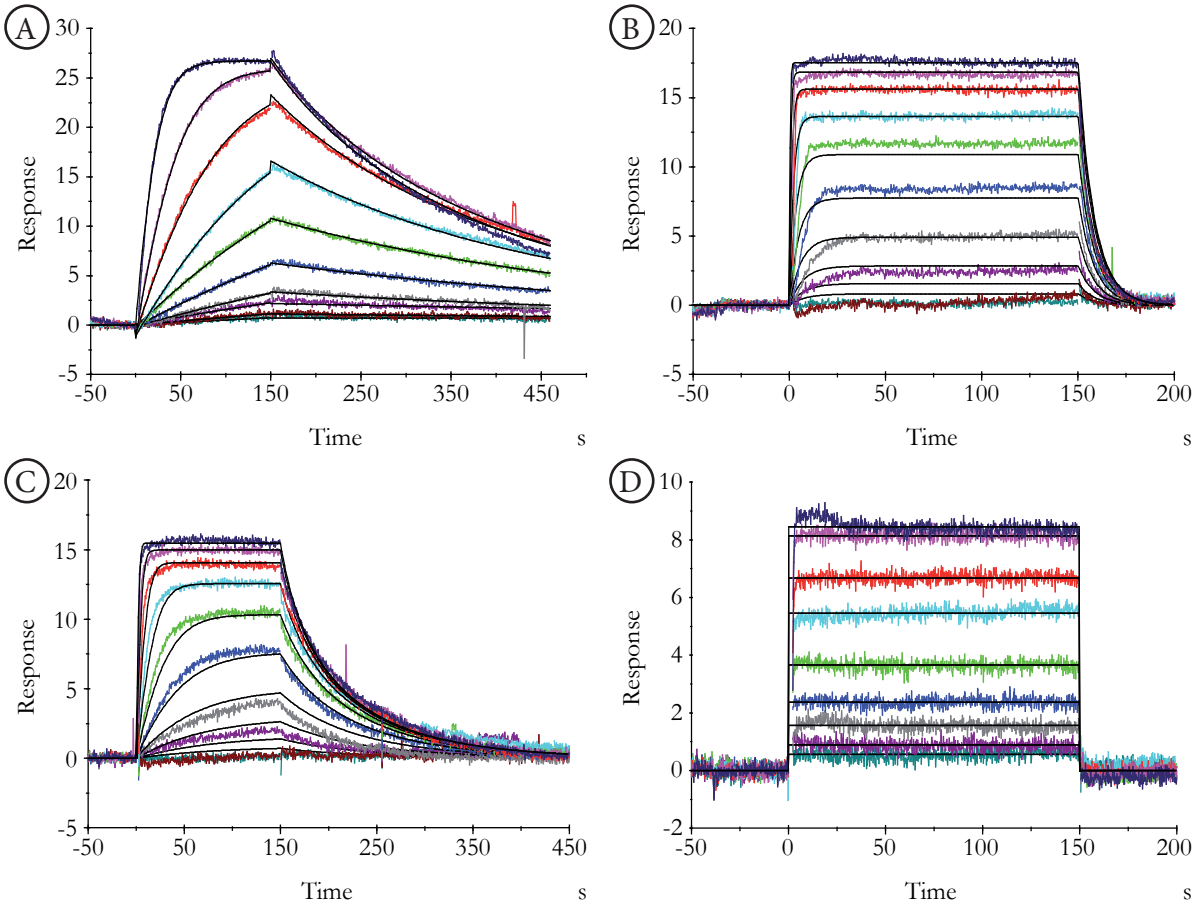

Figure 19: CypD SPR titrations with different ligands

The panels show the SPR traces of concentration series with the ligands CsA (A), CL1 (B), CL2 (C) and CL3 (D). CL1-3 are patentetd in WO2011/076784 A2. CypD with a C-terminal biotinylated Avi tag was coupled to a SA chip with a surface density of 1030 RU. The protein was non purified and directly taken from the cell free expression mix. The experiments were performed on a Biacore S51 instrument. The compound was injected in a 1:2 dilution series with 10 concentrations and 1 blank injection. The running buffer contained 20 mM Hepes, pH 7.4, 150 mM NaCl, 0.1 mM EDTA, 1 mM DTT, 0.0.5% Tween20. The maximal used compound concentration was 500 nM in A, 5 µM in B, 2 µM in C and 200 µM in D. The shown traces are double referenced, which means that the signal was referenced with a blank channel and the blank injection was subtracted. In addition, artefacts due to buffer mismatch at the beginning and the end of the injection were removed. The black lines represent a global fit of the data. The fitted data are k_{on}: $1.39 \cdot 10^5$ $M^{-1}s^{-1}$; k_{off}: $5.41 \cdot 10^{-3}$ s^{-1}; K_D: 39 nM for A; k_{on}: $5.6 \cdot 10^5$ $M^{-1}s^{-1}$; k_{off}: 0.12 s^{-1}; K_D: 212 nM for B; k_{on}: $4.4 \cdot 10^5$ $M^{-1}s^{-1}$; k_{off}: $3 \cdot 10^{-2}$ s^{-1}; K_D: 68 nM for C; K_D 20 µM for D

4.3.3. Determination of ligand binding sites on CypD using NMR analysis

NMR is a valuable tool to analyze protein ligand interactions, because the interaction can be measured in solution at temperatures that are close to the physiological relevant values. In addition, NMR allows for conformational flexibility and is not bound to the crystal lattice, in contrast to x-ray crystallography. Six different small molecule ligands were chosen to be analyzed, containing two positive controls that gave co-crystal structures (CL1 and CL7), to validate the NMR results. The fragments CL4 – CL8 have affinities for CypD of 1 mM – 10 mM and are therefore very weak binders. The analysis of the binding position was done taking advantage of chemical shift perturbations (CSPs) that occur upon ligand binding to a protein, due to the change in the local chemical environment around the binding site (Williamson 2013). This method would allow to discriminate between a binding in the proline pocket, the P2 pocket or outside of these pockets. This information can then be used for approaches like fragment linking, fragment merging or fragment growing (Hajduk 2007; Villemagne 2014). A CSP analysis in combination with a ligand titration yields the K_D of the binding as well as information about the binding position. The aim of this analysis was to confirm the binding of the chosen fragments and to gain information about the binding location. Therefore only endpoint measurements were done with the maximum soluble amount of ligand. Full titrations were not in the scope of this NMR analysis, because a K_D determination was performed with SPR.

As basis for the CSP analysis a complete peak assignment of CypD apo was needed. The assignment was achieved by the use of a HNCA (Kay 1990; Farmer 1992; Grzesiek 1992c), HNCACB (Grzesiek 1992b), HN(CO)CACB (Grzesiek 1992a) and a $^{15}N,^{1}H$ HSQC spectra, recorded on a Bruker Avance 500 MHz at 293 K. The assignment table is shown in Table 7 in the appendix. Interestingly some signals were much broader than others. This was the case for the region Thr52-His54, Gly65- Gly72 and Lys148-Ser149.

Before the titrations of CypD with the small molecules, the influence of DMSO on the spectra was tested, as it was reported that DMSO binds to the active site (Schlatter 2005). These findings

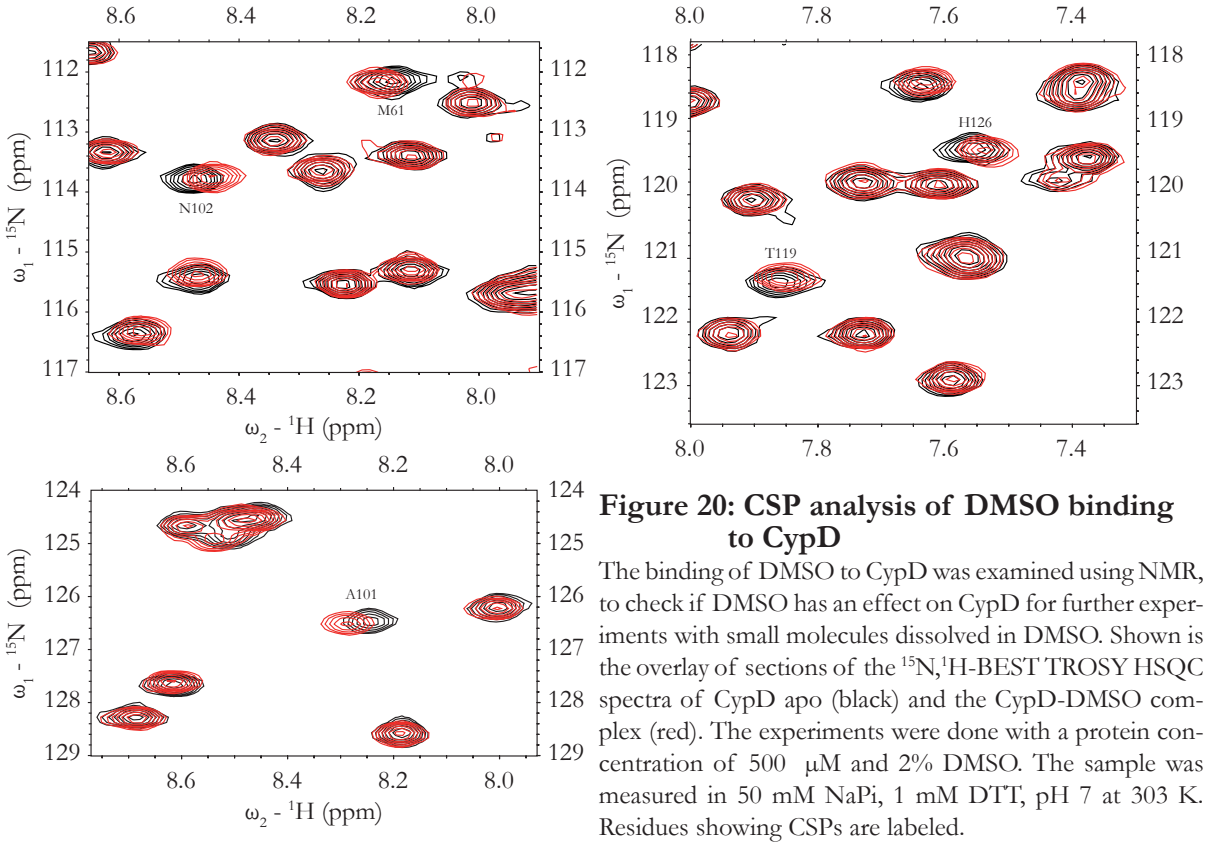

Figure 20: CSP analysis of DMSO binding to CypD

The binding of DMSO to CypD was examined using NMR, to check if DMSO has an effect on CypD for further experiments with small molecules dissolved in DMSO. Shown is the overlay of sections of the $^{15}N,^{1}H$-BEST TROSY HSQC spectra of CypD apo (black) and the CypD-DMSO complex (red). The experiments were done with a protein concentration of 500 µM and 2% DMSO. The sample was measured in 50 mM NaPi, 1 mM DTT, pH 7 at 303 K. Residues showing CSPs are labeled.

were confirmed by SPR (Data not shown) and NMR. The addition of 2% DMSO produced CSPs on several signals. Figure 20 shows sections of a $^{15}N,^{1}H$ HSQC overlay of the CypD apo and CypD in complex with 2% DMSO. The residues Met61, Cys62, Ala101, Asn102, Ile114, Thr119, Trp121sc and His126 show CSPs upon addition of DMSO. This list comprises many residues situated in the active site, which would disturb the analysis of the small molecules. Due to this finding the experiments with the fragments were done in absence of DMSO to get as clean data as possible. This approach comes with the costs of low solubility of the small molecules resulting in protein to ligand ratios below the K_D of the interaction. This situation does not allow to determine the K_D by NMR, but is still suited to analyze the binding position of the ligands.

CL 5 and CL7 were used as a positive control, because their affinity is in the range of the fragments that should be determined (K_D > 1 mM) and a co-crystal structure with CypD is available (data not disclosed; personal communication Daniel Schwarz Merck Serono). Figure 21 shows an overlay of the $^{15}N,^{1}H$ HSQC spectra of CypD apo and CypD in complex with CL7. The signals showing CSPs are labeled and highlighted with arrows, in cases where the shift is unclear. The spectra show that the addition of CL7 leads to large CSPs on a few residues, while most signals are not affected by the ligand binding. Significant CSPs are seen on the residues Met61, Gly72, Thr73, Asn102 and Ala103. Additionally the signals for Gly65 and Ser149, which were already very weak in the apo form, disappear. These findings match the expectations, as only the residues involved in ligand binding or close to the binding site should be affected. The CSPs upon ligand binding are quantified and mapped on the crystal structure of CypD. Figure 24 shows the crystal structure of CypD with a mapping of the observed CSPs. The determined binding position as well as the major interactions of CL7 with CypD is in line with the results gathered by x-ray crystallography.

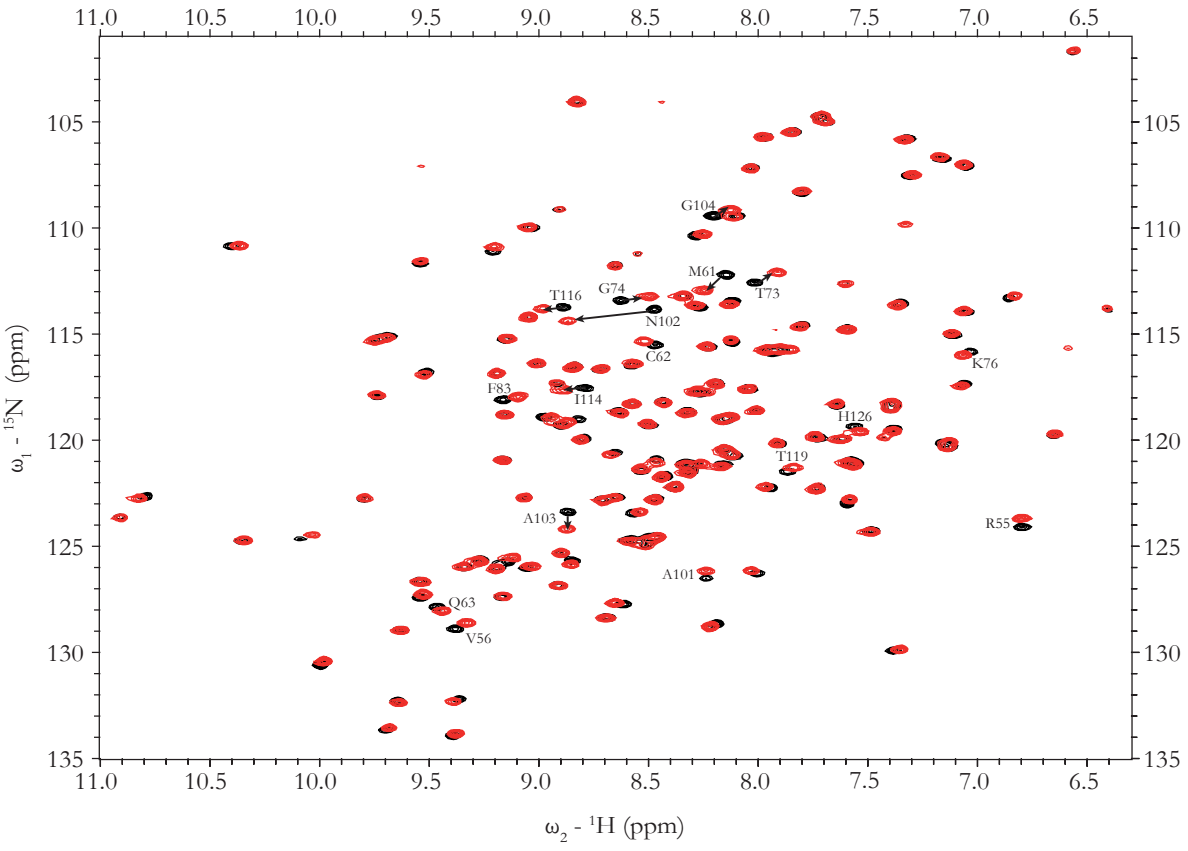

Figure 21: CSP analysis of CL7 binding to CypD

The binding of CL7 to CypD was examined using NMR. Shown is the overlay of the $^{15}N,^{1}H$-BEST TROSY HSQC spectra of CypD apo (black) and the CypD-CL7 complex (red). The ligand to protein ratio is 1:1 with a protein concentration of 500 µM. The sample was measured in 50 mM NaPi, 1 mM DTT, pH 7 at 303 K. The residues showing CSPs are labeled. Black arrows indicate the shift of the peak if necessary.

After the validation of the method with the positive controls, the experiments were expanded to the fragments with certified CypD binding, whose binding position in the CypD structure should be determined. The CSPs upon ligand binding are quantified and mapped on the crystal structure of CypD. Because the CSPs obtained with the fragments are very small, it was essential to tightly control the NMR sample preparation. The reference spectrum and the complex spectrum have to be measured in exactly the same buffer and using the same temperature to minimize the variations between the experiments. In addition, no DMSO could be used, since the CSPs produced by DMSO addition are in the same range as the CSPs produced by the fragments. Figure 22 shows sections of the spectra obtained with CL4 and CL6. The spectra show that the CSPs are very small but clearly above background. This is illustrated in figure 23, which shows a bar diagram containing the occurring CSP for each amino acid upon addition of CL6. For the CSP calculation the shift in both dimensions is considered, whereby the shift in the ^{15}N dimension is corrected with the factor 0.14 as described by (Williamson 2013). The diagram illustrates that although the CSPs are very small in general some are clearly larger than background.For CL4 CSPs are seen on the residues Phe60, Gln111, Ile117, Asp120 and Trp121. Upon addition of CL6, Thr52 Phe60, Ile117, Asp120 and Trp121 show CSPs above background. The spectra obtained for the other fragments are very similar to those shown for CL4 and CL6 and are therefore not presented. Figure 24 shows the crystal structure of CypD with a mapping of the observed CSPs of the fragments. The shifting residues are Met61, Gln63, Ala64, Thr73, Leu98, Ser99, Asn102 and Ala103 for CL5 and Thr52, His54, Phe60, Phe67, Thr68, His92, Ile117, Trp121, Leu122, Ser149, Arg151 and Lys154 for CL8. The fragments can be grouped in two classes based on their binding position. The ligands CL4, CL6 and CL8 are binding to a hydrophobic area including Phe60, Ile117, Leu122 and Trp121.The fragments are hydrophobic and contain an aromatic moiety. Therefore the ligand binding could be mediated by hydrophobic interactions with the residues and π-interactions with the Trp121 sidechain. CL8 shows in addition a strong interaction with Ser149 and Arg151. This could be mediated by polar interactions with the sidechains of the residues. Since the fragment is not large enough to cover the whole space between the hydrophobic area and the polar residues, the ligand could either have two different binding sites with probably different affinities, or an aromatic ring in the fragment could have long ranging ring current effects leading to a shift of the signals, without a direct interaction. With the current data both cases can not be distinguished, because it was not determined if simultaneous binding at both positions is possible or not. The ligands CL7 and CL5 in contrast show no binding to the hydrophobic area but bind well in the CypD binding pocket. Both ligands show major CSPs in the proline pocket as well as in the loop area around Asn102 and Ala103. In addition both ligands show CSPs on residues lining the P2 pocket suggesting a partial occupation of this space.

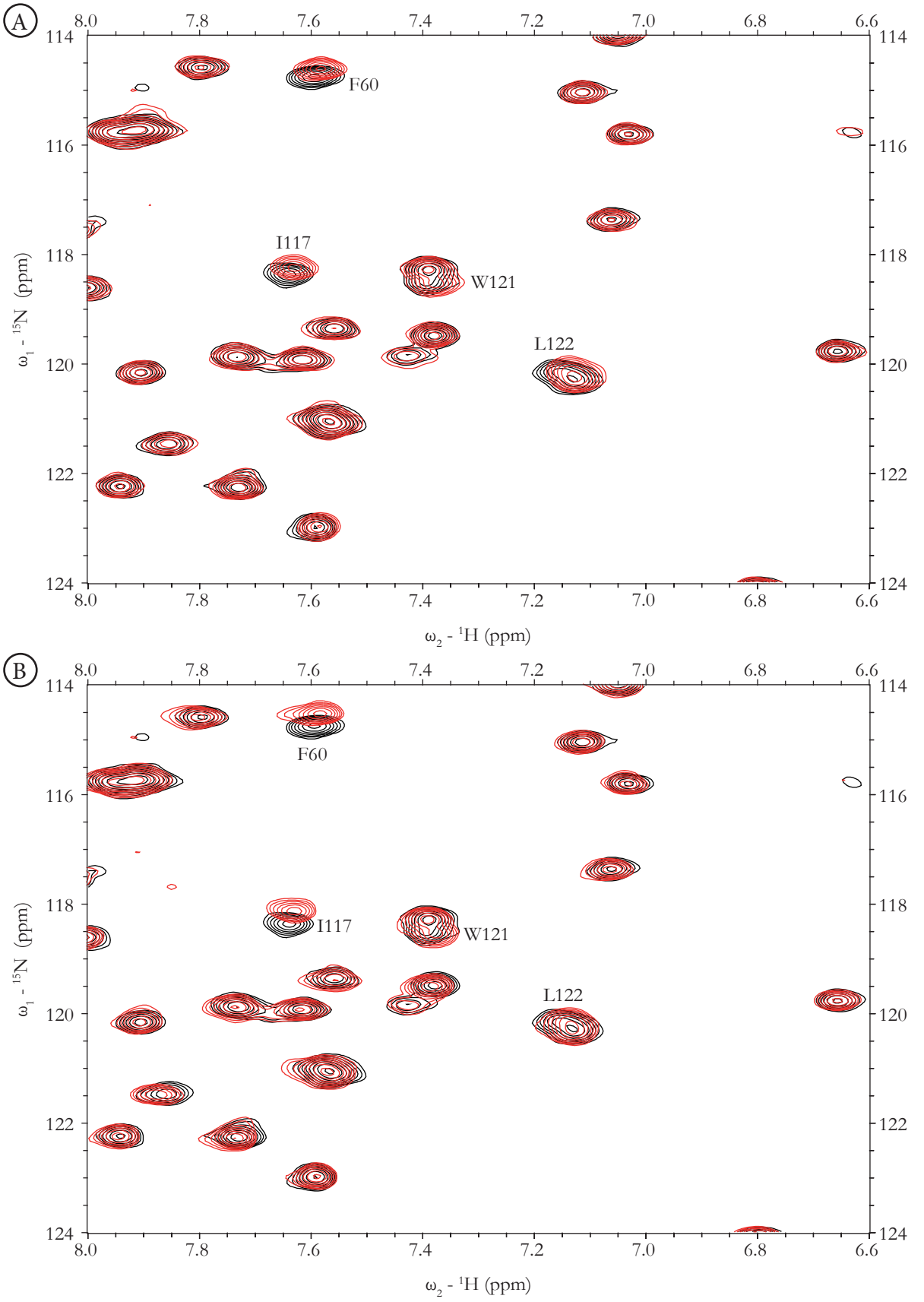

Figure 22: CSP analysis of CL4 and CL6 binding to CypD

The binding of CL4 and CL6 to CypD was examined using NMR. Shown is the overlay of a sector of the ^{15}N,^{1}H-BEST TROSY HSQC spectra of CypD apo (black) and the CypD-CL4 (A), CypD-CL6 (B) complex (red). The ligand to protein ratio is unclear, because some of the ligand stayed insoluble. The sample was measured in 50 mM NaPi, 1 mM DTT, pH 7 at 303 K. The residues showing CSPs are labeled.

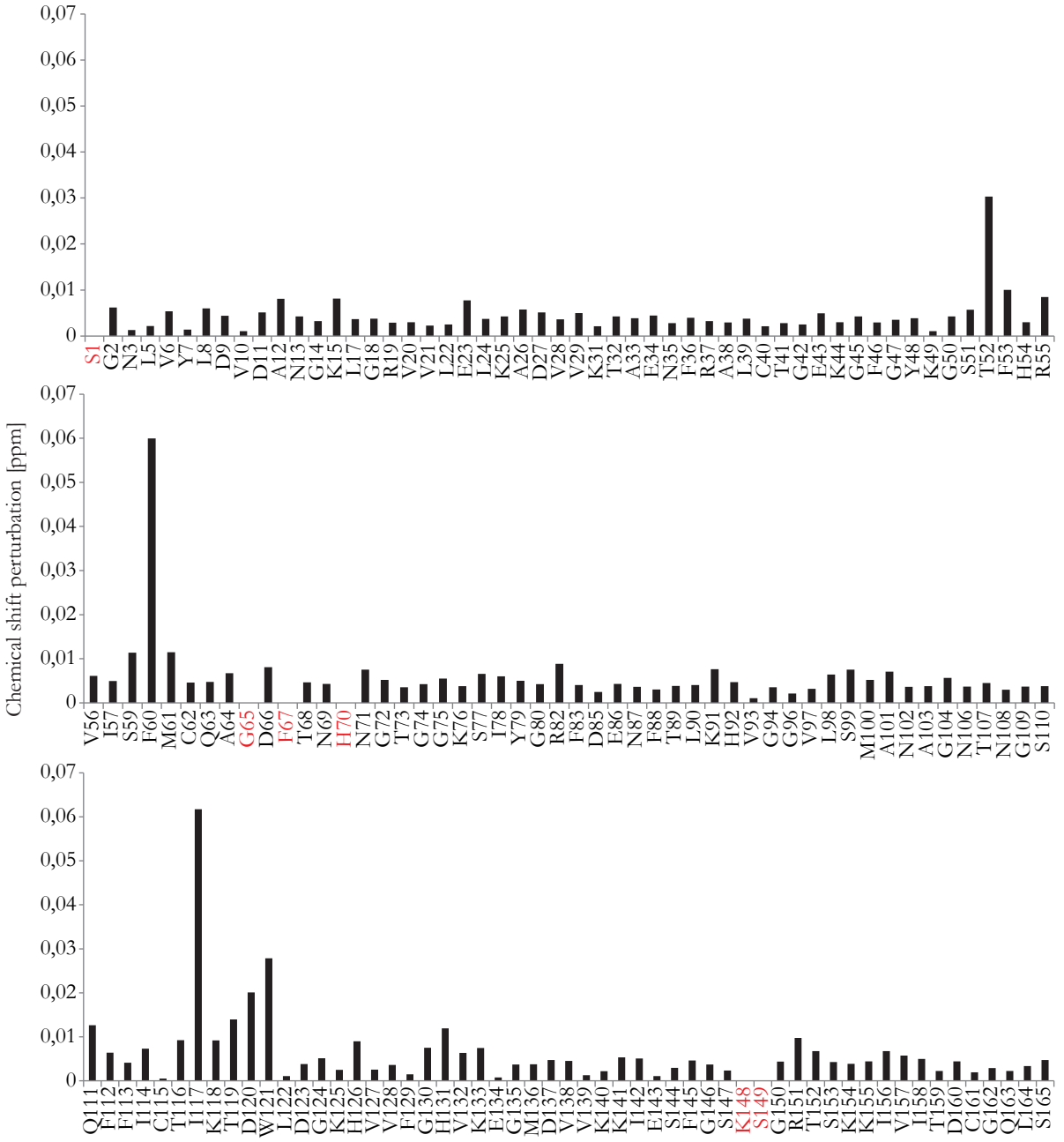

Figure 23: CSP mapping of CL6 binding to CypD

The binding of CL6 to CypD was examined using NMR. The occurring CSP upon ligand titration are quantified and shown as bar diagram. Signals that are not visible in either the reference or the complex spectrum are highlighted in red. Residues that show no signal in either of the $^{15}N,^{1}H$- HSQC spectra are not included in the graph. The chemical shift perturbation in the ^{15}N dimension is adjusted with the factor 0.14.

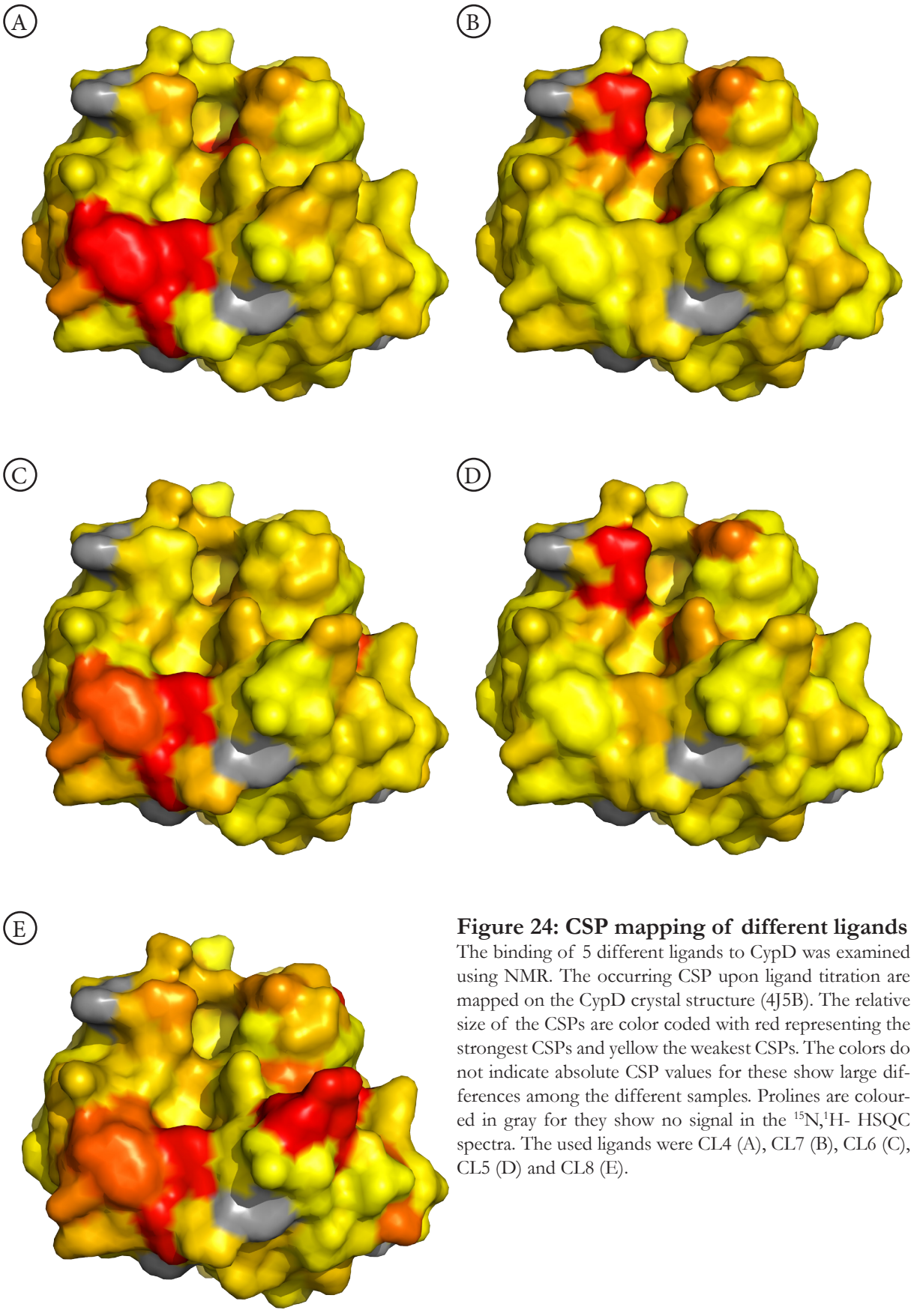

Figure 24: CSP mapping of different ligands
The binding of 5 different ligands to CypD was examined using NMR. The occurring CSP upon ligand titration are mapped on the CypD crystal structure (4J5B). The relative size of the CSPs are color coded with red representing the strongest CSPs and yellow the weakest CSPs. The colors do not indicate absolute CSP values for these show large differences among the different samples. Prolines are coloured in gray for they show no signal in the $^{15}N,^{1}H$- HSQC spectra. The used ligands were CL4 (A), CL7 (B), CL6 (C), CL5 (D) and CL8 (E).

4.4. Effect on CypD upon binding of CL1

CL1 was used as a positive control, because it is a tight binder (K_D = 212 nM) and a co-crystal structure with CypD is available (4J5B). Figure 25 shows an overlay of the ^{15}N,^{1}H HSQC spectra of CypD apo and CypD in complex with CL1. The signals showing CSPs are labeled and highlighted with arrows, in cases where the shift is unclear. The spectra show that the binding of CL1 to CypD produced changes in the ^{15}N,^{1}H HSQC spectra that cannot be explained by a simple rigid body binding of a ligand to a protein as it was the case for the other observed ligands. More peaks than expected show CSPs upon ligand binding and the signals of the complex are much broader than the signals of the apo protein. Due to the strong CSPs on many different peaks, the assignment of the peaks in the complex spectrum could not be done using the nearest neighbor assumption. This fact made it necessary to reassign the whole spectrum.

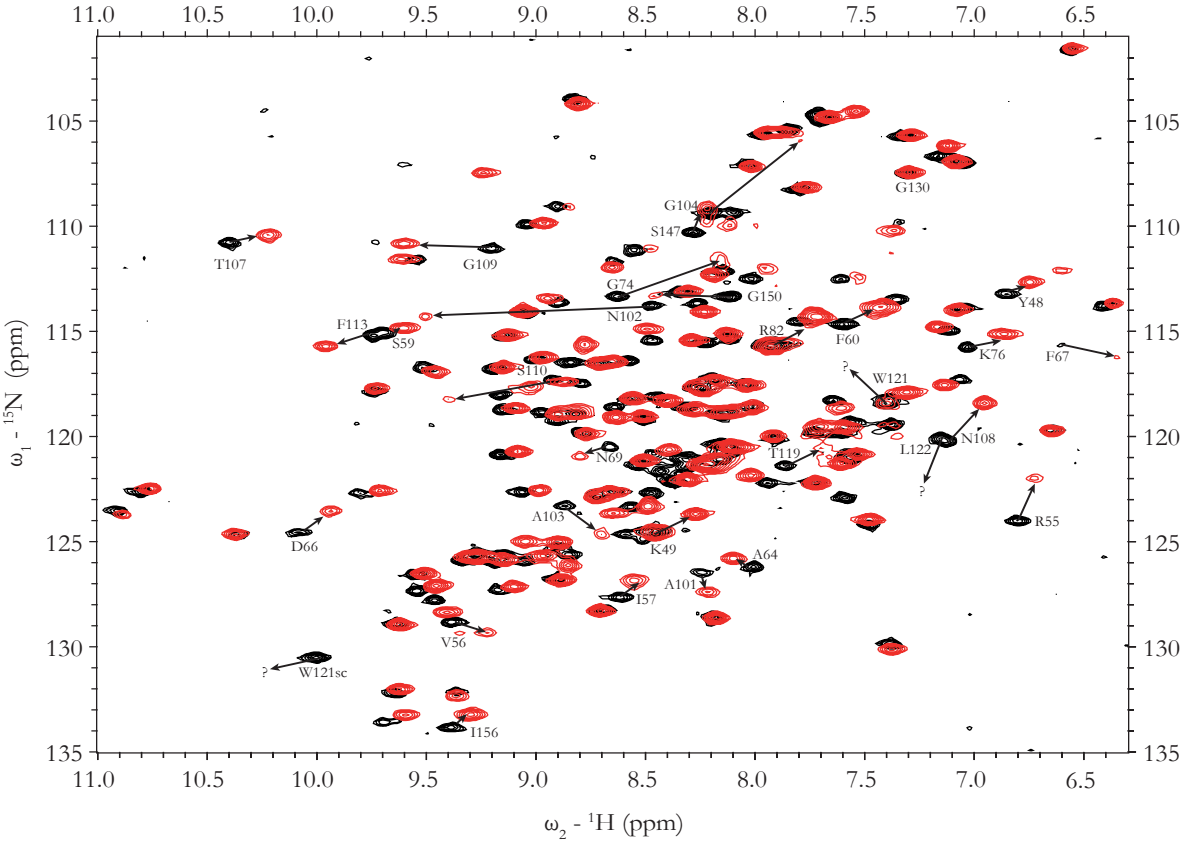

Figure 25: CSP analysis of CL1 binding to CypD

The binding of CL1 to CypD was examined using NMR. Shown is the overlay of the ^{15}N,^{1}H-BEST TROSY HSQC spectra of CypD apo (black) and the CypD CL1 complex (red). The ligand to protein ratio is 1:1 with a protein concentration of 500 µM. The sample was measured in 50 mM NaPi, 1 mM DTT, pH 7 at 303 K. The residues showing CSPs are labeled. Black arrows indicate the shift of the peak if necessary.

4.4.1. Cell free expression for triple selective labeling of CypD

The strong line broadening made it impossible to use NH detected 3D spectra for the signal assignment, needed to analyze the complex spectrum. The usually used HNCACB-, HNCA- and HNCO type spectra only showed a fraction of the expected peaks and had large gaps in the regions that show strong line broadening. These problems made it necessary to use another method for peak assignment. The possibility to express CypD in the cell-free expression systems allows the use of highly sophisticated labeling schemes like the scheme developed by Löhr et al. (Löhr

2015), because isotope scrambling can be inhibited. During expression the inhibitors O-Carboxymethylhydroxylamine hemihydrochloride (AOA), D-Malic Acid and D-Cycloserine are used to suppress isotope scrambling (Yokoyama 2011). These inhibitors suppress all scrambling except the action of transferases catalyzing the conversion of Glu to Gln and vice versa. The same is true for the conversion of Asp to Asn and vice versa. The conversion of Gln to Glu (Asn to Asp) can be inhibited by the addition of an excess of unlabeled Glu (Asp) (data not shown). The conversion of Glu to Gln however is slow, but it occurs and can produce unexpected peaks in the respective spectra. Nevertheless this scrambling only occurs on a fraction of the amino acids and the false signals can easily be identified by the peak intensity. Therefore only these few restrictions concerning the labeling of Gln, Glu, Asn and Asp have to be considered. The combination with timeshared experiments (Löhr 2014) accelerated the process. To show the relevance of this method for ligand screening projects in the pharmaceutical or biotech industry, all spectra are gathered on a Bruker Avance 500 MHz spectrometer without a cryo probehead. In contrast to high field spectrometers, which are often used in protein NMR, a 500 MHz spectrometer is available in many companies.

4.4.2. Triple selective labeling for straight forward assignment

The already mentioned problems using conventional assignment spectra made it necessary to assign the spectrum of the CypD-CL1 complex in another way. The triple selective labeling was expanded to a large set of differently labeled amino acids and used for the assignment. The labeling is based on 3 differently labeled samples. The labeling scheme for CypD is shown in Table 4. For each sample a set of 6 different triple resonance 2D experiments is performed. Only certain signals appear in these spectra, depending on the labeling pattern of the adjacent amino acids. Figure 26 shows which labeling pattern would give a signal in the different spectra. The labeling scheme is specifically designed for the individual amino acid sequence and therefore different for different proteins and even different mutants. For the determination of the optimal labeling scheme, the amino acid sequence, the special behavior of Asn/Asp and Gln/Glu, as well as the availability and the pricing of certain amino acids were considered. In addition, the labeling for CypD was optimized to observe important residues, that are involved in substrate binding or activity. This process is not yet automated and needs to be done manually. The used experiments are specifically designed to distinguish the labeling types including ^{12}C and ^{14}N nuclei. The experiments are triple resonance 2D experiments showing only the ^{1}H and ^{15}N frequencies. The experiment types are published by Löhr et al (Löhr 2014; Löhr 2015) and described in detail in the publications.

Table 4: Labeling scheme for CypD

The used labeling scheme for CypD. The scheme is based on three samples and defines the needed labeling for each amino acid type.

amino acid	sample 1	sample 2	sample 3
alanine	2-^{13}C	$^{13}C/^{15}N$	^{15}N
arginine	^{15}N	^{15}N	$^{13}C/^{15}N$
asparagine	^{15}N	$^{12}C/^{14}N$	^{15}N
aspartate	^{15}N	1-^{13}C	$^{12}C/^{14}N$
cysteine	$^{12}C/^{14}N$	1-^{13}C	^{15}N
glutamate	^{15}N	^{15}N	1-^{13}C
glutamine	$^{12}C/^{14}N$	^{15}N	$^{12}C/^{14}N$
glycine	2-^{13}C	2-^{13}C	$^{13}C/^{15}N$
histidine	1-^{13}C	^{15}N	^{15}N
isoleucine	^{15}N	$^{13}C/^{15}N$	^{15}N
leucine	$^{13}C/^{15}N$	2-^{13}C	$^{13}C/^{15}N$
lysine	$^{13}C/^{15}N$	^{15}N	$^{13}C/^{15}N$
methionine	$^{13}C/^{15}N$	^{15}N	1-^{13}C
phenylalanine	$^{13}C/^{15}N$	$^{13}C/^{15}N$	$^{13}C/^{15}N$
proline	1-^{13}C	1-^{13}C	1-^{13}C
serine	2-^{13}C	$^{13}C/^{15}N$	2-^{13}C
threonine	$^{12}C/^{14}N$	$^{13}C/^{15}N$	$^{13}C/^{15}N$
tryptophane	1-^{13}C	$^{12}C/^{14}N$	$^{12}C/^{14}N$
tyrosine	$^{13}C/^{15}N$	$^{12}C/^{14}N$	2-^{13}C
valine	$^{13}C/^{15}N$	$^{13}C/^{15}N$	$^{12}C/^{14}N$

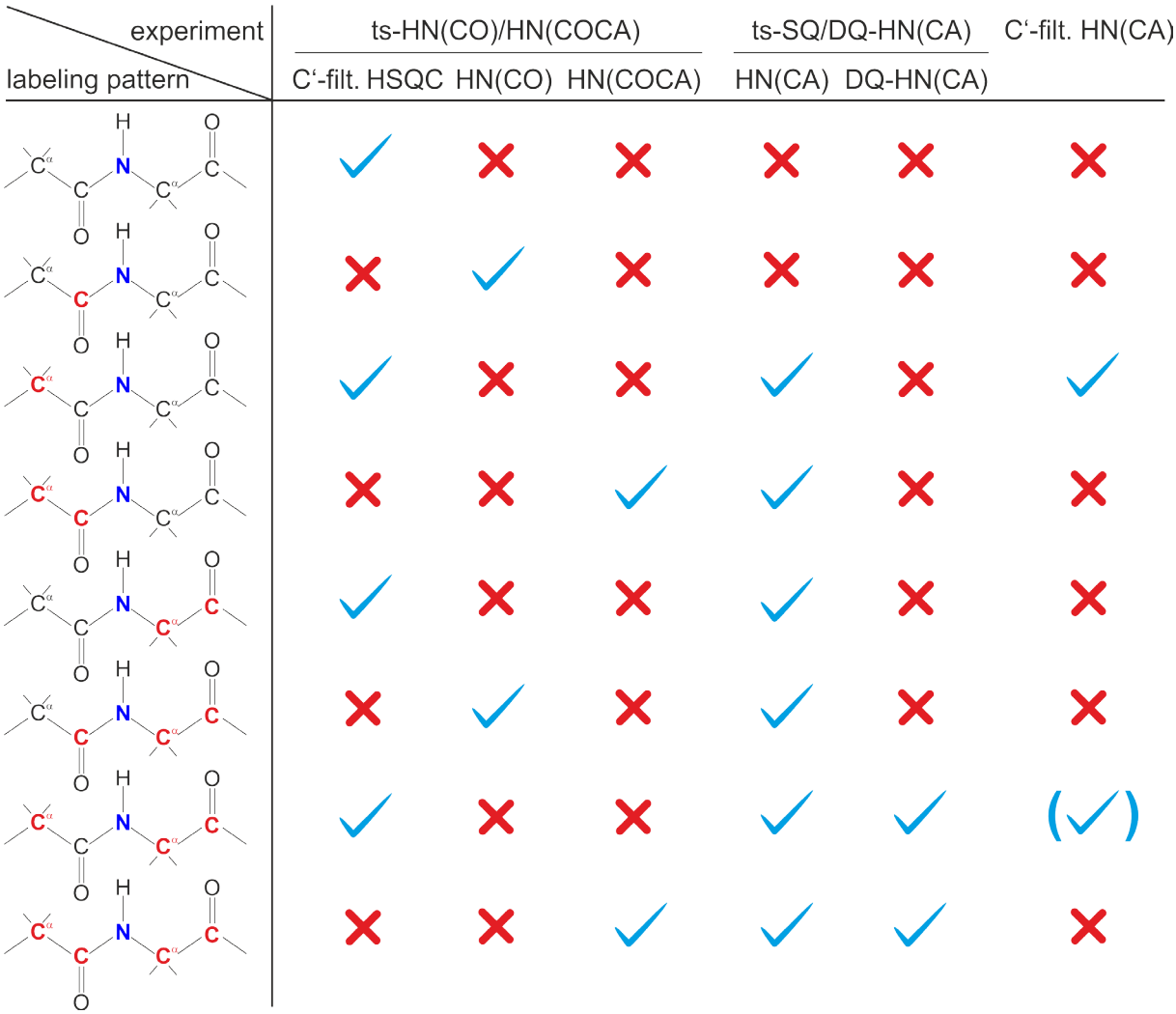

Figure 26: Overview of expected signals using triple selective labeling

The triple selective labeling uses three different experiments resulting in six spectra. The scheme shows the signals expected in each spectrum depending on the labeling pattern. Comparing the different spectra allows to identify unique pairs unambiguously. In the left column the labeling pattern is defined using red for 13C labeling and blue for 15N labeling. A red x shows that no signal is expected and a blue tick shows that a signal is expected. The tick in parentheses shows that a signal could occur but is usually invisible due to sensitivity limitation. This pattern is the basis for the triple selective labeling.

Because the amino acid sequence of the protein is known, the pattern of present or absent signals in the spectra contains information about their neighboring residues. This allows to identify unique amino acid pairs in the protein sequence and to assign them directly. In addition, only certain amino acids are ^{15}N labeled in each sample, giving information about the amino acid type of the signals that cannot be assigned directly. As a final step a 3D HNCA spectrum is used to close the gaps in the assignment. This procedure is fast, because many anchor points are present due to the assignment of unique pairs and the knowledge of the amino acid type of most signals facilitates the assignment. Figure 27 shows a few examples to demonstrate the assignment procedure. In the top part of the figure a section of the different spectra from all three samples are shown. In the bottom part the labeling scheme is shown for six amino acid pairs from CypD. The amino acid that can directly be assigned is highlighted with a colored ring. The example comprises three amino acids that are labeled in all samples (Arg151, Ile117, Lys15) and three amino acids that are labeled in only two samples (Leu122, His126, Val97). In sample 1 for example Arg151 is ^{15}N labeled and Gly150 is 2-^{13}C labeled. Therefore a signal is only expected in the C' filt. HSQC, SQ-HN(CA) and the C' filt. HN(CA). In sample 2 the pattern is the same as in sample 1. In sample 3 Arg151 is

$^{13}C,^{15}N$ labeled and Gly150 is also $^{13}C,^{15}N$ labeled. So the signal for Arg151 is only expected in the HN(COCA), SQ-HN(CA) and the DQ-HN(CA). There is only one signal that shows this pattern in the three samples and can therefore be unambiguously assigned. According to this example the assignment can be performed for many amino acid pairs. It is important to mention that amino acids that are not ^{15}N labeled in a sample, as it is the case for Leu122 in sample 2 for example, do not show any signal in all six spectra of this sample. Only a careful evaluation of all spectra from all samples allows the assignment of the signals. Besides speeding up the assignment, the triple selective labeling is well suited for cases with high signal overlap and/or low signal to noise. The 2D spectra are easy to analyze and the acquisition time is shorter than for conventional 3D experiments, allowing to use more scans in the same time. The spectra only contain the signals of amino acids that are ^{15}N labeled, reducing spectral overlap and complexity. In addition, these signals are spread over 6 different spectra adding a second layer of simplification to the spectra. The peak of Leu122 for example can be unambiguously assigned although it overlaps with the signal of Asn108 in the $^{15}N,^{1}H$ HSQC spectrum. The labeling scheme contains only one of the signals in some spectra, showing the exact position of both peaks. This can be seen for sample 3 where the C'filt HSQC shows the signal of Leu122, while the HN(COCA) of the same sample shows only Asn108 and the HN(CA) contains both signals illustrating the overlap. In this way the method allows to deconvolute overlapping signals. The simplification of the spectra is presented in figure 28 showing that the different spectra contain only a subset of the peaks present in the $^{15}N,^{1}H$ HSQC making the assignment clearer and easier. This approach resulted in a good backbone assignment of the CypD-CL1 complex. The assignment table is shown in Table 8 in the appendix.

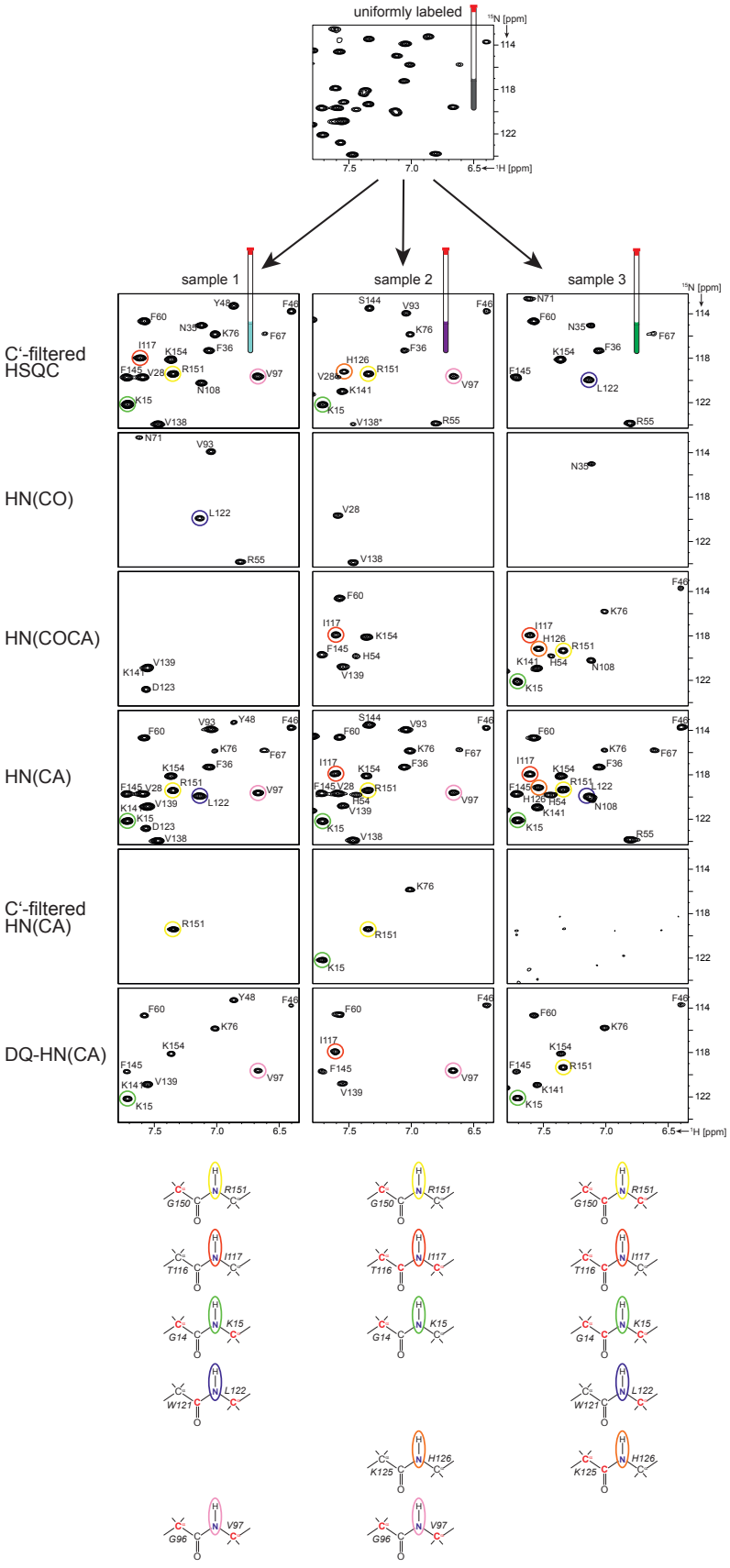

Figure 27: Assignment strategy

This figure shows how combinatorial labeling helps to assign the $^{15}N,^{1}H$ HSQC peaks of CypD. The top part of the figure shows a section of the spectrum of uniformly labeled CypD. This sections is then shown as an array of spectra. The array shows the same section in dependence on the specific experiment and the corresponding sample. The specific signal pattern is exemplified on six different amino acids which are color coded with a ring. The example comprises three amino acids that are labeled in all samples (Arg151, Ile117, Lys15) and three amino acids that are labeled in only two of the samples (Leu122, His126, Val97). The specific peak pattern allows the direct and unambiguous assignment of the highlighted peaks. In one of the sections the contour level is reduced to the noise level to show the absence of a signal.

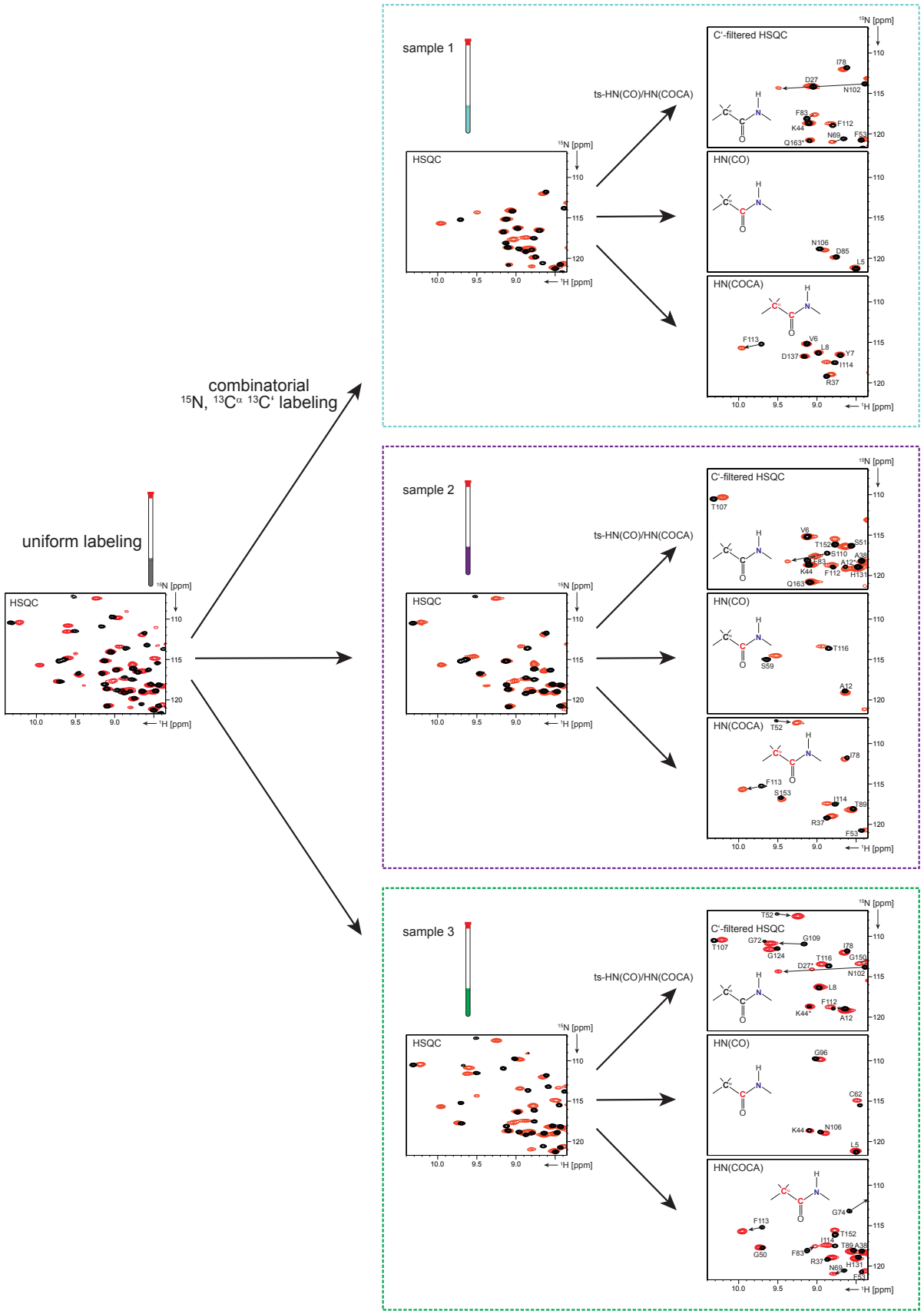

Figure 28: Spectra simplification using combinatorial labeling

Combinatorial labeling reduces signal overlap and simplifies spectra. On the left side a section of the $^{15}N^{1}H$ HSQC in figure is shown. The first level of clarification is achieved, because only a few amino acids are ^{15}N labeled in each sample, reducing the peak number in each spectrum. On the second level these signals are separated in three different spectra using time shared experiments, leading to a reduced signal overlap and a further reduction in peak number.

4.4.3. CSP analysis upon binding of CL1

Combinatorial labeling made it possible to get the assignment of the $^{15}N,^{1}H$ HSQC of CypD in complex with CL1. Having this assignment, the occurring CSPs upon CL1 binding can be analyzed and quantified in the same way as it was done for the other ligands. Figure 21 shows an overlay of the $^{15}N,^{1}H$ HSQC spectra in the apo form and in complex with CL1. Some residues that show very prominent CSPs are highlighted and the shift is illustrated by an arrow if needed. Figure 29 shows a bar diagram containing the occurring CSP for each amino acid. For the CSP calculation the shift

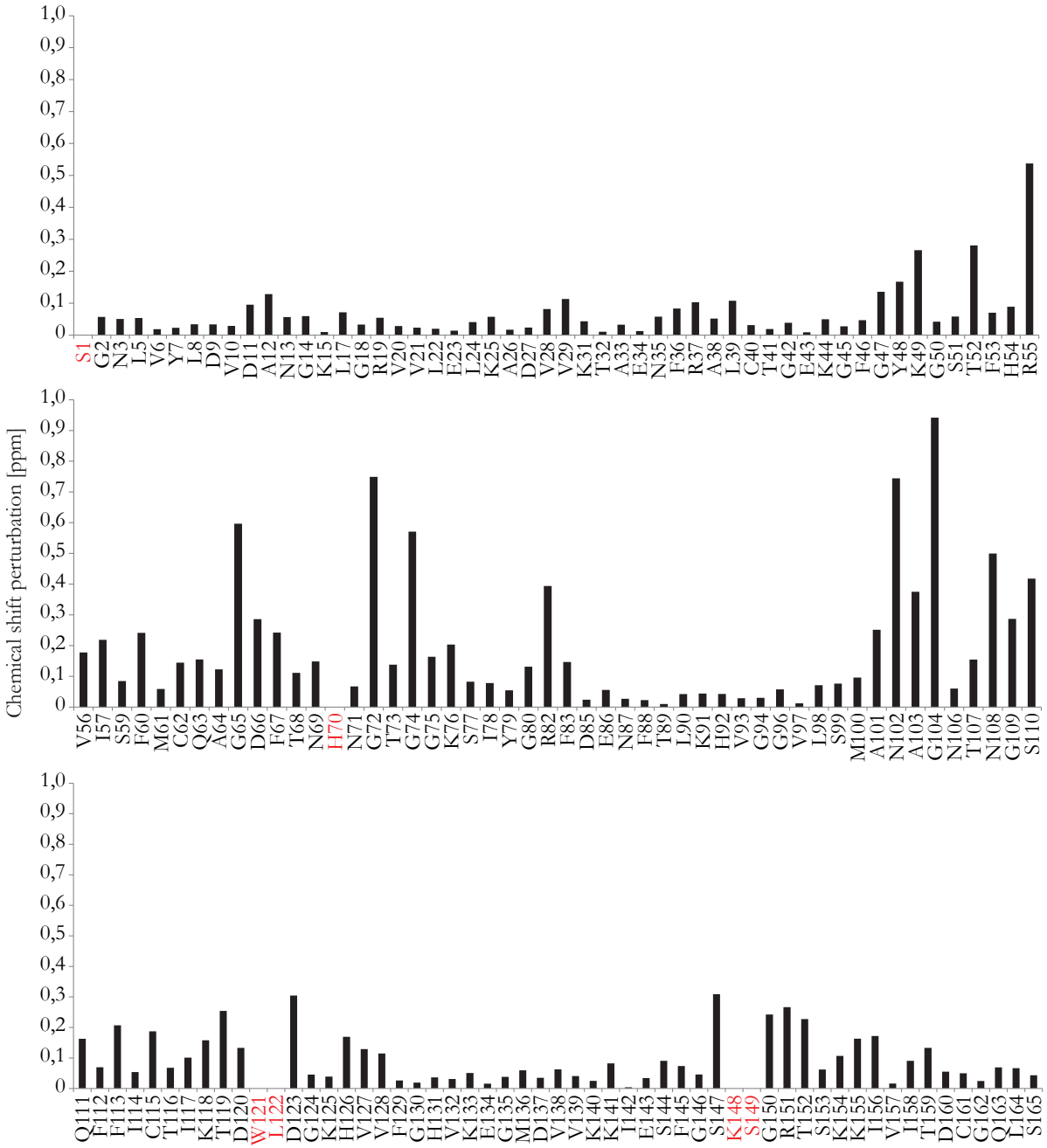

Figure 29: CSP mapping of CL1 binding to CypD

The binding of CL1 to CypD was examined using NMR. The occurring CSP upon ligand titration are quantified and shown as bar diagram. Signals that appear or disappear upon ligand binding are highlighted in red. Residues that show no signal in either of the $^{15}N,^{1}H$- HSQC spectra are not included in the graph. The chemical shift perturbation in the ^{15}N dimension is adjusted with the factor 0.14. Figure shows these CSP mapped on the crystal structure of CypD.

in both dimensions is considered, whereby the shift in the ^{15}N dimension is corrected with the factor 0.14 as described by (Williamson 2013). The CSPs are very large for some signals like Gly104, Gly72, Asn102, Gly65, Gly74 and Arg55 which all show a CSP of more than 0.5 ppm. A mapping of all CSPs on the crystal structure (Figure 30) shows that the strongest CSPs are clustered around the active site and fit well to the expectations based on the co-crystal structure. In this respect the NMR data support the binding position of CL1 seen in the crystal structure. The anilin moiety of CL1 is well occupying the P2 pocket of CypD making use of interactions with Thr107. In addition, CL1 contains a proline like region which is well situated in the proline pocket making interactions with the residues lining the proline pocket (see section 1.3.2). Important H bonds between CL1 and CypD are mediated by Asn102, Ala103 and His126. These interactions occur in the region between the proline and the P2 pocket. The catalytic Arg55 sidechain flips upon binding of CL1 in an alternative conformation. Interestingly Trp121 is not contacted and shows no changes in the crystal structure.

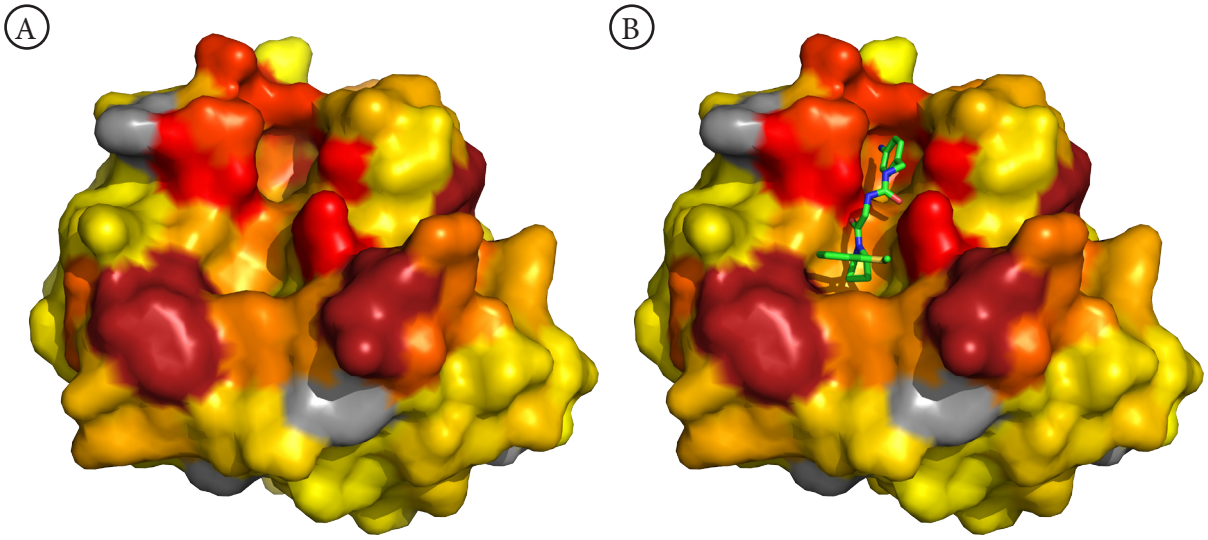

Figure 30: CSP mapping of CL1 and comparison to the x-ray structure
The binding of CL1 to CypD was examined using NMR. (A) The occurring CSP upon ligand titration are mapped on the CypD crystal structure (4J5B). The relative size of the CSPs are color coded with red representing the strongest CSPs and yellow the weakest CSPs. Prolines are coloured in gray for they show no signal in the $^{15}N,^{1}H$- HSQC spectra. The signals of the residues colored in dark red are broadened below the detection limit. A quantification of the CSPs is shown in figure (B) The crystal structure of CypD with CL1 bound (4J5B). The coloring was adapted from the CSP mapping to compare the results.

However the co crystal structure does neither explain the signal broadening seen in the NMR spectra nor the large number of shifting signals, because the co-crystal shows only small conformational differences to the apo structure. Also the disappearance of the peaks for Trp121, Leu122, Lys148 and Ser149 is still puzzling, because these residues are not contacted by CL1 and show no changes comparing the apo and the complex crystal structures. The NMR results gathered so far suggest a conformational change and therefore challenge the x-ray results.

4.4.4. Structure calculation to identify the potential conformational change

Based on the NMR observations a structure determination of CypD was performed to gain information about the potential conformational change induced by CL1. The sidechain assignment of CypD apo was performed using a H(CCO)NH TOCSY, CC(CO)NH TOCSY (Grzesiek 1993), $^{13}C,^{1}H$ HSQC/HMQC spectra and Yamazaki type experiments (Yamazaki 1993) to assign the aro-

matic signals. The distance restraints for structure calculation were extracted from a 3D ^{15}N-NOESY, a ^{13}C-NOESY of the aliphatic region and a ^{13}C-NOESY of the aromatic region. The structure calculation was performed by Dr. Sina Kazemi (Institute for Biophysical Chemistry, Goethe University, Frankfurt, Germany) using CYANA (Güntert 2004). The NOE crosspeak assignment was automatically performed by CYANA prior to the structure calculation. The energy of the final structure bundle was minimized using OpalP (Koradi 2000). Table 5 summarizes the main statistics of the structure calculation. The structure calculation yields a bundle of 20 structures. The bundle shows a backbone RMSD of 0.78 Å showing that the calculation converged and resulted in a tight bundle. Only the loop from Gly65 to Gly80 shows larger structural flexibility. For representation usually one structure from the bundle is shown. It turned out that this structure is not necessarily representative for the bundle. Therefore the regmean (Gottstein 2012) algorithm is used to get a representative structure. Figure 31 shows an overlay of the regmean structure and the crystal structure of CypD apo (3QYU). The calculated CypD apo structure and the crystal structure show the same fold. The central β-sheet as well as the α-helices that pack against this core are very close in the two structures. The position of the loops however diverges significantly. This leads to a RMSD between the backbone atoms of the regmean structure and the x-ray structures of 2.29 Å.

Table 5: Summary of the NOE restraints used in the structure calculation of the CypD apo form.
NOE crosspeak assignment was automatically performed by CYANA.

Distance bounds		Number	Percentage
All	:	1791	100.0%
Intraresidue, |i-j|=0	:	420	23.5%
Sequential, |i-j|=1	:	495	27.6%
Short-range, |i-j|<=1	:	915	51.1%
Medium-range, 1<|i-j|<5	:	260	14.5%
Long-range, |i-j|>=5	:	616	34.4%
Limit -2.99 Å	:	49	2.7%
Limit 3.00-3.99 Å	:	702	39.2%
Limit 4.00-4.99 Å	:	874	48.8%
Limit 5.00-5.99 Å	:	166	9.3%

The structure is defined by 1791 NOE restraints from which 616 are long range

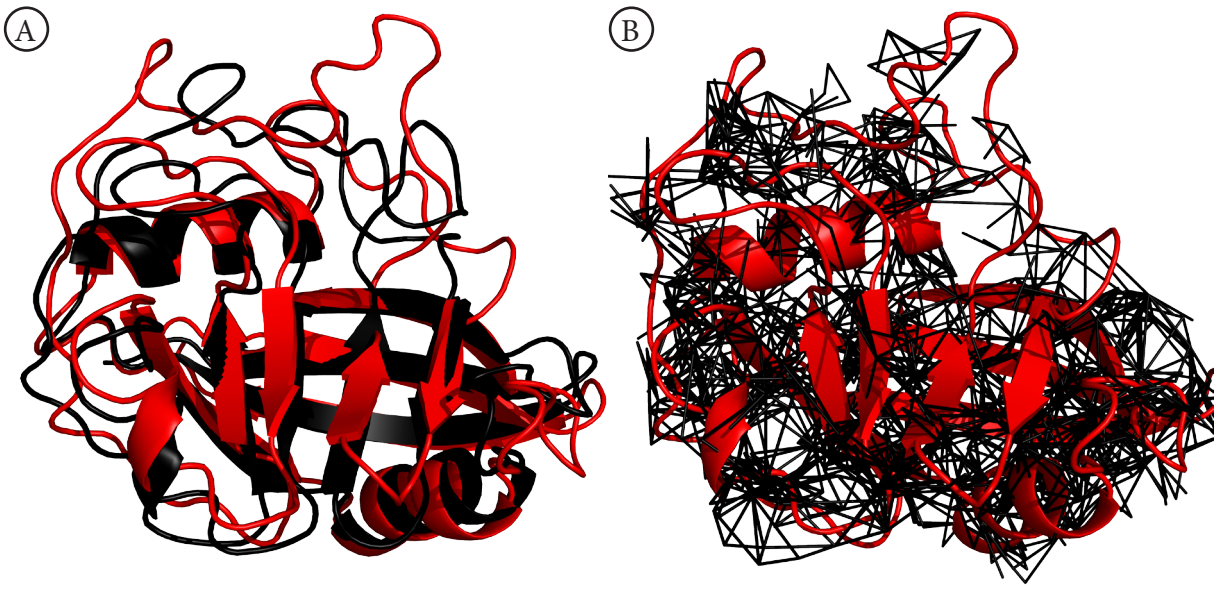

Figure 31: Structure of CypD apo
(A) Overlay of the structure calculated for CypD without any ligand bound (red) and the crystal structure of CypD (3QYU, black). The structure was calculated with CYANA using the measured NMR restraints. The resonance assignment was done manually, while the NOE assignment was performed by CYANA. (B) The calculated structure of CypD overlaid with the upper limit restraints used for structure calculation. The upper limits are represented as black lines and are derived from NOESY spectra.

restraints. Figure 31 illustrates the upper limit restraints in the calculated structure. This shows that the well-structured and folded regions are tightly defined by the restraints, while the loops are mostly defined by short and medium range restraints. This leads to a certain fold of the loops but leaves a degree of flexibility, because the loop positions are not defined by long range restraints. Overall the similarity in the fold is sufficient to confirm the already published data and shows that CypD apo adopts the same structure in solution as in the crystal.

Having confirmed the apo structure, the structure calculation was expanded to the CypD-CL1 complex. The amide signals of the complex were assigned using triple selective labeling (see sections 1.3.7 and 4.4.2). The NH detected spectra used for the assignment of the apo structure could not be performed due to the signal broadening in the complex. A HCCH TOCSY (Bax 1990), 3D ^{13}C NOESYs of the aliphatic and the aromatic region as well as ^{13}C,^{1}H HSQC/HMQC spectra of the aliphatic, methyl and aromatic region were used to assign the sidechain signals. The automated assignment was done by Dr. Sina Kazemi using FLYA (Schmidt 2012) for automated spectra assignment. The automated assignment was supported with the N and H^N shifts gathered with triple selective labeling and some C^α and C^β signals that could be extracted from a HNCA, HN(CO)CA, HNCACB and a HN(CO)CACB spectrum. For all other frequencies the CypD apo shifts were used as statistic for the automated assignment. Figure 32 shows the summary of the automatic assignment. The green bars represent resonances that are in agreeement with the manual assignment. The dark blue bars represent assignments which the algorithm considers to be strong, which means that this assignment turns out to be constant in multiple different assignment rounds. The light blue bars represent assignments that the algorithm considers to be weak. The settings leading

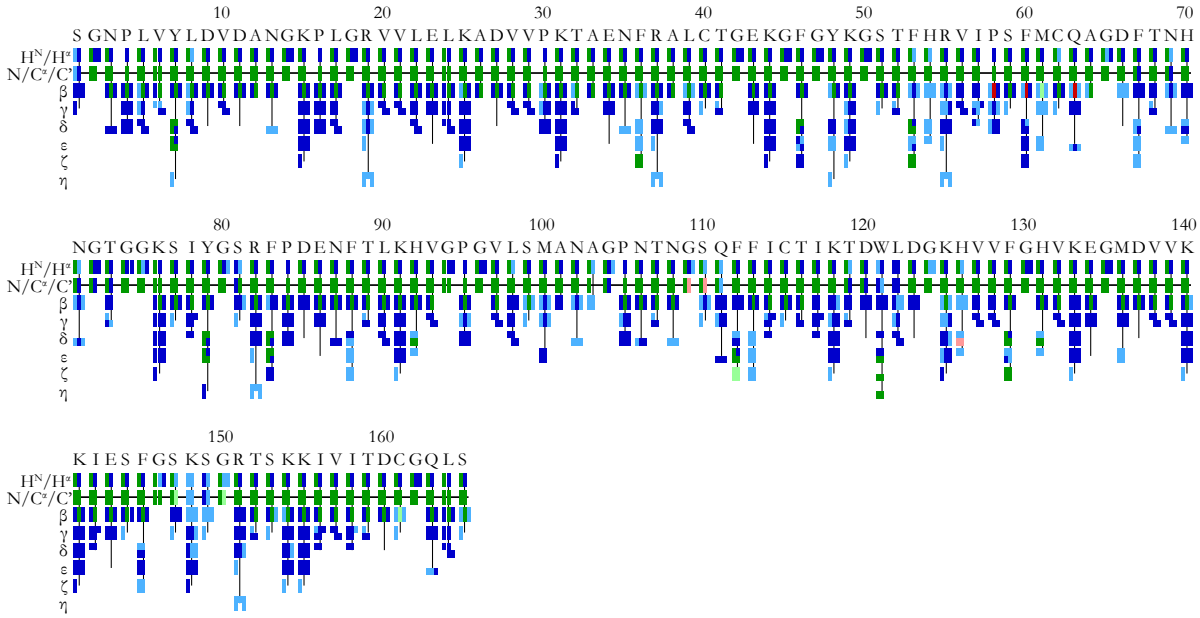

Figure 32: Automatic assignment statistics of the CypD-CL1 complex

The signals of the CypD-CL1 complex were assigned using FLYA (Schmidt 2012) for automated assignment. The assignment was performed using a hybrid approach between manual and automated assigned. The N and H^N resonances as well as some C^α and C^β shifts were assigned manually and set as fixed to support the automated assignment. The missing resonances were automatically assigned on the basis of a HCCH TOCSY, 3D ^{13}C NOESYs of the aliphatic and the aromatic region as well as ^{13}C,^{1}H HSQC/HMQC spectra of the aliphatic, methyl and aromatic region. To further support the assignment the resonances of CypD apo were used as a statistic with a standard deviation of 0.1. These settings lead to the most strong assignments. In the assignment summary, green bars represent assignments that are in agreement with the manual assignment, dark blue bars represent strong assignments and light blue bars represent weak assignments. Strong assignments mean that the algorithm repeatedly got the same assignment for the specific resonance and is therefore confident with the assignment. Weak assignments mean that this assignment showed some deviation in the different cycles. The pale red bars represent assignments that are in disagreement with the manual assignment but considered as weak ssignments.

to the most strong assignments were considered to be the best result. This was achieved when the standard deviation to the apo shifts was set to 0.1, which means only very little deviation. The final assignment including manually and automatic assigned resonances is shown in Table 8 in the appendix.

With the complete assignment of the CypD-CL1 resonances a structure calculation was performed. As basis for the NOE restraints a 3D ^{15}N NOESY, a ^{13}C NOESY of the aliphatic region and a ^{13}C NOESY of the aromatic region was used as in the case of the CypD apo structure. The structure calculation was again performed using CYANA. The statistics of the structure calculation are shown in Table 6. Although the automatic NOE crosspeak assignment identifies 495 long range NOEs the final structure calculation does not converge in one structure. Figure 33 shows an overlay of the regmean structure and the crystal structure of CypD apo (3QYU) as well as a representation of the upper limit restraints used for the structure calculation. The missing structure in the active site region is represented by a bundle backbone RMSD of 2.28 Å. The backbone deviation of the regmean structure from the crystal structure (3QYU) is 8.72 Å.

Table 6: Summary of the NOE restraints used in the structure calculation of the CypD-CL1 complex.
NOE crosspeak assignment was automatically performed by CYANA.

Distance bounds		Number	Percentage
All	:	1744	100.0%
Intraresidue, |i-j|=0	:	522	29.9%
Sequential, |i-j|=1	:	501	28.7%
Short-range, |i-j|<=1	:	1023	58.7%
Medium-range, 1<|i-j|<5	:	226	13.0%
Long-range, |i-j|>=5	:	495	28.4%
Limit -2.99 Å	:	37	2.1%
Limit 3.00-3.99 Å	:	686	39.3%
Limit 4.00-4.99 Å	:	840	48.2%
Limit 5.00-5.99 Å	:	181	10.4%

The part of the protein, which does not contain the active site, including 4 β-sheet strands and 2 α-helices was well defined in the final bundle. In contrast the part of the protein containing the active side, was largely unfolded. Analysis of the upper limit restraints (figure 33) shows

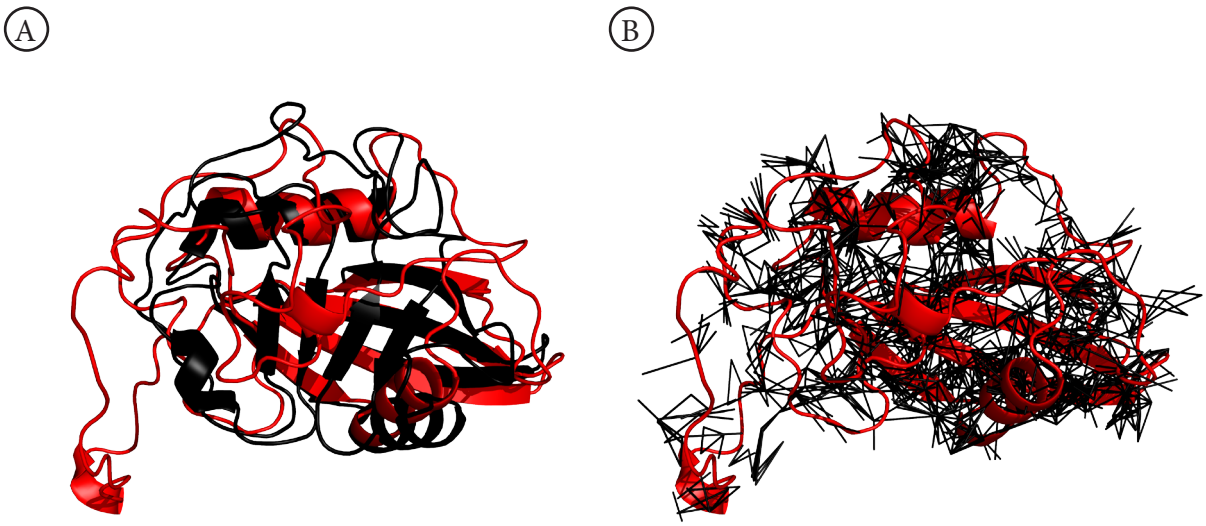

Figure 33: Structure of CypD bound to CL1
(A) Overlay of the structure calculated for CypD bound to CL1 (red) and the crystal structure of CypD (3QYU, black). The structure was calculated with CYANA using the measured NMR restraints. The backbone resonance assignment was done manually, while the sidechain assignment and the NOE assignment was performed by CYANA. (B) The calculated structure of CypD overlaid with the upper limit restraints used for structure calculation. The upper limits are represented as black lines and are derived from NOESY spectra.

that this is due to missing long range NOEs in this region resulting in a lack of restraints. In the region of the active side all NOE restraints are short or medium range. While these restraints are sufficient to provide some structure for the individual parts of the loops, they are not able to define the missing 4β-strands or to define the position of the loops, relative to the protein core. The good results for some parts of the protein suggest a correct peak assignment. The missing restraints are therefore probably due to a lack of NOE crosspeaks. The large overall amount of 1744 NOE crosspeaks suggests that the quality of the spectra in general is sufficient for a structure calculation. Only the NOE restraints for certain parts of the protein are missing. This observation is not in accordance with the assumption that CypD undergoes a conformational change upon binding of CL1. If this was the case, a defined new structure should have been the result of the calculation. Instead the conformation of the active side seems to be undefined by the NMR data. This seems to be the result of a severe signal broadening in some parts of the protein, which was already seen in the $^{15}N,^{1}H$ HSQC spectra. These observations suggest change in protein dynamics upon ligand binding instead of a defined conformational change.

4.4.5. Assessment of protein dynamics

The hypothesis that CypD undergoes dynamic changes in complex with CL1 is supported by several features in the spectra. Dynamics in the intermediate exchange regime (exchange rates in the millisecond time frame) would explain the observed line broadening in the spectra. These dynamics could originate from different sources. The possibility of the ligand binding event being in the intermediate exchange is not supported by any data. The SPR experiments show a k_{off} rate of 0.12 s^{-1} which means that the residence time of CL1 in the complex is in the range of seconds, which would be slow exchange in the NMR timeframe. This is supported by NMR titration experiments, that show a reduction of the apo peak and a corresponding increase in the complex peak signal depending on the protein:ligand ratio (data not shown). This is a clear indication of slow exchange. Thus the protein seems to undergo motions with time constants that are in the intermediate exchange.

Figure 34 shows a comparison of signal intensities in the apo protein and in the complex of CypD with CL1. For this analysis the peak heights of the individual peaks are normalized to the strongest peak, which is set to 1. This normalization was necessary, because all peaks in the complex show line broadening due to increased relaxation. The change in relaxation affected the T_1 and the T_2 relaxation time (data not shown). Still some areas experience more signal broadening than others. The broadening affected the areas that had broad signals in the apo state and expanded to other areas of the protein. The region from Arg55 to Ala64 shows line broadening in the apo form. In the complex this broadening is expanded from Thr52 to Lys76. In addition, the regions from Met100 to Gly104 and from Ser110 to Val127 are affected in the complex. Finally the region from Ser147 to Thr152 shows much broader signals in the complex. Strikingly the signals of Leu122, Trp121, Lys148 and Ser149 were broadened below the detection limit. Figure 35 visualizes the line broadening on the crystal structure of CypD for an easier identification of the positions of the affected residues in the structure. The colors range from yellow (only weak broadening) to red (strong broadening). In accordance with the observations during structure calculation, for the whole area around the active site, a large decrease in signal intensity occurs, which is indicative for dynamic motions in the intermediate exchange regime.

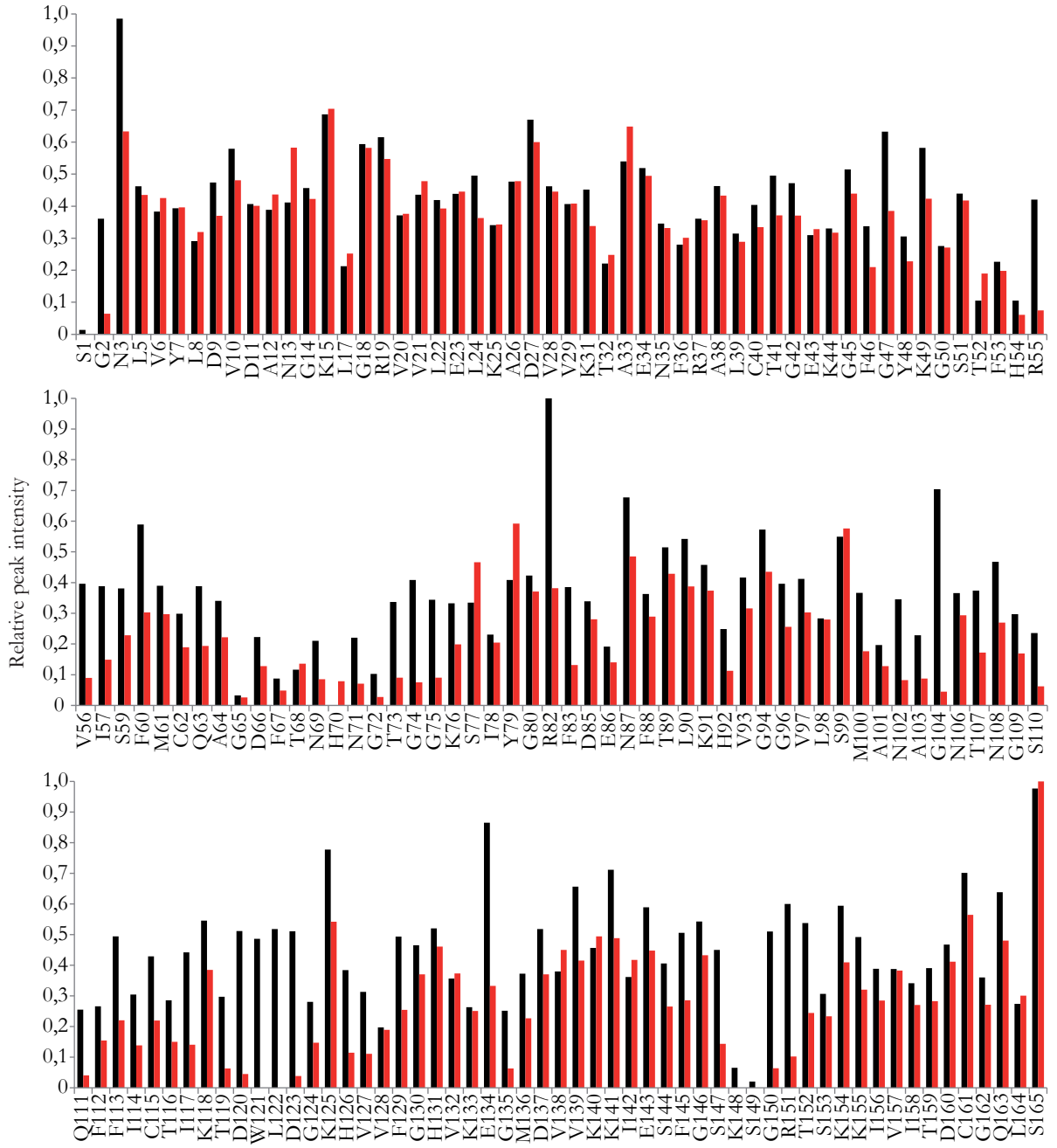

Figure 34: Analysis of peak heights as measure of peak broadening

The bars represent the relative peak heights of CypD apo (black bars) and CypD in complex with CL1 (red bars). The peaks heights were normalised on the strongest peak, which was set to 1. The relative peak heights were compared, because the signals show large intensity differences between the apo and the complex form. Residues that show no signal in the $^{15}N,^{1}H$- HSQC spectra are not included in the graph. The data show that some residues show significant peak broadening in the apo form and that additional residues become broadened. The broadening is probably due to dynamics in the protein. The visualization of the relative peak heights on the crystal structure are shown in figure 35

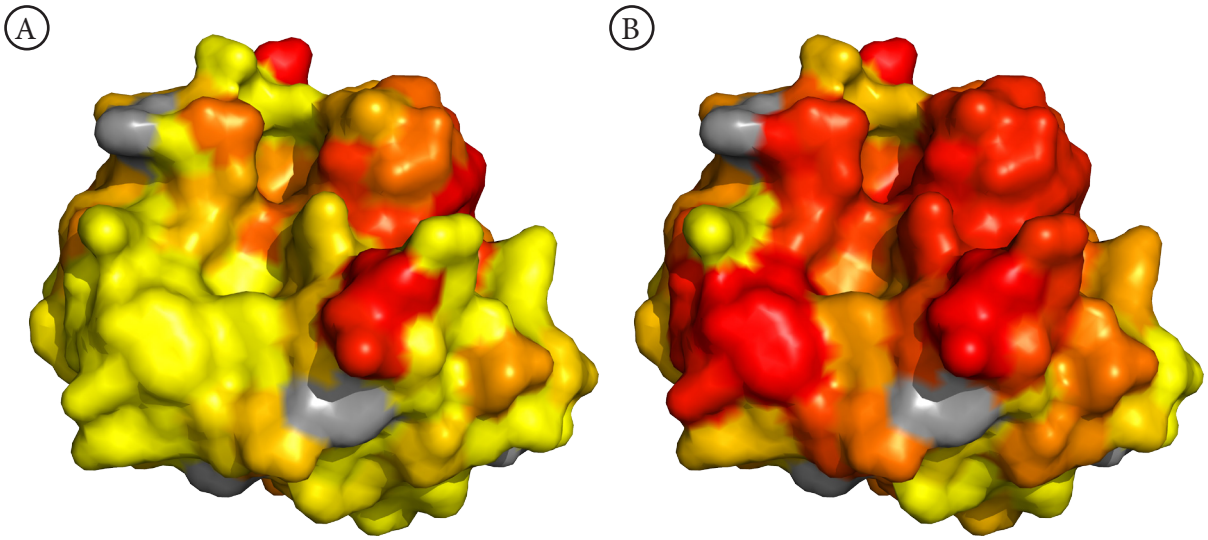

Figure 35: Visualization of peak broadening on the structure
The relative peak intensities shown in figure 34 are visualized as colors on the crystal structure of CypD (4J5B). The peaks heights were normalised on the strongest peak, which was set to 1. The colors represent the relative peak heights of CypD apo (A) and CypD in complex with CL1 (B) with yellow being not broadened and red being significantly broadened. The yellow colored residues have at least 50% of the maximum peak height. The colors do not indicate absolute peak heights for these show large differences among the different samples. Prolines are coloured in gray for they show no signal in the $^{15}N,^{1}H$- HSQC spectra. (B) The crystal structure of CypD with CL1 bound (4J5B). The coloring was adapted from the CSP mapping to compare the results.

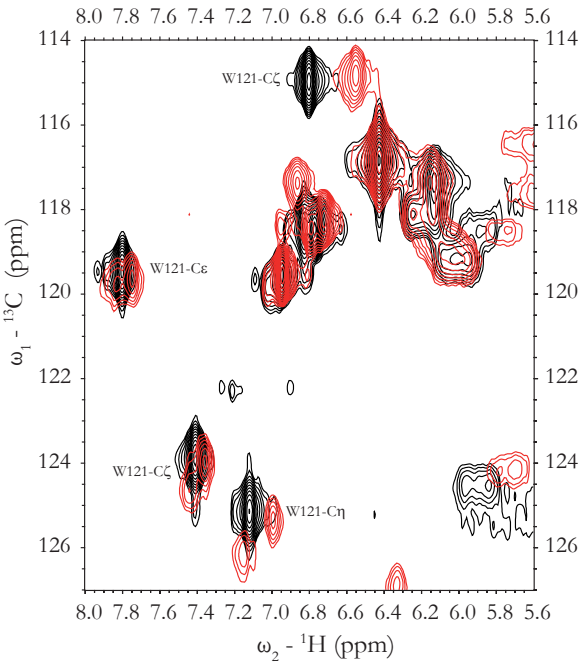

Figure 36: CL1 dependend peak splitting
The binding of CL1 to CypD was examined using NMR. Shown is the overlay of a section of the $^{13}C,^{1}H$- SOFAST HMQC spectra of CypD apo (black) and the CpD-CL1 complex (red). The ligand to protein ratio is 1:1 with a protein concentration of 500 µM. The sample was measured in 50 mM NaPi, 1 mM DTT, pH 7 at 293 K. The Trp121 signals show CSPs and split upon addition of ligand suggesting two alternative conformations.

In addition to the signal broadening, some residues show a splitting of the peaks upon addition of CL1. Figure 36 shows the aromatic signals of Trp121 in the complex, which are one of the most obvious examples for this splitting. The unique standard shifts of tryptophane in combination with the assignment of the apo spectra allowed an assignment of these signals. The spectrum shows clearly that the apo signals are shifted and split in two signals, whereby none of the complex peaks overlap with the apo peaks. This shows that all of the protein is in complex with the inhibitor and no free CypD is left. Additionally it suggests, that the protein is oscillating between two different conformations, with Trp121 being affected by the conformational change.

To support the idea of the protein changing between two structures in the ms timeframe $^{15}N,^{1}H$ HSQC spectra were recorded at different fields and different temperatures to probe if the signals are affected by the changes. If the described observations originate from protein dynamics, these parameters should have an effect on the signals. For the experiments the

used magnetic field was varied between 500 MHz and 900 MHz. In addition, the temperature was varied between 273 K and 303 K. While these changes had no effect on the spectra of CypD apo, except from the temperature dependent shift of the peaks, the spectra of the complex showed changes. Especially the change of the field strength lead to a split of several peaks in two different peaks. This observation suggests that the higher field shifted the protein dynamics from the intermediate to the slow exchange revealing the presence of two different conformations of the corresponding residues. Figure 37 shows the most prominent examples for this signal splitting. This selection contains some interesting residues. Arg55, which is an important catalytic residue in the active site shows a split of the signal in two peaks with similar intensity. Similar observations can be made for Ser59, Met100, Ile114, Leu122 which are part of the proline pocket or very close to

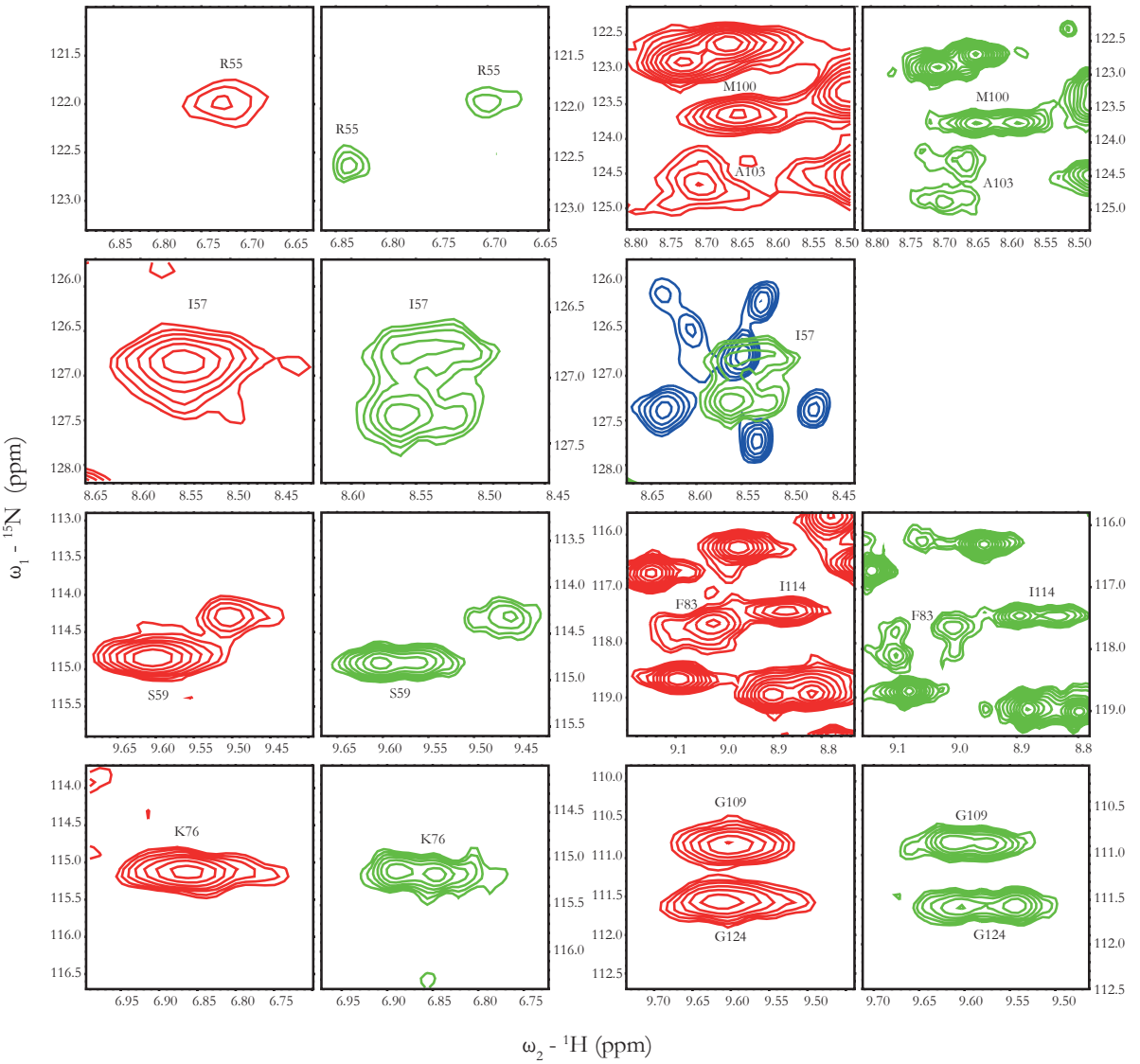

Figure 37: Field and temperature dependend peak splitting

Shown is an array of sections from ^{15}N,^{1}H HSQC spectra recorded at different temperatures and magnetic fields. All spectra are recorded with CypD in complex with CL1. The spectrum in red is recorded at 500 MHz proton frequency and 303 K. The spectrum in green is recorded at 900 MHz proton frequency and 303 K. The spectrum in blue is recorded at 900 MHz proton frequency and 273 K. All labeled peaks show a field dependent splitting of the signal. In most cases the signals split in two signals with similar intensity at 900 MHz. For I57, F83 and A103 the signals split in four signals with different intensities. A special case is seen for I57 which splits in many different peaks at 900 MHz and 273 K. Apart from the shown peaks most other peaks show no field dependent shift or splitting. The spectra at 900 MHz are recorded with batch 3 of CL1, while the spectra at 500 MHz are recorded with batch 2 of CL1. The ligand to protein ratio is 1:1. The sample was measured in 50 mM NaPi, 1 mM DTT, pH 7.

residues in the pocket. Besides this the two residues Ile57 and Phe83 show a splitting in at least four different peaks. For these residues the split peaks exhibit different intensities suggesting that the different states are not equally populated. Interestingly the signal for Ile57 splits further in at least seven different signals when the temperature is reduced to 273 K.

In summary, the described observation supports the hypothesis, that the binding of CL1 to CypD induces dynamic conformational changes in CypD. These protein dynamics are most prominent around the active site and the ligand binding pocket. It seems as if the protein is changing between at least two different conformations, that are nearly equally populated. The exchange rate between the different states occurs in the intermediate exchange when measured at 500 MHz and 303 K and are therefore in the ms timeframe.

.

5. Discussion

5.1. Acid sensing channels (ASIC)

5.1.1. Cell free expression of human AISC1

One of the objectives of this thesis was to deliver challenging human membrane proteins for small molecule screens in a drug discovery process. The expression of these proteins was performed using a cell free expression system based on *E.coli* lysate to profit from its advantages.

Concerning cell free expression, ASIC1a is a demanding target protein. With more than 60 kDa per monomer it is a rather large protein. It needs to form trimers for correct folding and activity and it contains a large soluble part as well as a transmembrane domain. On top the protein contains seven disulphide bonds in close proximity that need to be formed for correct folding. These different issues were tackled during the optimization of the expression. The expression of the full length polypeptide was achieved using tag variation. The expression of the codon optimized construct with an AT tag yielded full length protein in sufficient amount with only a little amount of smaller incomplete fragments.

After expression the problem of correct protein folding was tackled. During this optimization a folding environment needs to be created that supports the folding of the soluble part and the transmembrane part at the same time. On one hand, the transmembrane domains of proteins need a hydrophobic environment in order to be stabilized in solution. This environment can be delivered by detergents or lipids. On the other hand, detergents often interfere with the correct folding of soluble proteins or protein domains, because they stabilize the hydrophobic polypeptide stretches in solution and therefore prevent the formation of the hydrophobic protein core, which is important for the folding of soluble proteins. Lipids are less prone to disturb the folding of soluble proteins, because they usually self-assemble in larger structures like planar bilayers, liposomes or hexagonal phases. This organization in larger structures is less disturbing for the protein folding, because the amount of soluble monomers is very low, preventing them to interfere with protein folding in contrast to detergent micelles that are in constant exchange between the monomeric and the micellar state. The disadvantage of these lipid structures is, that they are insoluble and that the transmembrane domains of proteins need to insert spontaneously in these relatively stable structures. In summary the D-CF expression mode most probably disturbs the folding of the soluble domain, while expression in liposomes does not provide enough accessible membrane surface for an efficient insertion of the transmembrane parts. The use of nanodiscs could be a solution for this situation. Nanodiscs are small and stable lipid bilayer patches. On one side, they have the advantage of lipids not to interfere with the expression machinery or the folding of soluble proteins or protein domains. On the other side they behave like soluble particles that exhibit a large membrane area, that is equally distributed over the expression volume increasing the probability of spontaneous membrane protein insertion. Interestingly the nanodisc screen yielded indeed some full length ASIC1a in the soluble fraction of the expression (see figure 13).

The issue of disulphide bond formation could be addressed in several ways. The cell free reaction mixture is usually kept in a reducing environment to provide optimal conditions for the whole transcription and translation machinery. Reports from Sutro Biopharma (San Francisco, USA) (Yin 2012; Zimmerman 2014; Xu 2015) are dealing with this issue in the context of cell free antibody

production. They describe a treatment of the *E.coli* extract with iodacetamine and combine this with the supply of a redox system and different chaperones to succesfully fold proteins with disulfide bonds. This method could be applied to improve the folding of ASIC1a, if the correct disulfide bond formation is not achieved otherwise.

After many steps of optimzation it turned out that a fast and easy activity assay is absolutely crucial to evaluate the impact of changes in the expression system. The establishment of such an activity test was not possible, due to a lack of a positive control. By that time we had no supply of functional ASIC1a which could have served as a tool to find the optimal assay conditions. Therefore the project was set on hold until Proteros (München, Germany) provided functional chicken ASIC1a expressed in insect cells. With this protein interaction studies using SPR were performed and we succeded in setting-up binding active surfaces. As positive control the peptide toxin PcTx1 was used, which binds in the soluble domain of ASIC1a and is only able to bind the trimeric form of the protein. Therefore toxin binding is a good hint for correct folding. The binding of the toxin was evaluated and showed the same binding kinetics as described perviously (Dawson 2012).

This binding in combination with a pulldown assay could possibly be exploited to create a high troughput activity assay for the optimzation of the cell free expression. The toxin could be attached to beads and used to pull correctly folded ASIC1a from the cell free reaction mixture, if present. PcTx1 seems to be a good choice for this assay, because it was reported to bind very tight to ASIC1a and exclusively to the trimeric form (Dawson 2012). This assay would allow to have a quick assessment of protein folding without prior purification, allowing to use the full screening potential of cell free protein expression

5.1.2. Binding analysis of small molecules

The binding analysis of ASIC1a ligands was performed with chicken ASIC1a from insect cells using SPR. The immobilization of ASIC1a to the surface was performed using amine coupling to NTA chips. The successful coupling was verified with PcTx1 as positive control. After successful analysis of toxin binding the analysis was expanded to small molecules. As described in the results (section 4.2.3) a variety of different ligands was tested, but none of the measured results fitted to a simple 1:1 binding model.

SPR is sensitive to changes in the refractive index of the sample, which shows a correlation with changes in complex mass in a certain range. The trimeric ASIC1a is approximately 180 kDa plus the detergent micelle, which is 72 kDa for DDM (Strop 2005). The investigated small molecules however have masses between 300 Da and 800 Da. A binding event of the small molecules is therefore challenging to observe by SPR. Nevertheless amiloride, which is a general blocker of the whole channel family should bind to ASIC1a. The co-crystal of ASIC1a with amiloride (4NTX) (figure 3) supports this binding. Since no binding could be observed by SPR several different buffer conditions were tested. During the optimization process, different pH were chosen to induce different conformations in ASIC1a, as well as the used detergents to see if unspecific detergent effects mess up the data. A general trend that could be observed is that titrations without CHAPS showed much higher signals than the titrations with CHAPS. However these signal look like unspecific binding, because the signal intensity doubles with a doubling of the concentration and no saturation of the protein is visible, even at ligand concentrations that are at least 100 fold above the expected active concentrations. This suggests that CHAPS attenuates unspecific effects from the used ligands.

Interestingly Dawson et al have published a co-crystal of ASIC1a with amiloride and performed SPR binding tests with ASIC1a and PcTx1, as well as the small molecule A-317567. In the paper however they show no SPR analysis of amiloride and for A-317567 they show only one trace with

a ligand concentration of 100 μM, which ca 50 times higher than the described IC_{50} value (Dube 2005).

5.1.3. Possible problems with small molecule binding analysis and outlook

Some of the used compounds showed effects on cell based and electrophysiological assays (data collected by cooperation partners). Therefore a binding to ASIC1a is highly probable. Similar to the observations with amiloride, some conditions show binding curves with negative signal amplitudes while other show no binding signal at all. The conditions without CHAPS show signals where the highest used concentrations look like binding signals (see figure 15 C+D). An evaluation of the whole titration series however suggests that these signals are unspecific binding and do not fit a 1:1 binding model. The lack of binding can be due to many reasons. In the following some reasons are presented and discussed.

ASIC1a isoforms

While the electrophysiological experiments were performed with the human isoform of ASIC1a, the SPR experiments are performed with the chicken isoform expressed in insect cells. The choice of different expression hosts as well as different isoforms can influence the binding of small molecules significantly. For the binding position of the tested molecules is unknown, it is hard to predict if the differences between the isoforms abolish the binding or shift the affinity by orders of magnitude. In addition to differences in the protein sequence between the isoforms, the use of different expression hosts may result in altered post translational modifications of the proteins, which could influence the small molecule binding. This possible problem was approached using amiloride as a general blocker with a broad specificity. This molecule should be able to bind to different isoforms and is probably only little influenced by post-translational modifications.

Detergent effects

All SPR measurements with ASIC1a were done in detergent. Since the investigated small molecules are largely hydrophobic, they could partition in the detergent micelles reducing the concentration of "free" ligand in solution significantly. Additional they could insert in the micelle surrounding the transmembrane domain of ASIC1a and therefore produce unspecific binding signals. Besides the possibility to cover the ligands by packing them into a micelle, the detergents could mask hydrophobic binding pockets in ASIC1a and therefore compete with the small molecule binding. This behavior would result in no binding of the ligands. To approach these problems the hydrophobic environment was varied in the different experiments to see if the signals change depending on the used detergent. Although the influence of the used detergent was analyzed, DDM was present in every condition, because the protein was purified and stored in DDM. This issue could also be approached by reconstituting ASIC1a in nanodiscs. This method would still allow to immobilize the proteins as single soluble particles on the chip surface, but would eliminate the presence of the detergents and therefore the described effects. The small molecules could still exhibit unspecific binding to the used nanodiscs, but the reduction of the apparent ligand concentration as well as the masking of hydrophobic pockets in the protein would be eliminated using nanodiscs. For the reconstitution the optimal lipid to MSP to ASIC1a ratios need to be determined as well as an efficient DDM removal. This optimization requires multiple 100 μg of protein for the SEC analysis and was therefore not performed.

Protein immobilization

The protein was immobilized to the chip surface using amine coupling. A NTA chip was used to attract the proteins to the chip surface, using the N-terminal His tag. Afterwards the protein was covalently bound to the surface to ensure a high surface stability during the whole experiment.

Because the N-terminus is very near to the transmembrane part of the protein, the amine coupling could distort the organization of the transmembrane domains. This distortion could prevent the binding of small molecules but doesn't need to affect the toxin binding, for this occurs only in the soluble part of the protein. This problem could be approached using site specific biotinylation of ASIC1a. The biotin tag could be used to couple the protein to the surface applying less stress to the transmembrane domain. Issues with this method are the need for single biotinylation of the protein and the lack of information about the biotinylation site. For single biotinylation a lot of protein is needed, because the biotin is applied in sub stoichiometric amounts to drive the reaction to single biotinylation. If the biotinylation occurs in the soluble domain, the binding of peptide toxins could be altered due to steric reasons. This would result in altered binding stoichiometrys, because one to two binding sites could be blocked by the bound streptavidin. Still this method could be suitable for the analysis of small molecule binding.

Conformational selection

ASIC1a is a pH sensitive ion channel and able to adopt multiple conformations. For some proteins a conformational change is induced by an external stimulus, while some proteins sample multiple conformations constantly. For ASIC1a it could be possible that the protein samples multiple conformations, while only few conformations are able to bind the small molecule ligand. In this case the k_{on} rate of the small molecule could be determined by the speed in which the different conformations are sampled and the percentage of the binding competent population. This phenomenon could lead to very long k_{on} rates or a small amount of binding competent protein on the surface. Both effects could explain the observed lack of binding. This possibility was approached by using different pH values during the experiments to influence the protein conformation ensembles. In addition the protein was presaturated with PcTx1 to lock ASIC1a in a specific conformation. None of these conditions led to the observation of small molecule binding. The co-crystal of ASIC1 with amiloride showed that amiloride binding was only visible if the ASIC conformation was locked using MitTx. MitTx locks ASIC1 in an open conformation, while PcTX1 locks the protein in a closed conformation. Therefore it is possible that PcTx1 is not the right choice for the observation of amiloride binding. In addition conformational selection would be invisible during cell based or electrophysiological assays, because in these assays the ASIC1 is incubated with the ligand for longer time periods (>1h) before the activity is triggered by a pH change. So the ligand would have enough time to bind a significant amount of ASIC1a even if the binding competent population is very low or the conformational sampling slow.

Analysis method

As already mentioned SPR signals are dependent on changes in the refractive index, which changes in correlation to the complex mass. The mass increase in the ASIC1a detergent complex trough binding of a small molecule is very little, leading to a very small SPR signal and the need to produce chip surfaces with a high density of immobilized protein and with high stability. The choice of other analysis methods could help to analyze and observe the binding of small molecules. A popular method in this case would be the use of calorimetric methods like ITC or DSC. ITC and DSC work with label free protein and have no need for protein immobilization. In addition the protein is observed in equilibrium, which makes the method less sensitive to conformational selection. One of the major drawbacks of these methods is the high consumption of protein.

In summary it is strange that no binding could be observed for any of the small molecules. At least amiloride as general blocker should be binding to the used ASIC1a. Therefore the question arises if there is another intrinsic problem which was not considered so far. The fact that no SPR analysis of small molecules binding to ASIC is published, although many binding molecules have been identified and even co-crystal structures are available confirm that there must be some tweak to the SPR experiments which is not published so far.

5.2. Cyclophilin D (CypD)

5.2.1. Expression of CypD and SPR analysis of different ligands.

The cell free expression of CypD yielded acceptable amounts of CypD without extensive optimization. CypD was used with a N-terminal His tag, which is rich in AT bases and can therefore work as expression enhancing tag, similar to the tag variation performed for ASIC1a. Therefore the tag serves as purification tag, detection tag and expression enhancer at the same time. N-terminal tags are usually not used in cell free expression systems, because the cell free expression is prone to premature termination of the translation, leading to different C-terminal truncated side products. In the case of CypD this is no problem, because CypD is rather small, which is beneficial for the production of full length protein. In addition CypD is a soluble protein and harvested from the soluble fraction of the expression. All side products that do not fold properly and precipitate are therefore eliminated prior to the purification procedure. It is important to mention that upon cell free expression approximately 50% of the expressed CypD precipitates and is discarded before the purification. The cell free expression still yields around 1 mg of CypD per ml of reaction mixture after purification. This amount is sufficient to support a variety of different experiments including NMR. Although CypD can be efficiently produced in *E.coli* cells, the cell free expression of CypD was still performed to profit from the unique possibilities of this technique. In combination with the co-translational biotinylation the cell-free expression could serve as a brilliant tool for fast screening of different constructs, because the proteins can be immobilized directly from the reaction mix without prior purification. In addition, the cell free expression allows for efficient isotopic labeling of CypD. Although CypD expresses well in *E.coli*, the expression yield drops enormously when expression is performed in minimal media (data not shown). Labeled CypD is thus difficult to produce in *E.coli*, while the yield in the cell free expression is not affected by the use of isotopically labeled amino acids. On top cell free protein production allows to use inhibitors that efficiently suppress isotopic scrambling in the reaction mix. This allows the use of highly sophisticated labeling schemes, which was a key requisite for the in depth analysis of C1 with NMR.

5.2.2. SPR experiments with CypD

The SPR analysis of CypD was performed on one hand as an activity assay to assess the quality of cell free produced protein, on the other hand the binding of different small molecule ligands was analyzed. Cyclosporin A is a natural product and very potent inhibitor of CypD. This inhibitor was used as a positive control to confirm the correct folding of CypD. The gathered results are very similar to the published results confirming that CypD is correctly folded. Interestingly the direct immobilization from the reaction mix leaded to highly active surfaces that were stable for over 20 h. The analysis showed that all tested small molecules interacted specifically with CypD but displayed a variety of different binding kinetics and binding affinities. While CsA displayed clearly SPR resolved k_{on} and k_{off} rates, with a complex half life time of approximately 5 min, they were too fast for CL3 and an equilibrium analysis had to be performed in order to determine the binding constant. The binding kinetics for CL1 and CL2 were in between. They could be resolved by SPR, but can be considered as rather fast k_{on} and k_{off} rates.

5.2.3. Determination of fragment binding sites using NMR

Merck Serono performed a fragment screen on CypD to find potential scaffolds for an efficient inhibitor development. From the 58 confirmed fragment hits (binding assay), only 6 yielded

a co-crystal structure. For the other fragments the binding site remained unknown. Therefore NMR was used as an orthogonal method to confirm fragment binding and to assign the amino acid residues involved in fragment binding. The approach was validated with two ligands that gave co-crystal structures. One of these ligands showed high affinity (CL1) and one had only a K_D in the mM range (CL7). The results for CL7 are in good agreement with the crystal structure and showed that the chosen approach works in principle. The results gathered for CL1 were unexpected and are discussed later. Before the approach is extended to the fragments with unknown binding position, DMSO alone was used as a negative control. It turned out that DMSO is specifically binding to CypD producing CSPs in the active site area. This finding is also in good agreement with the published data, because CypD co-crystallizes with DMSO. However this behavior disturbs the NMR measurements, because 2% DMSO are usually used to increase the solubility of the applied ligands. These 2% DMSO lead to CSPs in the $^{15}N,^{1}H$ HSQC and create therefore a considerable background signal, which makes the fragment binding analysis far more complicated. The experiments with the fragments are thus done without DMSO, accepting that this lowers the ligand solubility and makes it very difficult to determine the ligand concentration in the sample. This issue is acceptable, because the NMR experiments were only performed to find the binding position of the ligand. This analysis works even with sub stoichiometric ligand ratios or ligand concentrations below the respective K_D. The performed analysis is not suited to determine the binding K_D of the ligands or the binding stoichiometry, but it confirms the binding and reveals the binding position. Interestingly most tested fragments bind in a very similar region. CL4, CL6 and CL8 bind to a patch near the active site including Phe60, Ile117, Asp120 and Trp121. This region is slightly outside of the proline pocket, but still important for substrate binding (Davis 2010) and targeted by the natural inhibitor CsA. Schlatter et al performed a fluorescence based binding measurement of CypD with CsA. They found a change in tryptophan fluorescence due to water shielding (Schlatter 2005). This finding suggests that CsA is reaching out of the pocket and covers Trp121. The gained information about the fragment binding site can be used for the design of new inhibitor scaffolds or the improvement of existing scaffolds. The fact that the binding area is outside of the proline pocket shows that potential inhibitors could be enlarged to this area to gain specificity and affinity. Interestingly the binding area is not in a pocket but on an exposed surface of the protein. A large part of this surface is formed by the tryptophan sidechain. It can be speculated that the fragment binding is mediated by π-interactions since the fragments contain an aromatic moiety which could well interact with the aromatic Trp sidechain. It is also remarkable that, although the fragments have different structural scaffolds, they all bind in the same area.

After the identification of the binding site the question arises, why the fragments did not show up in a crystal structure. Figure 38 shows a representation of three CypD molecules packed in the crystal lattice (based on structure 4J5B). The residues Phe60, Ile117, Asp120 and Trp121 are colored red in the central CypD molecule. The red colored area is involved in crystal contacts to other CypD molecules. These crystal contacts might block the area and prevent the binding of the ligand after crystal soaking. In addition the binding of the fragments might prevent the formation of the crystal contacts and therefore successful crystallization. This would also explain why the interaction can be characterized by NMR and SPR, because these techniques are not dependent on the formation of a crystal.

As presented in the Introduction, the members of the cyclophilin family share a similar active site (Proline pocket). They mainly differ in the architecture of the P2 pocket. A fragment based inhibitor design is therefore a good choice to target CypD because it allows to find potential fragments that specifically occupy the P2 pocket and might provide selectivity over the other family members. For this approach however it is absolutely essential to have structural information about the binding site of the ligand. The NMR experiments can give information about the pocket that is occupied even if the orientation of the fragment in the pocket, as well as the specific interaction

sites, are not determined.

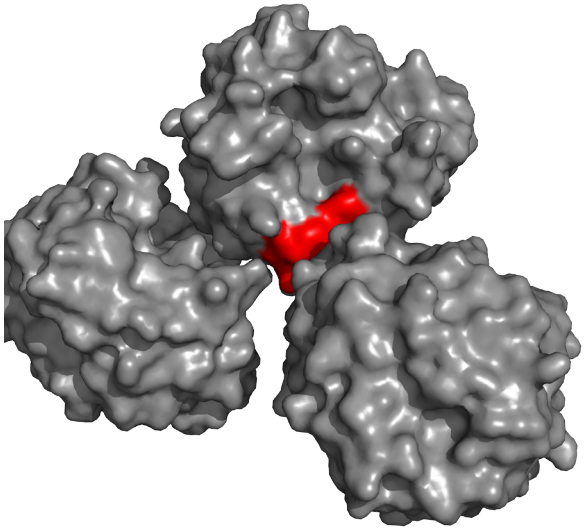

Figure 38: Crystal packing of CypD
This picture shows a part of the packing CypD adopts in the crystal (4J5B). In the central CypD molecule the residues Phe60, Ile117, Asp120 and Trp121 arecolored red because these residues comprise the main binding site of many tested fragments. The residues in this side are involved in crucial crystal contacts between the CypD molecules. This might explain why no co-cryystals with the fragments could be produced.

The determination of the ligand position with NMR would give very helpful information about important functional groups in the small molecule and help to optimize occupancy of the binding pocket. In principle these information can be gathered using NMR. For this approach NOE distance restraints between the ligand and the protein would be determined, which allows a structure calculation of the complex or gives helpful restraints for a ligand docking in the binding site. This approach was not followed, due to the very weak binding of most fragments in the mM range. The fragments exhibit a low residence time in the complex leading to exchange problems during the NOESY mixing time. In addition most fragments show low solubility in the NMR buffer which limits the amount of protein-ligand complex and therefore the sensitivity of the NMR experiments. These experiments would need careful optimization.

5.2.4. Effect of CL1 binding to CypD

As described in section 4.4 the addition of CL1 led to a different CSP pattern than all other tested ligands. Many signals in the $^{15}N,^{1}H$ HSQC spectrum shift upon ligand binding. This observation led to the hypothesis, that the protein undergoes a conformational change when bound to CL1. In addition to the large CSPs on many residues the general signal intensity decreased markedly. While the large and numerous CSPs made it necessary to reassign the spectra of the CypD-CL1 complex, the decrease in signal intensity made it very difficult to collect NH detected 3D experiments. Without these 3D spectra it is extremely difficult and time consuming to assign the signals. Therefore triple selective labeling was used to get the assignments of the N and the H^N resonances in the complex, which are needed for the determination of the CL1 binding position.

The general concept of the used labeling scheme was based on earlier published work (Löhr 2015) but was expanded to label much more amino acid types. This approach was combined with time shared experiments to shorten the needed experimental time (Löhr 2014). The used approach was based on three different samples. The cell free expression of the samples was very useful in this case, because inhibitors suppressing the isotope scrambling between the amino acids can be used. Only a few issues remain: the scrambling of glutamine to glutamate and asparagine to aspartate can be suppressed by using a tenfold excess of the corresponding glutamate/aspartate species. For cost reasons this is mainly applied when Glu/Asp were unlabeled. The other way around the scrambling is less efficient. Using an excess of Gln/Asn however dilutes the Glu/Asp signal below the detection limit and can therefore not be used (data not shown). Inhibitors like 6-diazo-5-oxo-L-norleucine or methionine sulfoximine are described to suppress this scrambling (Su 2011), how-

ever in this study they were found to be ineffective. The triple selective labeling allowed to assign the whole CypD-CL1 complex and revealed that some signals are not visible in the complex. This assignment would have been very complicated without this method.

In general the gathered information about the binding position of CL1 is in accordance with the data derived from the crystal structure. Key residues that show interaction between CypD and CL1 show strong CSPs in the NMR analysis. Therefore the binding mode seems to be identical in solution as well as in the crystal. Besides this determination of the binding site it was interesting to characterize the potential conformational change induced by the ligand. Again the problem of sensitivity using NH detected experiments made it necessary to use a HCCH TOCSY for sidechain assignment.

5.2.5. Automated assignment of the CypD-CL1 complex

The assignment of the CypD-CL1 complex was performed using automated signal assignment. For the automated assignment the FLYA algorithm was used (Schmidt 2012). The N and H^N resonances were all assigned using the triple selective labeling. In addition some C^α and some C^β shifts were extracted from a HNCA, a HNCACB and a HN(CO)CACB spectrum. These spectra contained only a subset of the expected peaks, and could only be efficiently used because the N and H^N resonances were already assigned. Due to the severe signal overlap in the HCCH TOCSY the manual assignment would have taken a long time, which was substantially decreased using the automated assignment. The parameters of the assignment were optimized by Dr. Sina Kazemi. The quality of the assignment was scored according to the amount of strong assignments as indicated by FLYA. To support the automated assignment all manually assigned resonances were set as fixed. The assignment was performed using this input in combination with the BMRB statistics. To improve the results gathered with these settings the resonance list of the manual CypD apo assignment was used as an input. This approach was chosen, because on the ^{13}C level, only a few signals showed CSPs, while many signals did not change compared to the apo state. The apo resonances were used as a statistic for the assignment in combination with different allowed deviations from this statistic. The standard deviation was varied from 0,1 to 1. The best results, that means the most strong assignments, were achieved when using a very low standard deviation of 0,1 from the apo shifts. The graphical summary of the automated assignment (figure 32) shows that most resonances could be assigned strong while nearly all manually assigned N, H^N, C^α and C^β shifts were confirmed by FLYA. Interesting are the C^α shifts of Gly109 and Ser110, because these are not in accordance with the automated assignment, although FLYA rates its own assignment as weak. Other interesting signals are the C^β shifts of Pro58, Phe60 and Gln63, because these are considered strong by FLYA and contradict the manual assignment. It should be noted that this area gives only very weak signals in the HN detected experiments, which could lead to artifact peaks in the HNCA and HNCACB type experiments and therefore to disturbances in the manual assignment. The respective signals should be revisited.

5.2.6. Structure calculation of the apo and the complex form

The structure calculation of CypD was performed using CYANA and automated NOE assignment. The calculation was based solely on NOE restraints. Although the overall amount of NOE restraints is high some regions are less covered than others. Especially the core region below the active site seems to include only few long range restraints. For this calculation the ^{13}C NOESY of the aromatic region was needed to get a compact structure. The final calculated structure was minimized using the OpalP forcefield. The structure shows basically the same fold as the reference crystal structure. The eight stranded β-sheet and the adjacent α-helices overlap very well, showing

that the well structured main part of the protein is identical in both structures. Interestingly the loops around the active site, especially the region from Asp66 to Asp85, show some significant deviation from the crystal structure. While the loop structure itself is well defined by a set of NOE restraints and potential hydrogen bonds, the loop position relative to the core deviates. This might be either a result of missing NOE restraints, or these loop regions are rather flexible in solution. Due to the large amount of NOE restraints it seems more likely that the loops are flexible in the native structure. This might be due to the need to fit a variety of different peptides from different substrate proteins in the active site, which would not be possible with a rigid peptide binding pocket. Therefore the flexible loops could support an induced fit mechanism for a broad range of substrates. The movement of the loop upon ligand binding is supported by the CSP data gathered for CL5 and CL7 (figure 24 B,D). Both ligands cause large CSPs in the loop region around Asn102, which could be explained with a ligand induced loop motion, as part of an induced fit mechanism. This finding questions the results seen by x-ray crystallography where the structure is nearly unchanged independent of the co-crystallized ligand. This view of a rock solid protein might be due to constraints of the crystal lattice forcing the protein in the seen conformation.

After the determination of the apo structure, the complex form was analyzed. The structure calculation was again solely based on NOE restraints. The NOE assignment was done automatically and based on three different 3D NOESY spectra. The resonances were taken from the automated assignment done with FLYA. The automatic NOE assignment assigned again a large number of NOE restraints. Still the structure calculation did not converge into a defined bundle. While half of the protein including four β-strands and the two core α-helices was well folded, the other half including the other four β-strands and the active site are largely disordered. The defined structure elements diverged from the reference crystal structure, but showed essentially the same fold. This suggests that the assignment of the signals is correct. A closer analysis of the used upper limit restraints showed that the reason for the missing folding is due a lack of NOE crosspeaks in the respective area. The signals of the active site residues are not visible, because they are very broad and disappear in the noise. This result is unexpected, because a conformational change would have resulted in a defined structure with a NOE pattern that differs from the apo structure. Instead a severe signal broadening and a structural state that is not defined by the NMR results is visible.

5.2.7. Dynamic motions occurring in CypD

The described findings do not support the hypothesis of a static conformational change. Instead the results fit better to dynamic changes in the protein. In NMR experiments there are three important time regimes in which changes can happen (Bain 2003). If two states are interconverting on timescales that are much slower than the shift difference between the two states, they are in slow exchange. This is characterized by two separated and sharp signals at the corresponding resonances of the two states. If the interconversion is on timescales that are much faster than the shift difference between the states, they are in fast exchange. This is characterized by a single sharp peak that is between the resonances of the two states. The exact position is determined by the distribution between the two populations. If both states are distributed equally the peak will appear in the middle of the two resonances for example. In the case that the interconversion between the two states is in the same time range as the shift difference the two states are in the intermediate exchange regime. The intermediate exchange is characterized by a largely broadened signal that is usually distributed between the two states. This exchange regime leads to sensitivity issues in the spectra, because the broad peaks have a bad signal to noise ratio. In the light of these exchange regimes it appears that the signal broadening might be due to an exchange between different states.

An analysis of the peak intensities shows that the signals get significantly broadened upon addition of CL1. In agreement with the observations during structure calculation the area around the

active site is mainly affected by this signal broadening. This suggests that specifically the active site is converting between different states in the intermediate exchange regime.

According to the SPR results, CL1 has a k_{off} rate of 0.12 s^{-1} at 25°C, which would translate in a complex half life time of ca. 6 seconds. This residence time would be in the slow exchange regime. This observation is supported by ligand titration experiments, which show a stepwise disappearance of the apo signals and a stepwise appearance of the complex signals, which is indicative for slow exchange. In summary the inhibitor is not binding in the intermediate exchange as suggested by the signal line broadening observed upon ligand binding.

Therefore the protein needs to undergo conformational changes on a timescale that corresponds to intermediate exchange. If the protein motions were in the intermediate exchange the signal would be dependent on the field strength used for the measurement as well as the temperature.

To investigate this, ^{15}N,^{1}H HSQC spectra were recorded at 500 MHz and at 900 MHz as well as at temperatures between 273 K and 303 K. As presented in figure 37 the signals change in a field dependent manner. When using higher field some of the signals split in two defined signals of approximately equal intensity. It is important to note that none of these split peaks are at the position of the apo spectrum, proving that the protein is saturated with ligand and the peak splitting is not due to a ligand bound and an unbound species. This suggests that the protein itself is oscillating between two different conformations. The measurement at higher field leads to a larger shift difference between the two single states. Since the exchange regime depends on the exchange rate in comparison to the shift difference, the higher field shifts the exchange regime towards the slow exchange regime. The appearance of two signals speaks for the existence of two different states. As an exception of this observation the signals of Ile57, Phe83 and Ala103 split in at least four different signals, suggesting more complex dynamics than just a two state model. In addition some signals are temperature dependent. Due to larger shifts produced by the temperature change not all signals could be assigned at 273 K. The signal of Ile57 is of special interest because it is isolated and can therefore be easily assigned. In addition to the splitting in four peaks at 303 K the signal splits in at least seven peaks when the temperature is lowered to 273 K.

A revision of the apo protein under the same conditions shows no signal splitting or temperature effects. This leads to the conclusion that the different states are induced by the ligand binding.

5.2.8. The working model of the CypD-CL1 complex

In summary different key points can be observed. As presented before the CypD-CL1 complex exhibits dynamics in the intermediate exchange regime. Because the ligand binding is in the slow exchange regime these dynamins have to be protein motions. The signals that show the most exchange broadening are located around the active site of the protein suggesting that the active site is involved in these motions. The field dependent peak splitting suggests an oscillation between two states. The proline like moiety in CL1 can be present in the *cis* and the *trans* conformation and shows uncatalyzed exchange between these conformations in solution (data not shown)

These observations lead to the model that CypD is able to catalyze the *cis/trans* isomerization of the proline like moiety in CL1. This leads to the effect that CypD is constantly undergoing the active cycle and the connected conformational changes. From the field dependent peak splitting it can be speculated that the protein adopts two different conformations during the active cycle and these conformations are populated equally. In contrast to natural peptide ligands, CL1 stays attached to the active site is not released after successful isomerization. A sampling of these different conformations is not observed in CypD apo suggesting that the conformational change is induced by the binding of a suitable ligand.

5.2.9. Comparison of the model to published data

The presented model of CypD undergoing catalysis in a two state model is supported by a recent publication of Chi et al. (Chi 2015). The authors investigated the protein dynamics in cyclophilin A (CypA) a close family member of CypD. They show two different NMR structures of CypA representing two relevant conformations in the catalytic cycle. They managed to calculate two structures from one dataset using the recently developed exact NOE (Vogeli 2012; Vogeli 2014). They claim that the protein motion during catalysis has an effect on a whole network of residues that change in an orchestrated way to enable the needed conformational changes. This network comprises most amino acids around the active site and even reaches out to the neighboring residues (Eisenmesser 2005; Chi 2015). They describe large scale motions of the active site loop (residues 64-74) which is involved in an induced fit mechanism. The behavior of the active site loop is in good agreement with the data presented in this thesis. The amino acids 64-74 show large CSPs upon ligand binding (figure 29) and a severe line broadening in the complex (figure 34) which supports the described involvement in ligand binding and the flexibility of the loop. In addition they report some residues that are important for ligand binding like His54, Phe60, Gln111, Phe113, Trp121 and His126, as well as side chains essential for activity like Gln63, Ser99, Phe113 and Arg55 (Chi 2015). These residues are also identified in CypD to be involved in the dynamics as seen by the CSPs upon ligand binding (figure 29) and the line broadening in the spectra (figure 34). In addition some of the signals that are close to these residues like Ile114, Arg55, Ser59 and Gly109 show a splitting of the signal which is indicative for two different structures (figure 37). It was also reported, that CypA is sampling these conformation even in the apo state (Fraser 2009; Chi 2015). This observation is not reflected in the gathered CypD data. Although also in the CypD apo sample some of the signals are broadened in the spectra, which might be due to dynamic exchange, the data do not support the presence of multiple different conformations. In this case relaxation dispersion experiments could reveal a second "hidden" state that is either very short-lived or only minor populated and might therefore be invisible in the used experiments. Le Maire et al. performed room temperature crystallography on CypD and do not report two different conformations (le Maire 2011), supporting the hypothesis that CypD apo is not sampling the different conformations in the same way as CypA.

Fraser et al. measured the dynamic motions in CypA by relaxation dispersion and describe them to be around 60 s^{-1} (Fraser 2009). This would perfectly fit with a motion in the intermediate exchange regime under the conditions we applied for the CypD measurements and supports therefore the hypothesis that the seen motion is indeed the exchange in the catalytic cycle of the protein. In summary the findings with CypA are very similar to the data gathered for CypD and support the model of CL1 stimulating the active cycle in CypD while blocking the active site for other substrates.

This finding leaves the question why the crystal structure of the CypD-CL1 complex (4J5B) shows only minor differences to the apo structure (3QYU). Fraser et al used room temperature crystallography to be able to see multiple sidechain positions in one crystal, which were invisible under cryo conditions (Fraser 2009). For Cyp it might also be true, that either the crystal lattice or the cryo conditions force the protein in the state that is seen in the structures, while the second conformation might be the energetically disfavored transition state of the catalysis.

5.2.10. Outlook on the CypD project

The CypD-CL1 complex system is a very interesting system for structural investigations of the CypD and its catalytic activity. CL1 enhances or induces large scale motions in CypD that are believed to represent the catalytic cycle. These motions and conformational changes could now be characterized using relaxation dispersion experiments or room temperature crystallography in

order to allow the population of both conformations. One of the drawbacks of the system is the motion in the intermediate exchange regime in the NMR experiments, leading to line broadening and bad signal to noise. Here mutations that influence the dynamics would be very helpful in order to move the dynamics to another timescale to improve the NMR conditions. Fraser et al describe that the S99T mutant in CypA slows down the protein dynamics (Fraser 2009). Due to the high homology between CypA and CypD this mutation could serve the same purpose in CypD. In addition the experiments could be expanded to a more detailed ligand observed analysis during catalysis, identifying the structural features of the ligand that are involved in the process. This information could be very valuable for a further ligand design, because it could be exploited to trap certain states of the protein or to induce a certain conformation.

6. Appendix

Table 7: Assignment table for CypD apo
All assignments were done manually.

Residue		N	H	CA	HA*	CB	HB*	CG	HG*	CD	HD*	CE	HE*
SER	1	117.9	8.51	58.2	4.52	64	3.9						
GLY	2	111.1	8.55	44.8	3.97								
ASN	3	122.1	8.38	51.2		37.9							
PRO	4			63.2	4.7	33	2.30/1.74	27.1	2.15/2.14	50.9	4.15		
LEU	5	121.4	8.54	53.2	5.55	44.8	1.72	26.8	1.91				
VAL	6	115.2	9.15	58.3	5.42	35.4	2.67		1.14/0.93				
TYR	7	116.6	8.72	55	6.19	42.8	2.80/2.56				6.58		6.43
LEU	8	116.3	9.01	53.8	4.76	45.1		26.2					
ASP	9	126	9.19	54.5	5.66	41.9	2.59						
VAL	10	118.9	8.14	60.2	5.56	35.3	1.75						
ASP	11	127.3	9.54	52.9	5.22	45.3	2.31						
ALA	12	118.6	8.64	50.2	5.08	21.6	0.78						
ASN	13	125.9	9.34	53.7	4.46	37.4	3.39/2.62						
GLY	14	104	8.83	45.7	4.12/3.71								
LYS	15	122.2	7.73	52.5		33.2							
PRO	16			64.1	4.6	32.4	2.36/1.90	27.6	2.12	51.1	4.01/3.71		
LEU	17	122.7	9.8	54.8	4.57	43.6	1.71	25.9	1.41		0.96/0.77		
GLY	18	104.9	7.69	44.1	4.65/3.73								
ARG	19	121.4	8.32	54.7	5.56	34.3	1.6	27.4		43			
VAL	20	126.6	9.55	61	4.61	34.4	2.07						
VAL	21	126.8	8.92	61.7	4.99	33.5	1.92		1.00/0.88				
LEU	22	128.9	9.64	53.5	4.95	43.1	0.96		1.59				
GLU	23	122.6	8.64	54.8	4.97	31.7	1.7	36.9	2.08/1.76				
LEU	24	124.6	8.51	52.1	4.88	42.9	2.02/1.31	26.9	1.25				
LYS	25	125.2	8.9	53.7	4.53	27.7	1.66/1.58	23.4	1.36/1.25		1.9	41.6	2.92/2.83
ALA	26	128.6	8.19	54.1	3.73	18.8	1.48						
ASP	27	114.1	9.04	55.1	4.24	38.4	2.84/2.74						

Residue		N	H	CA	HA*	CB	HB*	CG	HG*	CD	HD*	CE	HE*	CZ	HZ*
VAL	28	119.9	7.62	63.9	4.2	35.4	1.93		1.12/0.99						
VAL	29	113.7	8.27	57.6		31.7									
PRO	30			66.1	4.39	31.4	2.65/1.99	27.5	2.1	50.9	3.61/3.07				
LYS	31	122.6	10.79	60.2	4.06	31.6	1.71/1.43	26	1.39/1.21	29.2	1.49/1.39	41.9	2.67/2.60		
THR	32	124.7	10.35	67.5	3.98	68.7	4.16		0.85						
ALA	33	125.6	9.27	56	4.12	18.6	1.46								
GLU	34	117.5	8.04	58	4.5	28.2	2.27/1.73	33.7	2.49/2.02						
ASN	35	115	7.11	56.6	4.02	39.6	2.87/2.33								
PHE	36	117.3	7.06	61.9	4.05	40.3	3.21/3.14				7.17		6.99	128.9	5.9
ARG	37	119.2	8.9	60.6	3.62	30.3	1.84	24.5		41.3					
ALA	38	118.1	8.44	54.1		18.1	1.22								
LEU	39	122.2	7.95	57.2	3.81	40.9		26.6	0.91		0.56/0.91				
CYS	40	120.1	7.91	63.6	4.44	27	3.31/2.15								
THR	41	107.1	8.03	63.4	4.17	69.2	4.47		1.32						
GLY	42	108.2	7.8	45.7	3.84/3.55										
GLU	43	118.5	8.01	58.5	4.14	30.1	2.22/2.04	35.3	2.10/1.80						
LYS	44	118.7	9.15	54.3	4.32	30.3	1.66/0.93	24.9	1.08/1.03	27.5	1.46	42.2	2.85/2.68		
GLY	45	105.6	7.97	44.6	4.34/3.58										
PHE	46	113.8	6.41	54.2	4.65	39.5	3.15/2.70				6.64		7		
GLY	47	104.7	7.72	45.8	4.28/2.76										
TYR	48	113.2	6.86	57.7	4.37	38.7	3.11/3.06								
LYS	49	124.5	8.46	61	3.75	31.6	2.04	25.4	1.36	30	1.98/1.83	42.2	3.31/3.11		
GLY	50	117.9	9.74	45.5	4.47/3.65										
SER	51	116.4	8.58	58.5		64.8									
THR	52	107.1	9.61	61.4	5.89	73.5	4.34		1.24						
PHE	53	120.8	8.46	57.4	4.9	38.9					6.9		6.97	128.7	7.43
HIS	54	119.8	7.43	56.9	4.75	31.8	3.27/2.78				6.82				
ARG	55	124	6.8	54.8	4.96	32.5	1.05	28.2		43.4	3.17/2.99				

Residue		N	H	CA	HA*	CB	HB*	CG	HG*	CD	HD*	CE	HE*	CZ	HZ*
VAL	56	128.8	9.38	61.9	4.5	35.2	1.82		1.10/0.76						
ILE	57	127.7	8.62	57.4		40.8									
PRO	58			62.8		32.3		27.1		52.3					
SER	59	115	9.69	59	3.87	61.6	4.15/4.03								
PHE	60	114.7	7.59	57.2	5.05	38.3	3.27/2.99				7.22		7.21		
MET	61	112.1	8.15	54.8	5.19	35.2		28.4	1.03/0.78						
CYS	62	115.4	8.47	56.8	4.84	30.2	3.15/2.73								
GLN	63	127.8	9.46	54.9		30.8		33.6	2.57/2.05						
ALA	64	126.2	8.01	50.2		22.4									
GLY	65	103.9	8.4	47.1	4.04/2.83										
ASP	66	124.5	10.09	51.5		38.8									
PHE	67	115.7	6.63	56.1		39									
THR	68	109.8	7.35	62	4.55	68.7	4.04		0.74						
ASN	69	120.5	8.66	52.8		39.4									
HIS	70			57.4		28.5					6.77				
ASN	71	112.6	7.62	52.6		38.9									
GLY	72	110.8	9.73	45.2	4.66/3.39										
THR	73	112.5	8.02	62.6	4.46	70.9	4.27		1.09						
GLY	74	113.3	8.62	45.5	4.50/3.57										
GLY	75	109.4	8.1	43.2											
LYS	76	115.7	7.03	56	4.63	34.6	1.89/1.56	23.4	0.87	29.4	1.18	41.2	2.15		
SER	77	114.6	7.81	56.8	5.24	69.6	4.27/4.26								
ILE	78	111.7	8.65	63.7	4.23	37.3	1.71		0.72		0.47				
TYR	79	120.7	8.11	56.2	4.74	38.9	3.44/2.36				6.44		6.13		
GLY	80	106.7	7.17	44											
SER	81			62.8											
ARG	82	115.7	7.92	53.7	5.58	34.3	1.55	26.9	1.54/1.47	43.5	3.18/2.90				
PHE	83	118	9.17	55		39.5					7.32		7.58		

Residue		N	H	CA	HA*	CB	HB*	CG	HG*	CD	HD*	CE	HE*	CZ	HZ*
PRO	84			62.6	4	32.9	2.25/1.69	27.4	1.98/1.92	52					
ASP	85	119.8	8.8	54.8		40.9									
GLU	86	132.1	9.37	60.3	3.8	31.5	2.23/1.80	35	2.40/2.32						
ASN	87	107	7.05	52.9	4.12	39.6	3.38/2.74								
PHE	88	113.2	8.34	56	6.01	38.4	3.57/2.56								
THR	89	118.2	8.57	66.8	3.74	68.9			1.18						
LEU	90	119	8.16	54.5	4.46	40.8	1.51	27.3	1.81		0.83/0.91				
LYS	91	118.6	8.32	54.2	4.69	34.3	2.22/1.62	25.5	1.49/1.42	28.2	1.64/1.57	42.7	3.05		
HIS	92	123.5	10.91	56.9		25.9	3.10/2.86				6.6				
VAL	93	113.9	7.05	63.4	4.01	32.8	2.36		0.99/0.84						
GLY	94	105.7	7.32	45.7											
PRO	95			62.5		32		27.5		49.8					
GLY	96	109.9	9.04	44.9	4.49/3.26										
VAL	97	119.7	6.66	64.5	3.63	33.7	2.04		1.39/0.97						
LEU	98	129.9	7.38	53.1	4.83	44.2		25.7	-0.04		-1.5625				
SER	99	121.1	8.31	55.4	5.23	65									
MET	100	123.4	8.57	53.7		31.2		31.9							
ALA	101	126.5	8.25	51.9		19.9	1.39								
ASN	102	113.8	8.47	54.3	4.6	40.4									
ALA	103	123.3	8.87	50.3	4.81	19.2	1.32								
GLY	104	109.3	8.2	43.5											
PRO	105			64	4.38	32.1	2.33/1.82	27.8	2.14/1.98	49.3	3.64/3.52				
ASN	106	118.8	8.97	54.5	4	37	3.11/2.66								
THR	107	110.8	10.4	60.3	4.41	68.9	4.42		0.9						
ASN	108	120.2	7.13	55.7	4.25	39.7	1.54/0.98								
GLY	109	111	9.21	46	4.61/3.65										
SER	110	117.3	8.92	57.7	4.77	66.2									
GLN	111	124.9	8.52	57.8	5.3	32.1		35.7	1.87						

Residue		N	H	CA	HA*	CB	HB*	CG	HG*	CD	HD*	CE	HE*	CZ	HZ*
PHE	112	119	8.81	55.3	5.91	43.1	3.36/3.26				6.83		7.81	128.8	6.81
PHE	113	115.2	9.74	54.9	5.73	43.9	2.74				6.75		6.84		
ILE	114	117.5	8.79	59.2	5.05	40.8	1.6		0.76		0.97				
CYS	115	125.6	9.14	60.4		29.2	3.71/2.98								
THR	116	113.7	8.89	61.1	4.42	67.5			0.82						
ILE	117	118.3	7.64	59.8	4.38	44.1	1.81		0.96		1.13				
LYS	118	121	8.33	57.4		33.1	2	24.6	1.66	29.9	1.77	42	3.04/3.01		
THR	119	121.4	7.86	57.1	3.55	68			1.06						
ASP	120	121.7	8.43	56.4	4.2	39.7	2.90/2.70								
TRP	121	118.5	7.4	59.9	4.69	26.9	3.40/3.35				7.05		7.8		7.41/6.80
LEU	122	120.1	7.15	54.3	4.3	38.9	1.31	38.9	0.27		0.44/0.85				
ASP	123	122.9	7.59	55.9	5.24	39.3	2.75								
GLY	124	111.6	9.54	45	3.92/2.87										
LYS	125	115.7	7.9	56.4	4.15	35.3	1.84	25.2	1.27/1.23	29.3	1.69	42.4	3.02		
HIS	126	119.3	7.56	54.9	3.97	31.8	3.24				6.91				
VAL	127	124.7	8.6	63.8	4.21	33.3	2		1.00/1.14						
VAL	128	133.6	9.7	62.9	4.1	30.9	1.68		0.80/-0.00						
PHE	129	117.7	8.27	55.2	5.13	42	3.10/2.51				6.62		7.52	131.6	6.08
GLY	130	107.4	7.31	46.9	4.11/4.04										
HIS	131	119.1	8.51	55.5	5.12	34.7	3.12/2.82				6.95				
VAL	132	122.8	8.72	64.2	3.94	32.4	1.96		0.95/0.74						
LYS	133	132.2	9.65	56.6	4.51	35.1	1.71/1.67	25	1.58/1.52	29	1.78/1.67	42	3.03		
GLU	134	115.7	7.95	55.1	4.77	33.6	2.13/1.78	36	2.29/2.18						
GLY	135	109	8.9	46.3	4.94/4.17										
MET	136	122.6	9.06	56.7	4.53	29.8	2.05	33.1	2.77/2.64						
ASP	137	116.8	9.19	56.8	4.23	38.9	2.75/2.59								
VAL	138	124.2	7.48	66.1	3.39	30.9	2.4		1.03/0.56						
VAL	139	120.9	7.58	66.9	3.3	30.9	2.56		1.05/0.75						

Residue		N	H	CA	HA*	CB	HB*	CG	HG*	CD	HD*	CE	HE*	CZ	HZ*
LYS	140	117.3	8.19	58	4.15	30.2	1.66	24.3	1.67/1.57	26.9	1.69/1.60	41.3	2.96/2.88		
LYS	141	121	7.56	59.5	3.96	32.7	2.14/1.90	25.5	1.75/1.49	30.1	1.67	42.3	2.92		
ILE	142	121.1	8.16	67	3.33	38	2.05		0.47		0.06				
GLU	143	117.7	8.27	58.7	3.51	30.6	1.76	36.7	2.14						
SER	144	113.5	7.35	60.8	4.15	62.9	3.71								
PHE	145	119.8	7.73	57.5	5	39.2	3.57/2.99						7.27		
GLY	146	105.4	7.85	44.3	4.48/3.66										
SER	147	110.3	8.29	58		66.4									
LYS	148	121.5	9.08	60.2											
SER	149	109.8	8.15	59.2	4.41	64.5	4.14/3.99								
GLY	150	113.4	8.12	44.4	4.25/3.88										
ARG	151	119.4	7.38	56.7	4.45	30.6	1.75	27.3	1.75/1.67	43.3	3.26				
THR	152	116.5	8.84	59.8	5.48	71.4	4.6		1.31						
SER	153	116.7	9.52	59	4.42	63.5	4.19/4.04								
LYS	154	118.2	7.39	54.2	4.44	38	1.26	26	0.8	29.6	1.03	42.5	2.92/2.84		
LYS	155	122.7	8.47	56.8	4.23	32.2	1.88/1.77	25	1.44/1.21	29.4	1.65	41.9	2.90/2.84		
ILE	156	133.8	9.39	59.5	5.13	37.5	2.36		0.82		0.77				
VAL	157	128.3	8.69	61.4	4.51	35.6	2.14		0.82/0.76						
ILE	158	126	9.06	60.7	4.71	37.1	2.07		0.91		0.71				
THR	159	125.6	8.85	64.3	3.95	68.9	4.01		1.23						
ASP	160	115.3	8.12	53.4	4.96	44.7	2.96/2.92								
CYS	161	115.5	8.23	55.1	4.52	30.7	3.05								
GLY	162	101.6	6.57	45.5	3.84/3.37										
GLN	163	120.9	9.16	54.8	5.06	30.8	1.95/1.64	33	2.60/2.46						
LEU	164	127.3	9.17	55.6	4.55	43.5	1.67	27.4	1.66		0.89/0.77				
SER	165	120.4	8.15	60		64.4									

Table 8: Assignment table for CypD in complex with CL1

All NH assignments were obtained manually. The carbon assignments were produced by an automated signal assignment using FLYA.

Residue		N	H	CA	HA*	CB	HB*	CG	HG*	CD	HD*	CE	HE*	CZ	HZ*
SER	1	118,2	8,4	58,5	4,53	64	3.90/3.90		4,84						
GLY	2	111,1	8,47	44,8	3.98/3.98										
ASN	3	122,1	8,31	51,1	5,12	38	2.66/3.54				8.01/8.39				
PRO	4			63,2	4,7	32,9	1.74/2.32	27,1	2.19/2.19	51	4.03/4.17				
LEU	5	121,2	8,51	53,2	5,55	44,9	1.91/1.91	27	1,72		0.89/0.90				
VAL	6	115,2	9,13	58,3	5,4	35,4	2,69		0.93/1.13						
TYR	7	116,5	8,71	55	6,19	42,8	2.57/2.80				6.57/6.57		6.43/6.43		
LEU	8	116,2	8,97	53,6	4,95	45	1.39/1.92	26,4	0,92		0.89/0.92				
ASP	9	125,9	9,15	54,4	5,66	41,9	2.60/2.62								
VAL	10	118,8	8,1	60,2	5,52	35,3	1,74		0.87/0.90						
ASP	11	127,1	9,45	52,9	5,23	45,3	2.29/2.29								
ALA	12	119,1	8,63	50	5,08	21,6	0,76								
ASN	13	125,7	9,31	53,8	4,46	37,4	2.64/3.38				7.97/8.11				
GLY	14	104,2	8,81	45,7	3.69/4.13										
LYS	15	122,2	7,72	52,5	4,9	33,1	1.85/1.94	24,7	1.38/1.50	29,1	1.73/1.73	42,2	3.04/3.04		7,74
PRO	16			63,9	4,57	32,5	1.89/2.36	27,6	2.06/2.14	51,2	3.73/4.03				
LEU	17	122,6	9,71	54,7	4,57	43,5	1.67/1.68	26	1,41		0.75/0.94				
GLY	18	104,8	7,66	44,1	3.73/4.64										
ARG	19	121,3	8,23	54,7	5,56	34,4	1.60/1.61	27,2	1.60/1.60	43	3.13/3.34		8,32		
VAL	20	126,5	9,52	61,1	4,58	34,4	2,07		0.94/0.95						
VAL	21	126,8	8,89	61,8	4,99	33,4	1,94		0.89/1.00						
LEU	22	129	9,63	53,4	4,94	43,2	0.94/0.94	26,8	1,53		0.68/0.74				
GLU	23	122,6	8,66	54,8	4,96	31,7	1.71/1.71	36,9	1.76/2.10						
LEU	24	124,6	8,45	52,3	4,88	43	1.33/2.01	27	1,27		0.55/0.55				

Residue		N	H	CA	HA*	CB	HB*	CG	HG*	CD	HD*	CE	HE*	CZ	HZ*
LYS	25	125	8,9	53,8	4,52	27,4	1.59/1.67	23,5	1.26/1.36	27,5	1.91/1.91	41,6	2.84/2.91		6,96
ALA	26	128,6	8,18	54,1	3,74	18,8	1,49								
ASP	27	114,1	9,06	55,2	4,25	38,6	2.74/2.84								
VAL	28	119,6	7,59	63,8	4,22	35,3	1,94		1.00/1.12						
VAL	29	114,1	8,23	57,7	4,59	31,6	2,58		1.00/1.21						
PRO	30			66,1	4,4	31,4	2.00/2.64	27,4	2.00/2.10	50,8	3.09/3.62				
LYS	31	122,5	10,76	60,1	4,08	31,6	1.45/1.72	26	1.22/1.42	29,2	1.42/1.50	42	2.62/2.68		10,79
THR	32	124,6	10,37	67,5	4,02	68,7	4,17		0.88/2.58						
ALA	33	125,7	9,27	56	4,15	18,7	1,48								
GLU	34	117,6	8,03	58,3	4,52	28,2	1.75/2.29	33,6	2.04/2.49						
ASN	35	114,8	7,17	56,7	4,03	39,7	2.33/2.88				7.16/7.17				
PHE	36	117,6	7,14	62	4,08	40,4	3.15/3.29				7.13/7.14		6.99/7.00	128,9	5,81
ARG	37	118,9	8,81	60,6	3,65	30,1	1.85/1.95	24,4	0.94/1.66	41,3	2.85/2.95		4,84		
ALA	38	118,3	8,4	54,2	4,1	18,3	1,24								
LEU	39	121,9	8,02	57,1	3,86	41,3	1.57/1.57	26,6	0,92		0.59/0.92				
CYS	40	120	7,92	63,6	4,48	27	2.17/3.32		0,94						
THR	41	107,1	8,02	63,5	4,15	69,1	4,47		1.33/3.84						
GLY	42	108,2	7,77	45,6	3.52/3.84										
GLU	43	118,6	8,01	58,5	4,14	30	2.06/2.22	35,3	1.81/2.10						
LYS	44	118,7	9,09	54,2	4,32	30,3	0.93/1.65	24,9	1.05/1.07	27,5	1.46/1.46	42,1	2.69/2.85		4,83
GLY	45	105,6	7,95	44,7	3.56/4.32										
PHE	46	113,7	6,37	54	4,62	39,5	2.67/3.12				6.64/6.64		6.97/6.97	130,5	7,46
GLY	47	104,5	7,54	45,8	2.72/4.31										
TYR	48	112,7	6,74	58,6	4,3	39,4	3.00/3.12				6.64/7.10		6.79/6.86		
LYS	49	123,7	8,27	60,8	3,74	31,7	1.98/1.99	25,1	1.37/1.39	30,1	1.82/1.95	42,2	3.12/3.28		4,94
GLY	50	117,7	9,74	45,5	3.64/4.45										

Residue		N	H	CA	HA*	CB	HB*	CG	HG*	CD	HD*	CE	HE*	CZ	HZ*
SER	51	116,4	8,65	58,6	4,96	65,4	4.29/4.29		4,95						
THR	52	107,5	9,24	61	5,73	73	4,3		1.27/4.30						
PHE	53	120,6	8,39	57,6	4,98	39,3	1.88/3.00				6.90/6.91		6.97/7.05	128,7	7,45
HIS	54	120	7,35	56,8	4,97	31	2.78/3.12				6.86/6.86		6,94		
ARG	55	122	6,72	54,9	4,96	32,6	0.98/1.13	28,2	1.66/1.66	43,4	2.98/3.14		9,14		
VAL	56	129,4	9,23	62	4,51	35,1	1,82		0.75/1.09						
ILE	57	126,8	8,55	57,4	5,17	41	1,86		1.14/1.53/ 1.63		1,14				
PRO	58			62,5	4,36	32,8	1.71/2.26	27,4	1.91/2.01	51,8	3.75/3.84				
SER	59	114,8	9,6	59	3,85	61,7	3.97/4.07		9,61						
PHE	60	113,8	7,44	56,9	4,96	37,3	3.08/3.39				7.11/7.11		7.15/7.15	129,9	6,54
MET	61	112,3	8,2	54,5	5,13	35	1.61/2.69	28,2	0.95/0.95			20,3	1,14		
CYS	62	114,9	8,49	56,7	4,96	30,7	2.80/3.09		0,75						
GLN	63	128,4	9,41	55	4,52	30,7	2.32/2.55	33,4	2.04/2.48				7.17/7.17		
ALA	64	125,8	8,1	50,5	4,85	23,2	0,87								
GLY	65	102,6	7,7	47,2	2.74/4.02										
ASP	66	123,6	9,94	51,6	4,22	39	2.59/2.99								
PHE	67	116,2	6,35	55,7	4,56	39	2.60/3.96				7.09/7.10		7.06/7.45	130,4	5,88
THR	68	110,2	7,36	62,2	4,57	68,7	4,04		0.75/7.36						
ASN	69	121	8,79	52,8	4,14	39,3	2.77/3.42				8.08/8.56				
HIS	70	112,1	6,6	57,3	4,51	28,3	3.12/3.28				7.53/6.72		5,81		
ASN	71	112,4	7,51	52,8	4,14	39,4	2.77/3.55				7.30/8.56				
GLY	72	108	9,47	45,6	3.37/4.56										
THR	73	112,1	7,95	62,3	4,56	71,3	4,32		1.10/1.10						
GLY	74	111,6	8,15	45,6	3.43/4.57										
GLY	75	110	8,11	43,3	3.57/4.66										

Residue		N	H	CA	HA*	CB	HB*	CG	HG*	CD	HD*	CE	HE*	CZ	HZ*
LYS	76	115,1	6,86	55,9	4,65	35	1.55/1.84	23,4	0.85/0.96	29,5	1.15/1.15	41,1	2.12/2.12		7,18
SER	77	114,3	7,71	56,6	5,32	70,1	4.25/4.25		7,13						
ILE	78	112	8,65	63,9	4,21	37,3	1,74		0.73/-0.39/1.23		0,49				
TYR	79	120,5	8,08	56,1	4,76	39	2.38/3.46				6.43/6.43		6.15/6.15		
GLY	80	106,2	7,12	43,7	3.90/5.12										
SER	81	114,3	7,7	62,9	4,1	62,9	3.98/4.10		3,99						
ARG	82	114,2	7,74	53,4	5,66	34,4	1.59/1.68	26,3	1.48/1.49	43,4	2.98/3.14		4,37		
PHE	83	117,6	9,03	55,1	5,18	39,4	3.00/3.12				7.32/7.32		7.61/7.61	132,8	6,43
PRO	84			62,6	4	32,8	1.71/2.26	27,4	1.92/2.00	51,9	3.75/3.84				
ASP	85	119,9	8,77	54,8	4,16	40,8	1.93/2.40								
GLU	86	132,3	9,36	60,4	3,8	31,6	1.82/2.25	34,9	2.32/2.40						
ASN	87	106,9	7,08	52,9	4,14	39,5	2.77/3.42				7.08/8.36				
PHE	88	113,1	8,31	56,1	6,02	38,4	2.60/3.57				7.29/7.29		6.51/7.29	130,4	5,88
THR	89	118,2	8,56	66,8	3,76	69,1	3,76		1.20/8.59						
LEU	90	118,9	8,16	54,5	4,48	40,9	1.50/1.50	27,3	1,66		0.82/0.93				
LYS	91	118,7	8,28	54,3	4,7	34,4	1.61/2.23	25,7	1.42/1.49	28,3	1.59/1.65	42,7	3.07/3.07		6,07
HIS	92	123,7	10,87	56,7	4,42	25,9	2.88/3.09				0.93/6.51		6,9		
VAL	93	114	7,08	63,6	3,97	32,8	2,35		0.84/1.00						
GLY	94	105,7	7,29	45,6	3.63/4.40										
PRO	95			62,6	3,71	32,2	1.87/1.97	27,5	1.86/2.16	49,7	3.44/3.62				
GLY	96	109,9	8,96	44,9	3.25/4.46										
VAL	97	119,7	6,65	64,7	3,61	33,4	2,02		0.93/1.38						
LEU	98	130,1	7,37	53,2	4,78	44,4	0.33/0.53	25,6	-0,09		-1.63				
SER	99	121,3	8,21	55	5,29	64	2.74/3.80		1,38						
MET	100	123,6	8,65	54	5,58	32	2.29/2.79	32,1	2.42/2.42			16,9	2,24		

Residue		N	H	CA	HA*	CB	HB*	CG	HG*	CD	HD*	CE	HE*	CZ	HZ*
ALA	101	127,4	8,22	52,4	5,21	19,6	1,39								
ASN	102	114,3	9,5	55	4,52	41,1	1.47/2.03				8.22/8.03				
ALA	103	124,7	8,7		4,65	18,3	1,24								
GLY	104	105,9	7,78	43,4	3.57/3.60										
PRO	105			63,9	4,37	32,3	1.88/2.36	27,6	1.97/2.16	49,7	3.45/3.61				
ASN	106	119	8,9	54,5	4,02	37,2	2.64/3.09				8.80/8.90				
THR	107	110,4	10,21	60,4	4,38	68,7	4,3		0.82/3.14						
ASN	108	118,4	6,95	55,6	4,36	39,9	1.04/1.66				6.95/6.95				
GLY	109	110,8	9,59	45,6	3.48/4.63										
SER	110	118,2	9,39	56,8	4,64	66,1	3.67/3.82		2,74						
GLN	111	125,4	8,62	58,3	5,4	32,9	1.71/2.26	35,3	1.73/1.93				8.51/8.64		
PHE	112	118,7	8,82	55,6	6,09	43	3.43/3.44				6.88/6.88		7.84/7.84	128,7	6,79
PHE	113	115,7	9,96	55,3	5,77	43,6	2.69/2.70				6.75/6.88		6.78/6.97	130,4	5,87
ILE	114	117,4	8,86	59,1	5,04	41,2	1,57		0.74/0.85/ 1.85		0,95				
CYS	115	125	9,05	60,8	4,41	29,4	2.93/3.72		4,69						
THR	116	113,4	8,95	61	4,42	67,6	4,4		0.80/1.96						
ILE	117	118,7	7,62	59,8	4,33	44	1,77		0.93/1.28/ 1.40		1,08				
LYS	118	121,4	8,19	57,5	3,75	33,1	1.93/2.13	24,5	1.66/1.72	30	1.76/1.76	42,1	3.00/3.00		7,94
THR	119	120,5	7,69	57,2	3,54	68,1	2,87		1.01/3.80						
ASP	120	122,1	8,41	56,7	4,23	39,5	2.72/2.88								
TRP	121	119,6	7,59	59	4,58	27	3.33/3.46				7,05		7.75/9.28		7.37/6.55
LEU	122	117,9	7,3	54,2	4,44	38,3	1.27/1.27	38,8	0,33		0.33/0.75				
ASP	123	124	7,77	55,9	5,25	39,5	2.72/2.87								
GLY	124	111,6	9,61	44,8	2.94/3.96										

Residue		N	H	CA	HA*	CB	HB*	CG	HG*	CD	HD*	CE	HE*	CZ	HZ*
LYS	125	115,7	7,93	56,9	4,21	35,2	1.82/1.93	26	1.22/1.33	29,5	1.61/1.62	42,2	3.05/3.11		4,84
HIS	126	119,7	7,72	55	3,91	31,3	3.34/3.33				7.92/6.93		7,28		
VAL	127	124,4	8,47	63,9	4,23	33,5	2,04		1.01/1.16						
VAL	128	133,2	9,6	63	4,01	31	1,67		-0.02						
PHE	129	117,6	8,26	55,5	5,12	42,1	2.55/3.12				6.63/6.63		7.46/7.60	131,7	6,16
GLY	130	107,4	7,29	46,9	3.99/4.12										
HIS	131	119	8,51	55,5	5,11	34,6	2.81/3.10				8.72/6.94		6,91		
VAL	132	122,9	8,72	64,1	3,91	32,4	1,96		0.74/0.94						
LYS	133	132	9,62	56,5	4,51	35,1	1.68/1.69	24,9	1.51/1.54	29,1	1.68/1.79	42,1	3.01/3.04		9,66
GLU	134	115,8	7,93	55,2	4,77	33,5	1.79/2.12	36	2.19/2.29						
GLY	135	109,1	8,85	46,3	4.16/4.93										
MET	136	122,6	8,99	56,7	4,52	29,9	2.02/2.12	33,1	2.62/2.77			16,8	1,96		
ASP	137	116,7	9,15	56,8	4,22	38,9	2.59/2.74								
VAL	138	124	7,48	66,1	3,4	31	2,4		0.56/1.04						
VAL	139	120,8	7,53	67	3,32	30,8	2,55		0.74/1.04						
LYS	140	117,4	8,18	58,1	4,13	30,1	1.66/1.76	24,4	1.57/1.66	26,9	1.59/1.68	41,4	2.86/2.95		8,21
LYS	141	121,3	7,6	59,5	3,96	32,7	1.90/2.14	25,5	1.50/1.73	30	1.76/1.76	42,2	2.90/2.91		7,61
ILE	142	121,1	8,16	67	3,32	37,9	2,06		0.43/1.76/ 1.76		0,1				
GLU	143	117,8	8,23	58,7	3,51	30,5	1.75/1.75	36,8	2.11/2.11						
SER	144	113,8	7,42	60,9	4,15	62,9	3.75/3.75		7,44						
PHE	145	119,5	7,7	57,7	4,98	39,3	2.99/3.55				7.09/7.28		7.28/7.28	132	7,28
GLY	146	105,5	7,89	44,3	3.58/4.48										
SER	147	109,1	8,21	57,6	3,75	66,1	3.67/3.87		3,98						
LYS	148	118,9	8,81	60,5	3,66	29,6	1.26/1.27	23,2	0.84/1.25	29,6	0.83/1.26	42,3	2.84/2.92		4,84
SER	149	109,9	8,23	58,6	4,35	63,9	3.90/4.21		7,06						

Residue		N	H	CA	HA*	CB	HB*	CG	HG*	CD	HD*	CE	HE*	CZ	HZ*
GLY	150	113,3	8,46	45,2	3.88/4.44										
ARG	151	118,4	7,42	56,4	4,49	30,1	1.76/1.76	26,9	1.74/1.74	43,3	3.26/3.38		8,23		
THR	152	115,6	8,77	59,8	5,5	71,2	4,6		1.28/5.50						
SER	153	116,9	9,46	59	4,41	63,5	4.06/4.16		4,17						
LYS	154	117,9	7,3	54,2	4,45	37,9	1.10/1.25	25,8	0.75/0.82	29,4	1.04/1.05	42,3	2.85/2.92		7,09
LYS	155	123,4	8,5	56,9	4,21	32,4	1.78/1.88	25	1.21/1.45	29,4	1.66/1.66	42	2.85/2.91		8,51
ILE	156	133,2	9,29	59,5	5,12	37,4	2,3		0.76/1.32/ 1.50		0,7				
VAL	157	128,3	8,7	61,2	4,55	35,8	2,12		0.75/0.84						
ILE	158	125,7	8,97	60,9	4,69	36,9	2,11		0.90/0.92/ 1.89		0,72				
THR	159	126,1	8,86	64,3	3,95	69,1	3,96		1.24/2.60						
ASP	160	115,1	8,13	53,4	4,95	44,7	2.94/2.94								
CYS	161	115,4	8,29	55	4,52	30,7	3.04/3.08		4,76						
GLY	162	101,5	6,56	45,5	3.36/3.83										
GLN	163	120,7	9,08	54,8	5,06	30,8	1.66/1.96	33,1	2.48/2.62				8.70/9.15		
LEU	164	127,1	9,1	55,6	4,57	43,5	1.66/1.66	27,3	1,66		0.78/0.89				
SER	165	120,5	8,11	60,1	4,28	64,2	3.90/3.90		1,51						

Table 9: Predicted protein parameters.
The listed parameters of the used constructs are predicted using ProtParam (Wilkins 1999)

Construct	Number of amino acids	Molecular weight	Theoretical pI	Extinction coefficient
His-CypD43-207	189	20.573	8.32	12950
CypD43-207	165	17.730	9.06	9970
AT-hASIC1a	549	62.535	5.92	51895
His-MSP1-Flag	225	26.304	5.61	26930
His-MSP1E3D1	272	31.962	6.00	28420

7. References

Abdine, A., M. A. Verhoeven, et al. (2011). „Cell-free expression and labeling strategies for a new decade in solid-state NMR." New biotechnology 28(3): 272-276.

Aceti, D. J., C. A. Bingman, et al. (2015). „Expression platforms for producing eukaryotic proteins: a comparison of E. coli cell-based and wheat germ cell-free synthesis, affinity and solubility tags, and cloning strategies." Journal of structural and functional genomics.

Alavian, K. N., G. Beutner, et al. (2014). „An uncoupling channel within the c-subunit ring of the F1FO ATP synthase is the mitochondrial permeability transition pore." Proceedings of the National Academy of Sciences of the United States of America 111(29): 10580-10585.

Andrey, F., T. Tsintsadze, et al. (2005). „Acid sensing ionic channels: modulation by redox reagents." Biochimica et biophysica acta 1745(1): 1-6.

Aoki, M., T. Matsuda, et al. (2009). „Automated system for high-throughput protein production using the dialysis cell-free method." Protein expression and purification 68(2): 128-136.

Askwith, C. C., C. Cheng, et al. (2000). „Neuropeptide FF and FMRFamide potentiate acid-evoked currents from sensory neurons and proton-gated DEG/ENaC channels." Neuron 26(1): 133-141.

Azzolin, L., N. Antolini, et al. (2011). „Antamanide, a derivative of Amanita phalloides, is a novel inhibitor of the mitochondrial permeability transition pore." PLoS ONE 6(1): e16280.

Baconguis, I., C. J. Bohlen, et al. (2014). „X-ray structure of acid-sensing ion channel 1-snake toxin complex reveals open state of a Na^+-selective channel." Cell 156(4): 717-729.

Baconguis, I. and E. Gouaux (2012). „Structural plasticity and dynamic selectivity of acid-sensing ion channel-spider toxin complexes." Nature 489(7416): 400-405.

Bain, A. D. (2003). „Chemical exchange in NMR." Progress in Nuclear Magnetic Resonance Spectroscopy 43(3–4): 63-103.

Baines, C. P., R. A. Kaiser, et al. (2005). „Loss of cyclophilin D reveals a critical role for mitochondrial permeability transition in cell death." Nature 434(7033): 658-662.

Baron, A. and E. Lingueglia (2015). „Pharmacology of acid-sensing ion channels - Physiological and therapeutical perspectives." Neuropharmacology.

Baron, A., L. Schaefer, et al. (2001). „Zn^{2+} and H^+ are coactivators of acid-sensing ion channels." The Journal of biological chemistry 276(38): 35361-35367.

Basso, E., L. Fante, et al. (2005). „Properties of the permeability transition pore in mitochondria devoid of Cyclophilin D." The Journal of biological chemistry 280(19): 18558-18561.

Basso, E., V. Petronilli, et al. (2008). „Phosphate is essential for inhibition of the mitochondrial

permeability transition pore by cyclosporin A and by cyclophilin D ablation.“ The Journal of biological chemistry 283(39): 26307-26311.

Bax, A., G. M. Clore, et al. (1990). „1H-1H correlation via isotropic mixing of 13C magnetization, a new three-dimensional approach for assigning 1H and 13C spectra of 13C-enriched proteins.“ Journal of Magnetic Resonance (1969) 88(2): 425-431.

Beebe, E. T., S. Makino, et al. (2014). „Automated cell-free protein production methods for structural studies.“ Methods in molecular biology 1140: 117-135.

Bissantz, C., B. Kuhn, et al. (2010). „A medicinal chemist‘s guide to molecular interactions.“ Journal of medicinal chemistry 53(14): 5061-5084.

Bohlen, C. J., A. T. Chesler, et al. (2011). „A heteromeric Texas coral snake toxin targets acid-sensing ion channels to produce pain.“ Nature 479(7373): 410-414.

Chi, C. N., B. Vogeli, et al. (2015). „A Structural Ensemble for the Enzyme Cyclophilin Reveals an Orchestrated Mode of Action at Atomic Resolution.“ Angewandte Chemie.

Chinopoulos, C. and V. Adam-Vizi (2012). „Modulation of the mitochondrial permeability transition by cyclophilin D: moving closer to F(0)-F(1) ATP synthase?“ Mitochondrion 12(1): 41-45.

Clarke, S. J., G. P. McStay, et al. (2002). „Sanglifehrin A acts as a potent inhibitor of the mitochondrial permeability transition and reperfusion injury of the heart by binding to cyclophilin-D at a different site from cyclosporin A.“ The Journal of biological chemistry 277(38): 34793-34799.

Davis, T. L., J. R. Walker, et al. (2010). „Structural and biochemical characterization of the human cyclophilin family of peptidyl-prolyl isomerases.“ PLoS biology 8(7): e1000439.

Dawson, R. J., J. Benz, et al. (2012). „Structure of the acid-sensing ion channel 1 in complex with the gating modifier Psalmotoxin 1.“ Nature communications 3: 936.

Denisov, I. G., Y. V. Grinkova, et al. (2004). „Directed self-assembly of monodisperse phospholipid bilayer Nanodiscs with controlled size.“ Journal of the American Chemical Society 126(11): 3477-3487.

Diochot, S., A. Baron, et al. (2004). „A new sea anemone peptide, APETx2, inhibits ASIC3, a major acid-sensitive channel in sensory neurons.“ Embo J 23(7): 1516-1525.

Diochot, S., A. Baron, et al. (2012). „Black mamba venom peptides target acid-sensing ion channels to abolish pain.“ Nature 490(7421): 552-555.

Dötsch, V., R. E. Oswald, et al. (1996). „Amino-acid-type-selective triple-resonance experiments.“ Journal of magnetic resonance. Series B 110(1): 107-111.

Du, H., L. Guo, et al. (2008). „Cyclophilin D deficiency attenuates mitochondrial and neuronal perturbation and ameliorates learning and memory in Alzheimer‘s disease.“ Nature medicine 14(10): 1097-1105.

Dube, G. R., S. G. Lehto, et al. (2005). „Electrophysiological and in vivo characterization of

A-317567, a novel blocker of acid sensing ion channels.“ Pain 117(1-2): 88-96.

Eisenmesser, E. Z., O. Millet, et al. (2005). „Intrinsic dynamics of an enzyme underlies catalysis.“ Nature 438(7064): 117-121.

Elrod, J. W., R. Wong, et al. (2010). „Cyclophilin D controls mitochondrial pore-dependent Ca^{2+} exchange, metabolic flexibility, and propensity for heart failure in mice.“ The Journal of clinical investigation 120(10): 3680-3687.

Escoubas, P., J. R. De Weille, et al. (2000). „Isolation of a tarantula toxin specific for a class of proton-gated Na^{+} channels.“ The Journal of biological chemistry 275(33): 25116-25121.

Farmer, B. T., 2nd, R. A. Venters, et al. (1992). „A refocused and optimized HNCA: increased sensitivity and resolution in large macromolecules.“ Journal of biomolecular NMR 2(2): 195-202.

Fayaz, S. M., Y. V. Raj, et al. (2015). „CypD: The Key to the Death Door.“ CNS & neurological disorders drug targets 14(5): 654-663.

Fraser, J. S., M. W. Clarkson, et al. (2009). „Hidden alternative structures of proline isomerase essential for catalysis.“ Nature 462(7273): 669-673.

Galat, A. and S. M. Metcalfe (1995). „Peptidylproline cis/trans isomerases.“ Progress in biophysics and molecular biology 63(1): 67-118.

Gao, J., B. Duan, et al. (2005). „Coupling between NMDA receptor and acid-sensing ion channel contributes to ischemic neuronal death.“ Neuron 48(4): 635-646.

Gee, C. T., E. J. Koleski, et al. (2015). „Fragment screening and druggability assessment for the CBP/p300 KIX domain through protein-observed 19F NMR spectroscopy.“ Angewandte Chemie 54(12): 3735-3739.

Gething, M. J. and J. Sambrook (1992). „Protein folding in the cell.“ Nature 355(6355): 33-45.

Giorgio, V., E. Bisetto, et al. (2009). „Cyclophilin D modulates mitochondrial F0F1-ATP synthase by interacting with the lateral stalk of the complex.“ The Journal of biological chemistry 284(49): 33982-33988.

Gossert, A. D., A. Hinniger, et al. (2011). „A simple protocol for amino acid type selective isotope labeling in insect cells with improved yields and high reproducibility.“ Journal of biomolecular NMR 51(4): 449-456.

Gottstein, D., D. K. Kirchner, et al. (2012). „Simultaneous single-structure and bundle representation of protein NMR structures in torsion angle space.“ Journal of biomolecular NMR 52(4): 351-364.

Grunder, S. and M. Pusch (2015). „Biophysical properties of acid-sensing ion channels (ASICs).“ Neuropharmacology.

Grzesiek, S., J. Anglister, et al. (1993). „Correlation of Backbone Amide and Aliphatic Side-Chain Resonances in 13C/15N-Enriched Proteins by Isotropic Mixing of 13C Magnetization.“ Journal of Magnetic Resonance, Series B 101(1): 114-119.

Grzesiek, S. and A. Bax (1992a). „Correlating backbone amide and side chain resonances in larger proteins by multiple relayed triple resonance NMR.“ Journal of the American Chemical Society 114(16): 6291-6293.

Grzesiek, S. and A. Bax (1992b). „An efficient experiment for sequential backbone assignment of medium-sized isotopically enriched proteins.“ Journal of Magnetic Resonance (1969) 99(1): 201-207.

Grzesiek, S. and A. Bax (1992c). „Improved 3D triple-resonance NMR techniques applied to a 31 kDa protein.“ Journal of Magnetic Resonance (1969) 96(2): 432-440.

Güntert, P. (2004). „Automated NMR structure calculation with CYANA.“ Methods Mol Biol 278: 353-378.

Guichou, J.F., Colliandre, L. et al. (2011). „New inhibitors of cyclophilins and uses thereof“ International patent, patent number WO 2011/076784 A2

Guo, H. X., F. Wang, et al. (2005). „Novel cyclophilin D inhibitors derived from quinoxaline exhibit highly inhibitory activity against rat mitochondrial swelling and Ca^{2+} uptake/ release.“ Acta pharmacologica Sinica 26(10): 1201-1211.

Haberstock, S., C. Roos, et al. (2012). „A systematic approach to increase the efficiency of membrane protein production in cell-free expression systems.“ Protein expression and purification 82(2): 308-316.

Hajduk, P. J. and J. Greer (2007). „A decade of fragment-based drug design: strategic advances and lessons learned.“ Nature reviews. Drug discovery 6(3): 211-219.

Halestrap, A. P. (2009). „What is the mitochondrial permeability transition pore?“ Journal of molecular and cellular cardiology 46(6): 821-831.

Halestrap, A. P., C. P. Connern, et al. (1997). „Cyclosporin A binding to mitochondrial cyclophilin inhibits the permeability transition pore and protects hearts from ischaemia/reperfusion injury.“ Molecular and cellular biochemistry 174(1-2): 167-172.

Halestrap, A. P., G. P. McStay, et al. (2002). „The permeability transition pore complex: another view.“ Biochimie 84(2-3): 153-166.

Hein, C., E. Henrich, et al. (2014). „Hydrophobic supplements in cell-free systems: Designing artificial environments for membrane proteins.“ Engineering in Life Sciences 14(4): 365-379.

Henrich, E., C. Hein, et al. (2015). „Membrane protein production in Escherichia coli cell-free lysates.“ FEBS letters.

Huber, W., S. Perspicace, et al. (2004). „SPR-based interaction studies with small molecular weight ligands using hAGT fusion proteins.“ Anal Biochem 333(2): 280-288.

Immke, D. C. and E. W. McCleskey (2001). „Lactate enhances the acid-sensing Na^{+} channel on ischemia-sensing neurons.“ Nature neuroscience 4(9): 869-870.

Immke, D. C. and E. W. McCleskey (2003). „Protons open acid-sensing ion channels by catalyzing relief of Ca^{2+} blockade.“ Neuron 37(1): 75-84.

Jahnke, W., R. M. Grotzfeld, et al. (2010). „Binding or bending: distinction of allosteric Abl kinase agonists from antagonists by an NMR-based conformational assay." Journal of the American Chemical Society 132(20): 7043-7048.

Jasti, J., H. Furukawa, et al. (2007). „Structure of acid-sensing ion channel 1 at 1.9 A resolution and low pH." Nature 449(7160): 316-323.

Jeremy Craven, C., M. Al-Owais, et al. (2007). „A systematic analysis of backbone amide assignments achieved via combinatorial selective labelling of amino acids." J Biomol NMR 38(2): 151-159.

Jobe, S. M., K. M. Wilson, et al. (2008). „Critical role for the mitochondrial permeability transition pore and cyclophilin D in platelet activation and thrombosis." Blood 111(3): 1257-1265.

Junge, F., S. Haberstock, et al. (2011). „Advances in cell-free protein synthesis for the functional and structural analysis of membrane proteins." New biotechnology 28(3): 262-271.

Junge, F., B. Schneider, et al. (2008). „Large-scale production of functional membrane proteins." Cell Mol Life Sci 65(11): 1729-1755.

Kai, L., E. Orban, et al. (2015). „Co-translational stabilization of insoluble proteins in cell-free expression systems." Methods in molecular biology 1258: 125-143.

Kainosho, M., T. Torizawa, et al. (2006). „Optimal isotope labelling for NMR protein structure determinations." Nature 440(7080): 52-57.

Kajitani, K., M. Fujihashi, et al. (2008). „Crystal structure of human cyclophilin D in complex with its inhibitor, cyclosporin A at 0.96-A resolution." Proteins 70(4): 1635-1639.

Kallen, J., V. Mikol, et al. (1998). „X-ray structures and analysis of 11 cyclosporin derivatives complexed with cyclophilin A." Journal of molecular biology 283(2): 435-449.

Kallen, J., R. Sedrani, et al. (2005). „Structure of human cyclophilin A in complex with the novel immunosuppressant sanglifehrin A at 1.6 A resolution." The Journal of biological chemistry 280(23): 21965-21971.

Kay, L. E., M. Ikura, et al. (1990). „Three-dimensional triple-resonance NMR spectroscopy of isotopically enriched proteins." Journal of Magnetic Resonance (1969) 89(3): 496-514.

Kellenberger, S. and L. Schild (2002). „Epithelial sodium channel/degenerin family of ion channels: a variety of functions for a shared structure." Physiological reviews 82(3): 735-767.

Kim, H. C. and D. M. Kim (2009). „Methods for energizing cell-free protein synthesis." Journal of bioscience and bioengineering 108(1): 1-4.

Kim, T. W., J. W. Keum, et al. (2006). „Simple procedures for the construction of a robust and cost-effective cell-free protein synthesis system." J Biotechnol 126(4): 554-561.

Kokoszka, J. E., K. G. Waymire, et al. (2004). „The ADP/ATP translocator is not essential for the mitochondrial permeability transition pore." Nature 427(6973): 461-465.

Koradi, R., M. Billeter, et al. (2000). „Point-centered domain decomposition for parallel molecular

dynamics simulation.“ Computer Physics Communications 124(2–3): 139-147.

Krauskopf, A., O. Eriksson, et al. (2006). „Properties of the permeability transition in VDAC1(-/-) mitochondria.“ Biochimica et biophysica acta 1757(5-6): 590-595.

Krishtal, O. A. and V. I. Pidoplichko (1980). „A receptor for protons in the nerve cell membrane.“ Neuroscience 5(12): 2325-2327.

le Maire, A., M. Gelin, et al. (2011). „In-plate protein crystallization, in situ ligand soaking and X-ray diffraction.“ Acta crystallographica. Section D, Biological crystallography 67(Pt 9): 747-755.

Leung, A. W., P. Varanyuwatana, et al. (2008). „The mitochondrial phosphate carrier interacts with cyclophilin D and may play a key role in the permeability transition.“ The Journal of biological chemistry 283(39): 26312-26323.

Linser, R., V. Gelev, et al. (2014). „Selective methyl labeling of eukaryotic membrane proteins using cell-free expression.“ Journal of the American Chemical Society 136(32): 11308-11310.

Löhr, F., A. Laguerre, et al. (2014). „Time-shared experiments for efficient assignment of triple-selectively labeled proteins.“ Journal of magnetic resonance 248: 81-95.

Löhr, F., S. Reckel, et al. (2012). „Combinatorial triple-selective labeling as a tool to assist membrane protein backbone resonance assignment.“ Journal of biomolecular NMR 52(3): 197-210.

Löhr, F., F. Tumulka, et al. (2015). „An extended combinatorial ^{15}N, $^{13}C^{\alpha}$, and $^{13}C'$ labeling approach to protein backbone resonance assignment.“ Journal of biomolecular NMR.

Lu, K. P., Y. C. Liou, et al. (2002). „Pinning down proline-directed phosphorylation signaling.“ Trends in cell biology 12(4): 164-172.

Luvisetto, S., E. Basso, et al. (2008). „Enhancement of anxiety, facilitation of avoidance behavior, and occurrence of adult-onset obesity in mice lacking mitochondrial cyclophilin D.“ Neuroscience 155(3): 585-596.

Merlini, L., A. Angelin, et al. (2008). „Cyclosporin A corrects mitochondrial dysfunction and muscle apoptosis in patients with collagen VI myopathies.“ Proceedings of the National Academy of Sciences of the United States of America 105(13): 5225-5229.

Millay, D. P., M. A. Sargent, et al. (2008). „Genetic and pharmacologic inhibition of mitochondrial-dependent necrosis attenuates muscular dystrophy.“ Nature medicine 14(4): 442-447.

Murray, J. B., S. D. Roughley, et al. (2014). „Off-Rate Screening (ORS) By Surface Plasmon Resonance. An Efficient Method to Kinetically Sample Hit to Lead Chemical Space from Unpurified Reaction Products.“ Journal of medicinal chemistry.

Navratilova, I., J. Besnard, et al. (2011). „Screening for GPCR Ligands Using Surface Plasmon Resonance.“ ACS medicinal chemistry letters 2(7): 549-554.

Nguyen, T. T., M. V. Stevens, et al. (2011). „Cysteine 203 of cyclophilin D is critical for cyclophilin D activation of the mitochondrial permeability transition pore.“ The Journal of biologi-

cal chemistry 286(46): 40184-40192.

Palmer, L. G. (1982). „Ion selectivity of the apical membrane Na channel in the toad urinary bladder.“ The Journal of membrane biology 67(2): 91-98.

Parker, M. J., M. Aulton-Jones, et al. (2004). „A combinatorial selective labeling method for the assignment of backbone amide NMR resonances.“ J Am Chem Soc 126(16): 5020-5021.

Poirot, O., M. Vukicevic, et al. (2004). „Selective regulation of acid-sensing ion channel 1 by serine proteases.“ The Journal of biological chemistry 279(37): 38448-38457.

Proverbio, D., E. Henrich, et al. (2014). Membrane Protein Quality Control in Cell-Free Expression Systems: Tools, Strategies and Case Studies. Membrane Proteins Production for Structural Analysis. I. Mus-Veteau, Springer New York: 45-70.

Quast, R. B., O. Kortt, et al. (2015). „Automated production of functional membrane proteins using eukaryotic cell-free translation systems.“ J Biotechnol 203: 45-53.

Rao, V. K., E. A. Carlson, et al. (2014). „Mitochondrial permeability transition pore is a potential drug target for neurodegeneration.“ Biochimica et biophysica acta 1842(8): 1267-1272.

Reckel, S., D. Gottstein, et al. (2011). „Solution NMR structure of proteorhodopsin.“ Angewandte Chemie 50(50): 11942-11946.

Reckel, S., S. Sobhanifar, et al. (2008). „Transmembrane segment enhanced labeling as a tool for the backbone assignment of alpha-helical membrane proteins.“ Proc Natl Acad Sci U S A 105(24): 8262-8267.

Reese, M. L. and V. Dotsch (2003). „Fast mapping of protein-protein interfaces by NMR spectroscopy.“ J Am Chem Soc 125(47): 14250-14251.

Roos, C., M. Zocher, et al. (2012). „Characterization of co-translationally formed nanodisc complexes with small multidrug transporters, proteorhodopsin and with the E. coli MraY translocase.“ Biochimica et biophysica acta 1818(12): 3098-3106.

Schagger, H. (2006). „Tricine-SDS-PAGE.“ Nat Protoc 1(1): 16-22.

Schagger, H. and G. von Jagow (1987). „Tricine-sodium dodecyl sulfate-polyacrylamide gel electrophoresis for the separation of proteins in the range from 1 to 100 kDa.“ Anal Biochem 166(2): 368-379.

Schinzel, A. C., O. Takeuchi, et al. (2005). „Cyclophilin D is a component of mitochondrial permeability transition and mediates neuronal cell death after focal cerebral ischemia.“ Proceedings of the National Academy of Sciences of the United States of America 102(34): 12005-12010.

Schlatter, D., R. Thoma, et al. (2005). „Crystal engineering yields crystals of cyclophilin D diffracting to 1.7 A resolution.“ Acta crystallographica. Section D, Biological crystallography 61(Pt 5): 513-519.

Schmidt, E. and P. Guntert (2012). „A new algorithm for reliable and general NMR resonance assignment.“ Journal of the American Chemical Society 134(30): 12817-12829.

Schneider, B., F. Junge, et al. (2010). „Membrane protein expression in cell-free systems.“ Methods in molecular biology 601: 165-186.

Schwarz, D., F. Junge, et al. (2007). „Preparative scale expression of membrane proteins in Escherichia coli-based continuous exchange cell-free systems.“ Nat Protoc 2(11): 2945-2957.

Shuker, S. B., P. J. Hajduk, et al. (1996). „Discovering high-affinity ligands for proteins: SAR by NMR.“ Science 274(5292): 1531-1534.

Staunton, D., R. Schlinkert, et al. (2006). „Cell-free expression and selective isotope labelling in protein NMR.“ Magn Reson Chem 44 Spec No: S2-9.

Strop, P. and A. T. Brunger (2005). „Refractive index-based determination of detergent concentration and its application to the study of membrane proteins.“ Protein science : a publication of the Protein Society 14(8): 2207-2211.

Su, X. C., C. T. Loh, et al. (2011). „Suppression of isotope scrambling in cell-free protein synthesis by broadband inhibition of PLP enymes for selective 15N-labelling and production of perdeuterated proteins in H2O.“ Journal of biomolecular NMR 50(1): 35-42.

Svarstad, H., H. Bugge, et al. (2000). „From Norway to Novartis: cyclosporin from Tolypocladium inflatum in an open access bioprospecting regime.“ Biodiversity & Conservation 9(11): 1521-1541.

Swinehart, D. F. (1962). „The Beer-Lambert Law.“ Journal of Chemical Education 39(7): 333.

Ugawa, S., T. Ueda, et al. (2002). „Amiloride-blockable acid-sensing ion channels are leading acid sensors expressed in human nociceptors.“ The Journal of clinical investigation 110(8): 1185-1190.

Vajpai, N., A. Strauss, et al. (2008a). „Solution conformations and dynamics of ABL kinase-inhibitor complexes determined by NMR substantiate the different binding modes of imatinib/nilotinib and dasatinib.“ The Journal of biological chemistry 283(26): 18292-18302.

Vajpai, N., A. Strauss, et al. (2008b). „Backbone NMR resonance assignment of the Abelson kinase domain in complex with imatinib.“ Biomolecular NMR assignments 2(1): 41-42.

Villemagne, B., M. Flipo, et al. (2014). „Ligand efficiency driven design of new inhibitors of Mycobacterium tuberculosis transcriptional repressor EthR using fragment growing, merging, and linking approaches.“ Journal of medicinal chemistry 57(11): 4876-4888.

Vogeli, B. (2014). „The nuclear Overhauser effect from a quantitative perspective.“ Progress in Nuclear Magnetic Resonance Spectroscopy 78: 1-46.

Vogeli, B., S. Kazemi, et al. (2012). „Spatial elucidation of motion in proteins by ensemble-based structure calculation using exact NOEs.“ Nature structural & molecular biology 19(10): 1053-1057.

Wang, P. and J. Heitman (2005). „The cyclophilins.“ Genome biology 6(7): 226.

Watashi, K., N. Ishii, et al. (2005). „Cyclophilin B is a functional regulator of hepatitis C virus RNA polymerase.“ Mol Cell 19(1): 111-122.

Weigelt, J., M. van Dongen, et al. (2002). „Site-selective screening by NMR spectroscopy with labeled amino acid pairs.“ Journal of the American Chemical Society 124(11): 2446-2447.

Wemmie, J. A., C. C. Askwith, et al. (2003). „Acid-sensing ion channel 1 is localized in brain regions with high synaptic density and contributes to fear conditioning.“ The Journal of neuroscience : the official journal of the Society for Neuroscience 23(13): 5496-5502.

Wemmie, J. A., M. P. Price, et al. (2006). „Acid-sensing ion channels: advances, questions and therapeutic opportunities.“ Trends in neurosciences 29(10): 578-586.

Wilkins, M. R., E. Gasteiger, et al. (1999). „Protein identification and analysis tools in the ExPASy server.“ Methods Mol Biol 112: 531-552.

Williamson, M. P. (2013). „Using chemical shift perturbation to characterise ligand binding.“ Progress in Nuclear Magnetic Resonance Spectroscopy 73: 1-16.

Wu, P. S., K. Ozawa, et al. (2006). „Amino-acid type identification in 15N-HSQC spectra by combinatorial selective 15N-labelling.“ Journal of biomolecular NMR 34(1): 13-21.

Xu, Y., J. Lee, et al. (2015). „Production of bispecific antibodies in „knobs-into-holes“ using a cell-free expression system.“ mAbs 7(1): 231-242.

Yamazaki, T., J. D. Forman-Kay, et al. (1993). „Two-dimensional NMR experiments for correlating carbon-13.beta. and proton.delta./.epsilon. chemical shifts of aromatic residues in 13C-labeled proteins via scalar couplings.“ Journal of the American Chemical Society 115(23): 11054-11055.

Yin, G., E. D. Garces, et al. (2012). „Aglycosylated antibodies and antibody fragments produced in a scalable in vitro transcription-translation system.“ mAbs 4(2): 217-225.

Yokoyama, J., T. Matsuda, et al. (2011). „A practical method for cell-free protein synthesis to avoid stable isotope scrambling and dilution.“ Anal Biochem 411(2): 223-229.

Zimmerman, E. S., T. H. Heibeck, et al. (2014). „Production of site-specific antibody-drug conjugates using optimized non-natural amino acids in a cell-free expression system.“ Bioconjug Chem 25(2): 351-361.

Zubay, G. (1973). „In vitro synthesis of protein in microbial systems.“ Annual review of genetics 7: 267-287.

Acknowledgements

I would like to thank Volker Dötsch for his support during my time as a student in his lab and for the supervision of my PhD thesis. I enjoyed my time in the group, where you managed to create a cooperative and creative working environment. I appreciate the space and the time you gave me for my personal and scientific development. I was able to pursue my own ideas, plan and develop my projects in nearly any way I wanted, work on a whole bouquet of different subjects and had the freedom to establish cooperations. In addition I would like to thank you for your great sense of humor, even in awkward or special situations.

Further I would like to thank Daniel Schwarz for his great support during the whole project. Thank you for establishing the cooperation that made my thesis possible and for all the organizational work connected with the project. Thank you for your great feedback on my data, my ideas, my presentations and my final thesis, as well as your ideas and help, especially during the critical and difficult times of the thesis.

I would further like to thank Jörg Bombke, Ansgar Wegener, Djordje Musil, Ulrich Graedler and Matthias Frech from the Merck MIB team for scientific input and support during the thesis, as well as Norbert, Ivonne, Eva and Gerlinde for their help in the MIB lab.

Special thanks go to Frank Löhr (Murph) for your enormous efforts with all my NMR samples. Your support and input saved my PhD thesis.

I would like to thank my cooperation partners, that helped me in a lot of projects even if the projects are not mentioned in this thesis. My thanks go to:

- Oliver Peetz for his MS measurements and for always having time for my samples, even on very short notice.
- Albert Konijnenberg for the cooperation on another MS project.
- Lilia Leisle and Chris Ahern for their big effort in synthesizing modified tRNAs and for their input during the cooperation project.
- Francis Valayaveetil and his lab for the great support on the protein refolding
- Martin Caffrey and Coilin Boland for their work on LCP crystallization of my samples.
- Ekaterina Zaitseva for electrophysiology measurements on a lot of samples.
- Sina Kazemi for all the work concerning the automated assignment and structure calculation as well as the fun during the music festivals and concerts.

I would like to thank Sigrid Oğuzer-Fachinger, who did a great job helping me with all the bureaucratic problems; Manfred Strupf, for being better than anyone else in fixing equipment, you kept the lab running and Brigit Schäfer for being the good soul of the lab.

But the most influence on my time had the people I worked with on an everyday basis in the lab. Here I'd like to thank Susanne Stefer for introducing me to the cell free expression and for the great cooperation during the first six months of my PhD, in which I worked with her on the Get project. I want to thank Sebastian Richers, who was probably the most helpful postdoc in the lab and had an endless amount of great tips, and hands on support. I want to thank Aisha Laguerre for her honest and open conversations and for sharing her postdoc wisdom on what a PhD thesis is about and how it works, as well as her ideas about life, the universe and everything. Further to the former lab members Gergor Deutsch, Robert Hänsel-Hertsch, Peter Tufar, Alena Busche, Sina Reckel, Alexis Rozenknop, Christian Roos and Stefan Haberstock for a warm welcome in the

group and a great start, as well as Jessie (for dance battles and singing in the hallway), Christian, Manni, Katharina, Susanne, Laura and Beate for help, input, feedback and everyday fun (and of course the special calendar photo shoots).

My thanks go to Alina Ornik. You‘ve been a great Hiwi student and the best diploma student I could wish for. Thank you for your work on the Pin1 project. I thank also Heidi Zetsche for the help during her Hiwi time

My special thanks go to Erik Henrich for a great cooperation on so many projects and constant ideas and help in the lab, as well as for the great fun after work. Special thanks also to Sebastian Kehrlößer for being a great friend, (ex) flat mate and colleague since high school. Thanks for the great time during the studies, the thesis and the holidays. You always had an open ear for problems, ideas and general silliness and always provided the right amount of input, feedback and mockery.

At last I want to thank my family and especially my girlfriend Viola, because they supported me when I was down, celebrated with me the good times and endured me for all these years, without any questions or rewards.